JOURNAL OF FOOD PROCESS ENGINEERING

D.R. HELDMAN
and
R.P. SINGH
COEDITORS

FOOD & NUTRITION PRESS, INC.

VOLUME 18, NUMBER 2 JUNE 1995

JOURNAL OF FOOD PROCESS ENGINEERING

All articles for publication and inquiries regarding publication should be sent to DR. D.R. HELDMAN, COEDITOR, *Journal of Food Process Engineering*, Food Science/Engineering Unit, University of Missouri-Columbia, 235 Agricultural/Engineering Bldg., Columbia, MO 65211 USA; or DR. R.P. SINGH, COEDITOR, *Journal of Food Process Engineering*, University of California, Davis, Department of Agricultural Engineering, Davis, CA 95616 USA.

All subscriptions and inquiries regarding subscriptions should be sent to Food & Nutrition Press, Inc., 2 Corporate Drive, P.O. Box 374, Trumbull, CT 06611 USA.

One volume of four issues will be published annually. The price for Volume 18 is $142.00, which includes postage to U.S., Canada, and Mexico. Subscriptions to other countries are $162.00 per year via surface mail, and $173.00 per year via airmail.

Subscriptions for individuals for their own personal use are $112.00 for Volume 18, which includes postage to U.S., Canada and Mexico. Personal subscriptions to other countries are $132.00 per year via surface mail, and $143.00 per year via airmail. Subscriptions for individuals should be sent directly to the publisher and marked for personal use.

The *Journal of Food Process Engineering* (ISSN 0145-8876) is published quarterly (March, June, September and December) by Food & Nutrition Press, Inc.—Office of Publication is 2 Corporate Drive, P.O. Box 374, Trumbull, Connecticut 06611 USA.

Second class postage paid at Bridgeport, CT 06602.

POSTMASTER: Send address changes to Food & Nutrition Press, Inc., 2 Corporate Drive, P.O. Box 374, Trumbull, Connecticut 06611 USA.

JOURNAL OF FOOD PROCESS ENGINEERING

JOURNAL OF FOOD PROCESS ENGINEERING

Journal of FOOD PROCESS ENGINEERING

VOLUME 18
NUMBER 2

Coeditors: D.R. HELDMAN
R.P. SINGH

FOOD & NUTRITION PRESS, INC.
TRUMBULL, CONNECTICUT 06611 USA

ISSN 0145-8876

Printed in the United States of America

CONTENTS

PARTICLE CONCENTRATION INFLUENCE ON LIQUID RESIDENCE TIME DISTRIBUTIONS IN A MODEL ASEPTIC PROCESSING SYSTEM[1]

JUN H. LEE[2], RAKESH K. SINGH[3] and D. SCOTT LINEBACK

Department of Food Science
Department of Agricultural Engineering[2]
Purdue University
West Lafayette, IN 47907

Accepted for Publication April 8, 1994

ABSTRACT

Residence time distributions (RTDs) of water as influenced by particle concentration and mutator speed (SSHE only) were investigated in a holding tube and a horizontal scraped surface heat exchanger (SSHE). Liquid mean residence times (LMRTs) were not significantly influenced by particle concentrations up to 30% in the holding tube. Variance, on the other hand, was significantly higher without particle loading, indicating a broader distribution. About 20% particle loading significantly reduced the LMRTs regardless of the mutator speed. In addition, an increase in the mutator speed significantly increased the variance regardless of the particle concentration, indicating a broader distribution. The variance in SSHE was not significantly influenced by the particle concentration, unlike the holding tube. The LMRTs calculated from volumetric flow rates were lower than those from pulse input experiments for both holding tube and SSHE.

INTRODUCTION

Residence time is the length of time a unit of product spends within the system boundaries. In aseptic processing of liquid foods, with or without particulates, one of the most important parameters affecting safety and quality of the aseptically processed products in continuous systems (heat exchanger and holding tube) is the residence time distribution (RTD). Thus, experimental

[1] Approved as Journal Paper No. 13,670 of the Purdue Agricultural Experiment Station, USA.
[2] Author Lee formerly with the Department of Agricultural Engineering, Purdue University, is now with Department of Food Engineering, Taegu University, KyungBuk KyungSan, Seoul, Korea.
[3] Address Correspondence to: Dr. Rakesh K. Singh, Dept. of Food Science, Smith Hall, Purdue University, W. Lafayette, IN 47907.

Journal of Food Process Engineering **18** (1995) 119–133.

determination of liquid and particle RTDs in those systems is essential for establishing an adequate thermal process.

Previous studies on particle RTDs in a holding tube (McCoy *et al.* 1987; Nesaratnam and Gaze 1987; Berry 1989; Dutta and Sastry 1990a,b; Hong *et al.* 1991; Yang and Swartzel 1991, 1992) and scraped surface heat exchanger (SSHE) (Taeymans *et al.* 1985, 1986; Alcairo and Zuritz 1990; NFPA 1990; Lee and Singh, 1991a,b,c, 1993) have shown the influence of process conditions on the particle RTDs. In addition, several researchers investigated RTDs of liquid medium in a SSHEs (Chen and Zahradnik 1967; Trommelen and Beek 1971; Milton and Zahradnik 1973; Cuevas *et al.* 1982) and holding tubes (Bosworth 1948, 1949; Dickerson *et al.* 1968; Scalzo *et al.* 1969; Palmer and Jones 1976; Hong *et al.* 1991; Sancho and Rao 1992). However, effect of particle concentration, which is one of the critical process parameters, on the liquid RTD has not been critically evaluated for conditions where particle concentration is the major variable.

The objectives of this study were to: (1) examine the effect of particle concentration on liquid RTDs in a holding tube and (2) study the effect of particle concentration, mutator speed, and their interaction on liquid RTDs in a horizontal SSHE.

MATERIALS AND METHODS

Experimental Setup

Holding Tube Assembly. A hold tube, 3.048 m section of stainless steel pipe (0.0525 m I.D.), was inclined 3.49° upward (6.06 cm inclination per linear meter) as specified by the Food and Drug Administration regulations. The injection port and conductivity meter (Presto-Tek Corp., Los Angeles, CA) were placed at the inlet and outlet of the test section, respectively (Fig. 1). A 90° elbow was connected immediately after the injection port to radially mix the tracer. The recycle loop, a 3.048 m, 0.0525 m I.D. plastic pipe (SaniTech, Sparta, NJ), was connected so that possible deviation of the particle flow pattern could be observed. A 0.0762 m I.D. inlet/outlet port Waukesha positive displacement pump (AMCA International, Waukesha, WI) with a 7.46 kW variable speed motor (Syncrogear Module, U.S. Electrical Motors, St. Louis, MO) was used to pump product through the system. Product was recycled through a 56.78 L stainless steel reservoir connected to the inlet port of the pump.

SSHE Assembly. A transparent horizontal SSHE (Contherm Division, Alfa-Laval, Inc., Newburyport, MA) was used for the study. The SSHE had an acrylic outer shield, thus making it possible to observe particle flow in the SSHE. Specific details of the system were described earlier (Lee and Singh

1991a). The mutator inside the SSHE was driven by a variable speed hydraulic power drive (Vickers Div. of Sperry Rand Corp., Troy, MI). The pump and reservoir used for the holding tube study were also used for the SSHE experiment. The injection port and conductivity meter (Presto-Tek Corp., Los Angeles, CA) were placed at the entrance and exit of the SSHE. Once again, a 90° elbow was located immediately after the injection port to mix the tracer. A long holding section after the SSHE was required to ensure recycled product would not return into the system during an experimental measurement period. In addition, tangential inlet and outlet ports for the SSHE were used to avoid bridging of the particles.

Experimental Procedure

Between 26.5 and 34.1 L of water (ρ_f = 998.2 kg/m^3), depending on conditions, were introduced into the reservoir, and the pump was turned on to circulate water for about 5 min to reach steady-state. Pump speed was adjusted to obtain the desired flow rate (480 ml/s for hold tube with Re = 11576 and 418 ml/s for SSHE runs), and mutator speed (60 and 110 rpm for SSHE runs only) was set using a Hasler tachometer (Hasler-Tel Co., Inc., New York, NY) and visual calibration.

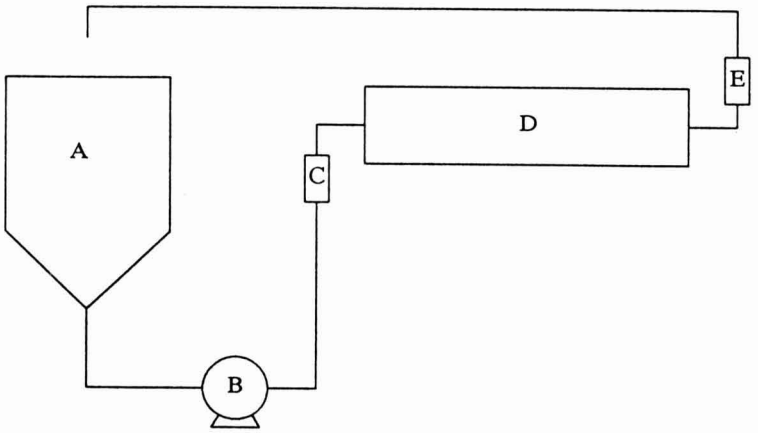

A. Feed reservior
B. Pump
C. Injection port
D. Hold tube or SSHE
E. Conductivity meter

FIG. 1. SCHEMATIC DIAGRAM OF EXPERIMENTAL PROCESSING SYSTEM

Once all process variables were set, the specified amount (depending on the particle concentrations; 0, 10, 20, and 30%, w/v) of potato particles (ρ_p = 1074.9 kg/m^3; precut in 12.7 mm cubes; Purdue University Food Store) were added to the reservoir and the mixture was recycled for about 5 min to achieve a steady-state condition. A 15-ml portion of tracer (2% NaCl) was injected through the injection port and electrical conductivity of the outlet liquid was recorded. Electrical conductivity versus time data were monitored and collected using a data acquisition system (TrendSetter; Acurex Corp., Autodata Div., Mountain View, CA) and personal computer (ZEOS® 386SX; ZEOS® International LTD., St. Paul, MN). Data were stored as ASCII files for subsequent analysis. Measurements were conducted under isothermal conditions (at room temperature) and replicated at least 5 times. Occasionally, water was replaced to reduce the electrical conductivity of the returning product.

Calculations

In order to experimentally determine the mean residence time and variance, E(t) curves were constructed from the original data (electrical conductivity versus time). E(t), the fraction of volume elements exiting the system at a particular time, is a normalized distribution defined as (Eq. 1):

$$\int_0^\infty E(t)dt = 1 \tag{1}$$

E(t) values were determined by establishing the baseline conductivity of the particle carrier fluid, integrating the area under the curve, then normalizing the data by dividing each individual data point by the total area. Normalized values were then plotted against time to obtain the E(t) curve.

To characterize the fluid distribution, mean and variance were calculated. For an E(t) curve, mean residence time, $\bar{t}$, is given by

$$\bar{t} = \int_0^\infty tE(t)dt = \sum t_i E(t_i)\Delta t \tag{2}$$

The theoretical mean residence time, $\bar{t}_T$, was based on volumetric flow rate, Q, and system volume, V,

$$\bar{t}_T = \frac{V}{Q} \tag{3}$$

If $\bar{t}_T$ and $\bar{t}$ do not agree, there may be channeling or bypassing in the equipment, so that the effective volume is less than the actual volume (Heppell 1985).

Variance, which indicated the spread of the distribution, was used to compare RTDs. For an E(t) curve, variance is given by

$$\sigma^2 = \int_0^\infty t^2 E(t)dt \tag{4}$$

Statistical Analyses

Statistical analyses were performed using the General Linear Model Program (SAS 1988) to test the effect of particle concentration and mutator speed (SSHE study only) on liquid RTD means and variances as calculated by Eq. 2 and 4 for a holding tube and horizontal SSHE. Main effects and two-way interaction were analyzed in SSHE experiments. Duncan's multiple range test was used to estimate significant difference among means at the 5% probability level (Duncan 1955).

RESULTS AND DISCUSSION

Holding Tube

Table 1 presents experimental liquid mean residence times (LMRTs) and variances along with predicted velocity ratios (VRs) as influenced by particle concentration in a holding tube. Even though statistical analysis indicated that LMRTs in the holding tube were not influenced by particle concentration up to 30%, a definite trend of decreasing LMRT with increasing particle concentration was observed (Fig. 2). This trend was explained by examining the shape of the E(t) curves. As particle concentration increased, the right-sided skew of the E(t) curve decreased (Fig. 3) thus causing the mean residence time ($\bar{t}$), as calculated from the E(t) curve, to decrease. However, the theoretical LMRT calculated from volumetric flow rate ($\bar{t}_T$ = 13.75 s) was 14.1–22.2% lower than the experimental LMRTs. Some of this variation may have been due to the tailing, or right-sided skew, observed in these experiments. Results obtained here are in agreement with Sancho and Rao (1992) who noted 8.8–17.3% difference for water flow in a holding tube. They also indicated that the former values were lower than the latter values in all cases. Hong *et al.* (1991) observed similar results that the experimental mean residence time was 0.975 times the theoretical mean residence time (standard deviation of ±4.16%) for a fluid in turbulent holding tube flow (Re = 13800). Himmelblau and Bischoff (1968) indicated that a 20% difference between the values was not too bad considering the approximations involved in the analysis as well as the experimental error such as determination of volumetric flow rate.

Variance was significantly affected by the particle concentration. The variance without particle loading was significantly higher than that with particles (Table 1). Low variance with 10–30% particle loading indicated that particle-particle interactions may reduce back-mixing so that the liquid portion of the product comes out more uniformly. The characteristic parameter (r) for tanks-in-series model, which can be used to describe nonideal flow, ranged between 32 and 65. As r increases, the skewness of the density function becomes less pronounced. For r large enough ($r \geq 50$), the function becomes close to a normal distribution with the product of mean and variance approximately equal to r (Olkin *et al.* 1980).

Figure 3 presents E(t) curves as influenced by particle concentration in a holding tube. Each curve drawn in Fig. 3 was an individual replication (no averaging) and was selected with respect to its similarity to the average variance listed for each particle concentration in Table 1. The distribution curves were sharper at higher particle concentrations and seemed to approach a normal distribution from a gamma distribution as particle concentration increased. Hong *et al.* (1991), however, reported that their distribution curves fitted a normal distribution.

TABLE 1.
LIQUID MEAN RESIDENCE TIMES, VARIANCES, AND PREDICTED VELOCITY RATIOS AS INFLUENCED BY PARTICLE CONCENTRATION IN A HOLDING TUBE

Particle Concentration (%)	LMRT (s)	Experimental Variance (s^2)	r[1] (-)	Predicted[2] $\frac{U_{pm}}{U_{fm}}$ (-)	Predicted[2] $\frac{U_{pf}}{U_{fm}}$ (-)
0	17.68[a]	9.74[a]	32	1.057	1.069
10	16.55[a]	7.19[b]	38	1.073	1.089
20	16.10[a]	3.98[c]	65	1.079	1.098
30	16.01[a]	5.19[bc]	49	1.081	1.100

[1] Characteristic parameter for tanks-in-series model, defined as $r = \bar{t}^2/\sigma^2$, where $\bar{t}$ and σ^2 are mean residence time and variance, respectively.

[2] Based on prediction equations from Yang and Swartzel (1992):

$$\frac{U_{pm}}{U_{fm}} = 0.933 Fr_p^{0.11}; \quad \frac{U_{pf}}{U_{fm}} = 0.912 Fr_p^{0.14}$$

[a-c] Means in the same column with the same superscript are not significantly different ($P < 0.05$).

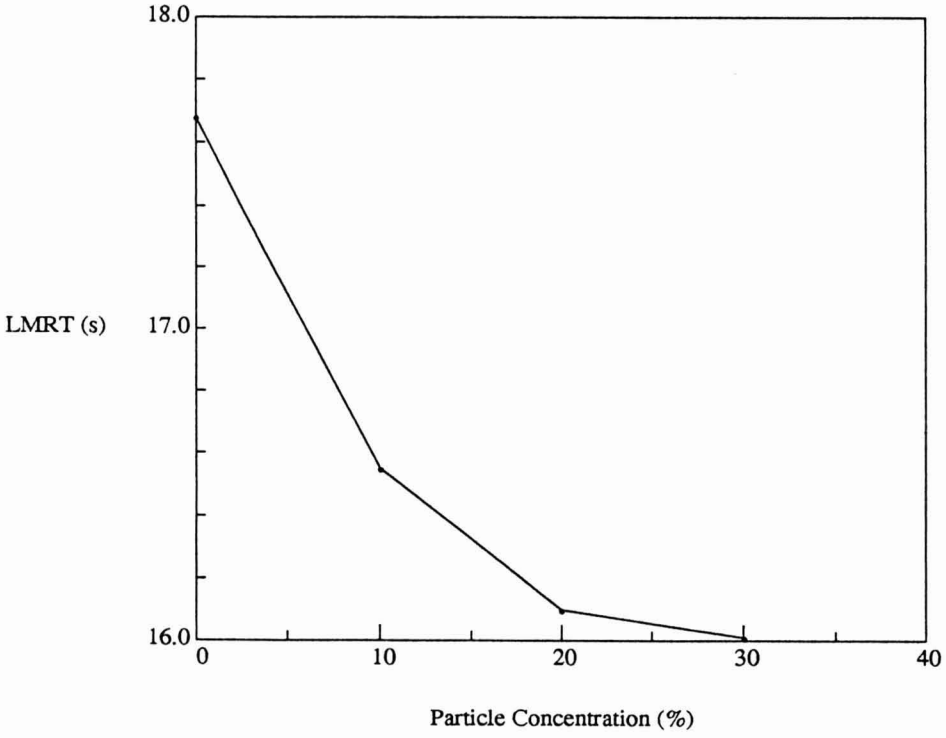

FIG 2. LIQUID MEAN RESIDENCE TIMES AS INFLUENCED BY PARTICLE CONCENTRATION IN A HOLDING TUBE (SYMBOL: • LMRT)

The velocity ratios (VRs) were estimated using the revised prediction equations from Yang and Swartzel (1992), which allowed determination of the U_{pm} and U_{pf} with known Fr_p and U_{fm} values with 95% confidence. These relationships were developed in the turbulent flow regions (Re = 11400–17600) in a straight round conduit (0.0508 m I.D.) under isothermal conditions (temperature range 16–22C). The carrier fluid was tap water and test particles were polystyrene spheres 19.1 mm diameter. These conditions were similar to those used in this study and, therefore, applicable with the assumption that no particle interaction influenced the mean particle residence time. This is supported by the findings that mean particle residence times were not affected by the particle concentration up to 10 and 20% for horizontal and vertical SSHEs, respectively where particle-particle interactions were more expected than in a holding tube due to the mutator mixing (Lee 1991).

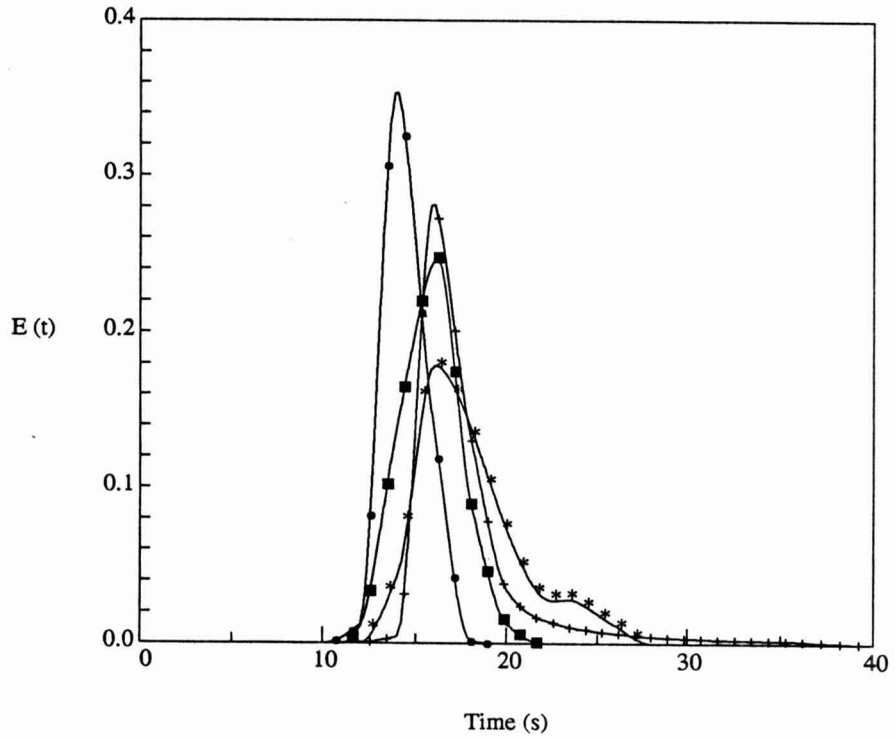

FIG. 3. E(t) CURVES AS INFLUENCED BY PARTICLE CONCENTRATION IN A HOLDING TUBE (SYMBOLS: + 0%; * 10%; • 20%; ■ 30%)

As shown by Table 1 mean particle velocities were predicted to be 1.057–1.081 times the mean fluid velocity and increased slightly as the particle concentration increased up to 30% in a holding tube. Velocities of the fastest moving particles were 1.069–1.100 times the mean fluid velocity and also increased as the particle concentration increased. In other words, the residence time ratios (τ) were greater than 0.909 and in such case, selection of the worst scenario of laminar flow ($\tau = 0.5$) for an adequate thermal process calculation in this turbulent flow region would result in overprocessing the fastest moving particles. For a known mean fluid residence time and hold tube length (calculated based on $\tau = 0.5$), particles with $\tau = 0.909$ would spend almost twice as long in the hold tube as necessary. This extra heat treatment delivered to the product will cause overall quality losses in terms of nutrient, color, texture, and other quality parameters.

SSHE

Table 2 presents LMRTs and variances as influenced by mutator speed and particle concentration in a horizontal SSHE. LMRTs were not significantly affected by mutator speed but were significantly influenced by particle concentration. An increase in mutator speed significantly increased the variance regardless of the particle concentration, resulting in broader distributions (Fig. 4). These results are consistent with findings of Chen and Zahradnik (1967) and Milton and Zahradnik (1973).

TABLE 2.
LIQUID MEAN RESIDENCE TIMES AND VARIANCES AS INFLUENCED BY MUTATOR SPEED AND PARTICLE CONCENTRATION IN A HORIZONTAL SSHE

Parameter	LMRT (s)	Variance (s^2)
Mutator speed (rpm)		
60	30.60[a]	68.84[a]
110	31.62[a]	97.86[b]
Particle concentration (%)		
0	33.44[a]	93.42[a]
10	30.35[bc]	77.96[a]
20	28.92[c]	75.93[a]
30	31.73[ab]	86.10[a]

[a-c] Means in the same column within parameter with the same superscript are not significantly different ($P < 0.05$).

Particle loading significantly reduced the LMRT of 20% particle concentration regardless of mutator speed. However, increasing particle concentration from 0 to 30%, 10 to 20%, and 10 to 30% did not significantly affect the LMRTs. As observed in the holding tube experiment, the theoretical LMRT ($\bar{t}_T = 20.93$ s) was considerably lower than experimentally determined values. Apparent back-mixing may have taken place as previously observed for particle flow in a horizontal SSHE (Lee and Singh 1991a). In addition, RTD of tracer material due to an imperfect pulse input as well as experimental error in determination of SSHE volume may have contributed to this difference. However, lower

theoretical LMRT was consistent with the findings for the holding tube experiment and was not unexpected. Unlike results obtained for the holding tube, variance in the SSHE was not significantly influenced by the particle concentration (Fig. 5). This was probably due to mixing induced by mutator rotation, which may have overshadowed the effect of particle concentration.

LMRTs and variances as influenced by two-way interaction between mutator speed and particle concentration in a horizontal SSHE are presented in Table 3. LMRT was significantly higher at 0% particles and a mutator speed of 110 rpm than under any other conditions. This was probably because flow restriction, induced by high tangential force, acted on the product at high mutator speeds. However, the average volume element of liquid stayed for a significantly shorter period when the SSHE was operated at 110 rpm with 20% particle concentration. LMRTs under other conditions were not significantly different.

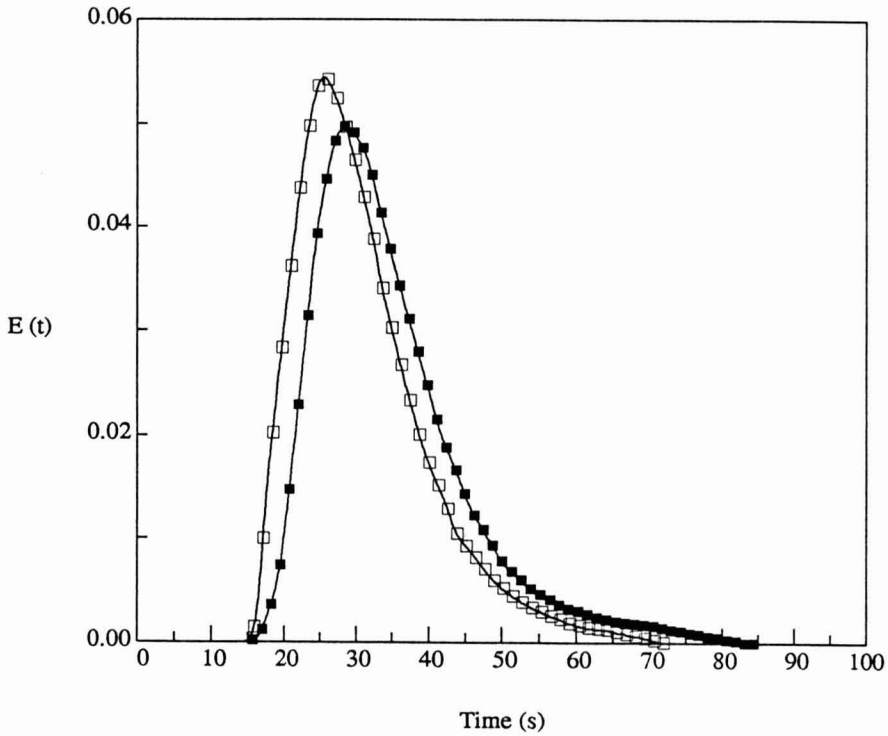

FIG. 4. E(t) CURVES AS INFLUENCED BY MUTATOR SPEED IN A HORIZONTAL SSHE (SYMBOLS: □ 60 rpm; ■ 110 rpm)

Effect of two-way interaction on variance can be distinctively divided into 2 groups depending on mutator speed. Variance was significantly higher when a mutator speed of 110 rpm was used regardless of the particle concentration with one exception; 60 rpm without particle loading. This indicated that back-mixing might be more significant without particle loading at the lower mutator speed. At 60 rpm, liquid RTDs became more uniform as particle concentration decreased. The effect of mutator speed on liquid RTDs in a horizontal SSHE was greater than the particle concentration. The number of tanks-in-series model varied from 8 to 17 depending on the mutator speeds and particle concentrations. For those relatively small r values, the skewness of the distribution function becomes more pronounced as it can be seen in Fig. 4 and 5.

Caution must be exercised in direct application of the results presented here to practical processing conditions; nevertheless, they provide fundamental insights into liquid RTDs as influenced by particle concentrations in a holding tube as well as SSHE. This variable with non-Newtonian fluid as a carrier at ultra high temperature processing conditions merits further study.

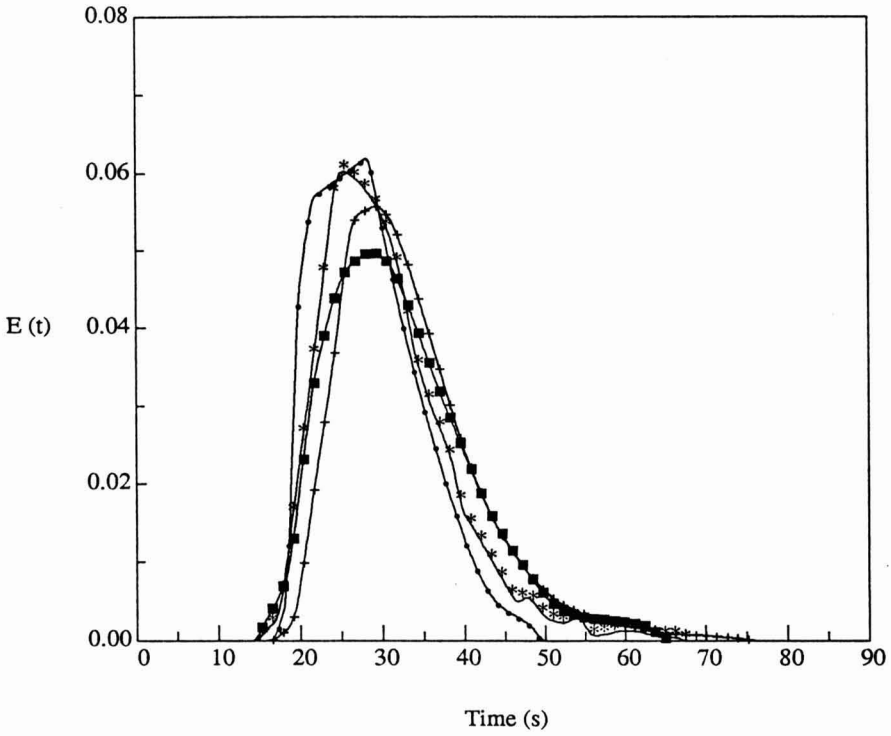

FIG. 5. E(T) CURVES AS INFLUENCED BY PARTICLE CONCENTRATION IN A HORIZONTAL SSHE (SYMBOLS: +0%; * 10%; • 20%; ■ 30%)

TABLE 3.
LIQUID MEAN RESIDENCE TIMES AND VARIANCES AS INFLUENCED BY TWO-WAY INTERACTION BETWEEN MUTATOR SPEED AND PARTICLE CONCENTRATION IN A HORIZONTAL SSHE

Two-Way Interaction		LMRT (s)	Variance (s^2)	r[1] (-)
Mutator speed (rpm)	Particle concentration (%)			
60	0	30.79[b]	103.50[a]	9
60	10	29.52[bc]	52.44[b]	17
60	20	31.00[b]	57.63[b]	17
60	30	31.08[b]	61.80[b]	16
110	0	36.09[a]	83.34[ab]	16
110	10	31.19[b]	103.48[a]	9
110	20	26.83[c]	94.24[a]	8
110	30	32.38[b]	110.39[a]	9

[1] Characteristic parameter for tanks-in-series model, defined as $r = \bar{t}^2/\sigma^2$, where t and σ^2 are mean residence time and variance, respectively.

[a-c] Means with the same superscript within a column are not significantly different ($P<0.05$).

CONCLUSIONS

Liquid mean residence times were not significantly influenced by particle concentration up to 30% in a holding tube. Variance, on the other hand, was significantly higher without particle loading, resulting in a broader distribution. A 20% particle loading significantly reduced the LMRTs regardless of the mutator speed. In addition, an increase in the mutator speed significantly increased variance regardless of particle concentration. In contrast to the holding tube results, SSHE variances were not significantly influenced by particle concentration. The theoretical LMRTs were lower than the experimentally determined LMRTs for both holding tube and SSHE. Thermal process calculations based on theoretical residence time will be conservative, however, will result in a considerable overprocessing of the liquid portion of the product.

ACKNOWLEDGMENT

This research was funded by the NRI Program of the United States Department of Agriculture.

NOMENCLATURE

D = Diameter of pipe (m)
d_p = Diameter or length of particle (m)
$E(t)$ = Normalized residence time distribution function
Fr_p = Particle Froude number, defined as $Fr_p = \frac{U^{2}_{fm}}{gd_p(\rho_p/\rho_f - 1)}$ (dimensionless)
g = Acceleration due to gravity (m/s^2)
Q = Volumetric flow rate (ml/s)
Re = Reynolds number, defined as $\frac{\rho_f D U_f}{\mu}$ (dimensionless)
t = Time (s)
t_i = Specified time (s)
t_p = Particle residence time (s)
$\bar{t}$ = Mean residence time (s)
$\bar{t}_T$ = Theoretical mean residence time (s)
U_f = Velocity of fluid (m/s)
U_{fm} = Mean velocity of fluid (m/s)
U_p = Velocity of particle (m/s)
U_{pf} = Velocity of fastest particle (m/s)
U_{pm} = Mean velocity of particle (m/s)
V = Volume (ml)
μ = Viscosity (N/m s)
ρ_f = Density of fluid (kg/m^3)
ρ_p = Density of particle (kg/m^3)
σ^2 = Variance of residence time (s^2)

τ = Residence time ratio, defined as $\tau = \frac{t_p}{\bar{t}}$, dimensionless

REFERENCES

ALCAIRO, E.R. and ZURITZ, C.A. 1990. Residence time distributions of spherical particles suspended in non-Newtonian flow in a scraped-surface heat exchanger. Trans. ASAE *33*: 1621.

BERRY, M.R. 1989. Predicting fastest particle residence time. In *Proceedings of the First International Congress on Aseptic Processing Technologies*, (J.V. Chambers, ed.), p. 6, Indianapolis, IN.

BOSWORTH, R.C.L. 1948. Distribution of reaction times for laminar flow in cylindrical reactors. Phil. Mag. *39*, 847.

BOSWORTH, R.C.L. 1949. Distribution of reaction times for turbulent flow in cylindrical reactors. Phil. Mag. *40*, 314.

CHEN, A.C.Y. and ZAHRADNIK, J.W. 1967. Residence time distribution in a swept surface heat exchanger. Trans. ASAE *10*, 508.

CUEVAS, R., CHERYAN, M., and PORTER, V.L. 1982. Performance of a scraped-surface heat exchanger under ultra high temperature conditions: A dimensional analysis. J. Food Sci. *47*, 619.

DICKERSON, R.W. JR., SCALZO, A.M., READ, R.B. JR. and PARKER, R.W. 1968. Residence time of milk products in holding tubes of high-temperature short-time pasteurizers. J. Dairy Sci. *51*, 1731.

DUNCAN,D.B. 1955. Multiple range and multiple F tests. Biometrics *11*, 1.

DUTTA, B. and SASTRY, S.K. 1990a. Velocity distributions of food particle suspensions in holding tube: Experimental and modeling studies on average particle velocities. J. Food Sci. *55*, 1448.

DUTTA, B. and SASTRY, S.K. 1990b. Velocity distributions of food particle suspensions in holding tube: Distribution characteristics and fastest-particle velocities. J. Food Sci. *55*, 1703.

HEPPELL, N.J. 1985. Comparison of the residence time distributions of water and milk in an experimental UHT sterilizer. J. Food Eng. *4*, 71.

HIMMELBLAU, D.M. and BISCHOFF, K.B. 1968. *Process Analysis and Simulation*, John Wiley & Sons, New York.

HONG, C.W., SUN PAN, B., TOLEDO, R.T., and CHIOU, K.M. 1991. Measurement of residence time distribution of fluid and particles in turbulent flow. J. Food Sci. *56*, 255.

LEE, J.H. 1991. Modeling and experimental studies on aseptic processing of particulate foods. Ph.D. thesis, Purdue University, West Lafayette, IN.

LEE, J.H. and SINGH, R.K. 1991a. Particle residence time distributions in a model horizontal scraped surface heat exchanger. J. Food Proc. Eng. *14*, 125.

LEE, J.H. and SINGH, R.K. 1991b. Process parameter effects on particle residence time in a vertical scraped surface heat exchanger. J. Food Sci. *56*, 869.

LEE, J.H. and SINGH, R.K. 1991c. Scraped surface heat exchanger orientation influence on particle residence time distributions. J. Food Sci. *56*, 1446.

LEE, J.H. and SINGH, R.K. 1993. Residence time distribution characteristics of particle flow in a vertical scraped surface heat exchanger. J. Food Eng. *18*, 413.

MCCOY, S.C., ZURITZ, C.A. and SASTRY, S.K. 1987. Residence time distribution of simulated food particles in a holding tube. ASAE Paper No. 87-6536, American Society of Agricultural Engineers, St. Joseph, MI.

MILTON, J.L. and ZAHRADNIK, J.W. 1973. Residence time distribution of a Votator pilot plant using a non-Newtonian fluid. Trans. of the ASAE *16*, 1186.

NFPA. 1990. Information Letter. No.3232, National Food Processors Assoc. Washington, DC.

NESARATNAM, R. and GAZE, J.E. 1987. Application of a particle technique to the study of particle sterilization under dynamic flow. Tech. Memo. No. 461, Campden Food Preservation Research Assoc., Chipping Campden, UK.

OLKIN, I., GLESER, L.J. and DERMAN, C. 1980. *Probability Models and Applications*, Macmillan Publishing Co., New York.

PALMER, J.A. and JONES, V.A. 1976. A research note prediction of holding times for continuous thermal processing of power loss fluids. J. Food Sci. *41*, 1233.

SANCHO, M.F. and RAO, M.A. 1992. Residence time distribution in a holding tube. J. Food Eng. *15*, 1.

SAS. 1988. SAS/STAT™ User's Guide, Release 6.03, SAS Institute, Cary, NC.

SCALZO, A.M., DICKERSON, R.W. JR., READ, R.B. JR. and PARKER, R.W. 1969. Residence times of egg products in holding tubes of egg pasteurizers. Food Technol. *23*(5), 80.

TAEYMANS, D., ROELANS, E. and LENGES, J. 1985. Influence of residence time distribution on the sterilization effect in a scraped surface heat exchanger used for processing liquids containing solid particles. In *Proceedings of IUFoST Symp. on Aseptic Processing and Packaging of Foods*, Sept. 9–12, Tylosand, Sweden, pp. 100–107.

TAEYMANS, D., ROELANS, E. and LENGES, J. 1986. Residence time distribution in a horizontal SSHE used for UHT processing of liquids containing solids. In *Food Engineering and Process Applications, Vol. l. Transport Phenomena*, (M. Le Maguer and P. Jelen, eds.) pp. 247–258, Elsevier Applied Science Publications, London.

TROMMELEN, A.M. and BEEK, W.J. 1971. Flow phenomena in a scraped-surface heat exchanger ("Votator" type). Chem. Eng. Sci. *26*, 1933.

YANG, B.B. and SWARTZEL, K.R. 1991. Photo-sensor methodology for determining residence time distributions of particles in continuous flow thermal processing systems. J. Food Sci. *56*, 1076.

YANG, B.B. and SWARTZEL, K.R. 1992. Particle residence time distributions in two-phase flow in straight round conduit. J. Food Sci. *57*, 497.

MATHEMATICAL MODELING OF SOLID-LIQUID TWO PHASE TUBE FLOW: AN APPLICATION TO ASEPTIC PROCESSING

YANSHENG LIU and CARLOS A. ZURITZ[1]

Department of Agricultural and Biological Engineering
The Pennsylvania State University
University Park, PA 16801

Accepted for Publication July 27, 1994

ABSTRACT

The sizing of holding tubes for continuous sterilization of foods containing large particles is affected by the flow behavior of the suspensions. Velocities of carrier fluid and model food particles in holding tube flow were numerically simulated through an iterative solution of the Navier-Stokes equations and particle dynamic equations in three dimensions. The Lagrangian approach was used to predict the individual particle trajectories under multiparticle tube flow. The physical domain included two straight tubes connected with a 180° bend. The system had an upward inclination of 1.194° (0.25 in./ft of straight run). The assumptions considered included Newtonian carrier, spherical and neutrally buoyant particles, and 10% v/v particle loading. The results indicate that the particles have a significant back-influence on the fluid flow field. The 180° bend strongly affected both fluid and particle flow fields, which further reinforced the interaction of the two phases. The fastest particle velocities were less than the fluid streamline velocities passing through the particles' center. The radial positions of the particles on the cross section of the holding tube changed very little in the first straight section, but experienced a significant shifting in the bend and second straight-tube sections due to secondary flow. The residence times of particles under secondary-flow effect are therefore different from those obtained under straight tube-only flow.

INTRODUCTION

Food and Drug Administration (FDA) approval for aseptic processing of low-acid foods containing large particles has been hampered by the lack of basic information regarding the flow behavior of food particles (Sastry *et al.* 1989). This information is needed for estimating residence time distributions (RTDs)

[1]Author to whom correspondence should be addressed.

Journal of Food Process Engineering **18** (1995) 135–163.

of particles and heat transfer coefficients (h_f) at the solid-liquid interfaces. Both RTDs and h_f are the parameters most difficult to predict in aseptic processing of particulate foods. RTDs are critical in sizing holding tubes. The fastest moving particles must achieve the desired thermal treatment to assure commercial sterility. Furthermore, the h_f depends on the relative velocity between the solid particle and the carrier liquid. Therefore, detailed and realistic flow behaviors of solid-liquid mixtures are necessary in designing aseptic processing systems. Simultaneous solutions of the continuity and momentum equations for the fluid and the dynamic equations for the particles may provide insights useful for designing aseptic systems.

The velocity distributions of fluid and particles in two-phase flow have been studied numerically and experimentally by several researchers. Due to the complex nature of particulate two-phase flow, most of the published research on the subject has been performed using experimental techniques (Toda and Ishikawa 1973; Auton 1973; Ohashi *et al.* 1980; Dutta and Sastry 1990a,b). Experimental methods, however, usually provide "end effect" results instead of a continuous accounting of the whole flow process. Therefore, experimental techniques in general present limitations in providing detailed data on flow fields. A thorough review of the pertinent two-phase flow literature was presented by Sastry and Zuritz (1987). The literature in two-phase flow field modeling and simulation applicable to aseptic processing of particulate foods is limited; only a few publications (Kaimal and Devanathan 1980; Durst *et al.* 1984; Berlemont *et al.* 1990; Lu *et al.* 1993) are available. However, most deal with two-phase turbulent flow.

Durst *et al.* (1984) used both the Eulerian and the Lagrangian methods to simulate the flow of solid-liquid mixtures in tubes. In the Eulerian approach, both solid and liquid phases are considered as a continuum. The equations of motion are written for each phase at every point in the computational domain. The two sets of equations are coupled through the volume fractions and the interfacial forces or momentum transfer relations. The Eulerian approach seems to have advantages in the cases where high particle concentrations occur and where the high void fraction of the fluid becomes a dominant flow controlling parameter. But it is limited in the sense that it cannot predict individual particle trajectories.

In the Lagrangian approach, only the fluid phase is considered as a continuum, with the particles dispersed throughout the fluid phase. The fluid acts as the carrier of the particles. This kind of flow is usually called dispersed two-phase flow or particulate two-phase flow. The conservation equations for the carrier phase are described by the standard equations of motion, while the Lagrangian frame of reference is applied in describing the motion of the particles moving through the carrier phase. The Lagrangian approach is better suited for predicting those particulate flows in which large particle accelerations

occur, and in providing information on individual particle trajectory. The system of equations for the two phases are coupled through source-like terms or interface drag forces including slip velocity between the phases.

The simulations performed by Durst *et al.* (1984) were for two-dimensional axisymmetric flows, while in the present situation we treat fully three-dimensional flows due to the existence of curvatures in the holding tube. The models by Durst *et al.* (1984) cannot be applied directly to aseptic processing because of their simplified flow situations. Also, the particle dimensions in their models are small in relation to the internal diameter of the pipe. In aseptic processing, particle sizes can be of the same order of magnitude than the internal diameter of the holding tube (up to 3-cm in a 5-cm diameter tube). The relative bigger particle size is the main characteristic in the modeling of aseptic processing of particulate two-phase flow. Non-Newtonian flow behavior of the carrier liquid, particle-particle interactions and particle-wall interactions further complicate the problem.

Previous works on flow behavior of two-phase flow pertaining to aseptic processing (Sastry and Zuritz 1987; Sastry *et al.* 1989; Dutta and Sastry 1990a,b) have predicted velocity profiles of particles in non-Newtonian tube flow through the use of simplified one-dimensional models. These models neither considered the back-influence of particles, nor the effect of 180° bends on the fluid flow field. These two factors are obviously very important for accurate numerical simulation of two-phase holding tube flow situations. Further study is therefore necessary to gain an improved understanding of the flow behavior of particles under these conditions.

Particulate two-phase flow in aseptic processing still poses a challenge to numerical simulation. The present study is a preliminary investigation on flow behavior of suspended model food particles in viscous flow through a "typical" holding tube. It is intended to provide a better understanding of the underlying phenomena involved in this complex two-phase flow system. The emphasis is to explore the back influence of particles and 180° bends on the fluid flow field.

MATHEMATICAL MODEL

The Lagrangian model was employed to simulate the particulate two-phase flow. The assumptions of the model were: (1) laminar flow; (2) Newtonian carrier fluid; (3) negligible particle-particle interactions and (4) constant physical properties.

The momentum transfer between the phases was carried along particle trajectories. The momentum transfer yielded additional terms that were included in the momentum equations of the fluid phase as a source term, and were dependent on the velocity difference between the two phases.

The physical domain studied included two, 3-m long each, straight tubes connected with a 180° bend. The internal diameters of the tubes and the bend were 5.08 cm corresponding to a commercial size holding tube OD. The curvature diameter of the 180° bend was 18.0 cm (centerline measurement). The whole system has an upward inclination of 1.194° (corresponding to the FDA requirement of 0.25 in./ft). The x-direction is taken as the axial direction, and the y- and z-axis are the vertical and horizontal directions, respectively, on the tube cross section. The corresponding velocities are u, v, w in the x, y, z directions, respectively.

There are 351 grid points along the tube axial direction, and 21 grid points on the horizontal (z-axis) and vertical (y-axis) directions, respectively, on the tube cross section. The grid points on the holding tube are illustrated in Fig. 1.

The model food particles are considered to have uniform spherical shape with diameter of 1 cm. Neutrally buoyant condition (particles with same density as the liquid phase) was assumed in the current simulation, although the model can handle nonneutrally buoyant conditions. The viscosity and average velocity of the liquid carrier investigated were 0.1 Pa · s (1 poise) and 30 cm/s, respectively, and the particle loading was 10% v/v. Under these conditions, the Reynolds number is about 150. The outlet pressure of the holding tube was assumed to be 10 Pa (100 dyne · cm^{-2}).

Equations of Motion of Fluid Phase

Since a 180° bend was included in the physical domain, the three dimensional Navier-Stokes equations of the fluid phase (including the source term S, which represents the back influence of particles on the fluid flow field) must be solved. The corresponding governing equations in vector form are given by:

$$\Gamma\frac{\partial Q}{\partial \gamma} + \frac{\partial E}{\partial \xi} + \frac{\partial F}{\partial \eta} + \frac{\partial G}{\partial \zeta} = \frac{\partial E_v}{\partial \xi} + \frac{\partial F_v}{\partial \eta} + \frac{\partial G_v}{\partial \zeta} + S \qquad (1)$$

where (ξ, η, ζ) represent a general nonorthogonal coordinate system. Γ is the preconditioning matrix. Here, an artificial temporal term is added to the continuity equation with a user-specified control parameter β. The incompressible system of equations is thus hyperbolic in time, so that a time marching technique can be used to solve the problem. When steady state is reached, the time derivatives vanish and the original continuity equation ($\nabla \cdot V = 0$) is recovered. The various matrices and vectors are given by:

$$\Gamma=\begin{bmatrix}\frac{1}{\beta} & 0 & 0 & 0\\ 0 & 1 & 0 & 0\\ 0 & 0 & 1 & 0\\ 0 & 0 & 0 & 1\end{bmatrix},\quad Q=\begin{bmatrix}\rho & P\\ \rho & u\\ \rho & v\\ \rho & w\end{bmatrix},\quad S=\begin{bmatrix}0\\ S_x\\ S_y\\ S_z\end{bmatrix} \tag{2}$$

$$E=\begin{bmatrix}\rho U\\ \rho Uu+\xi_x P\\ \rho Uv+\xi_y P\\ \rho Uw+\xi_z P\end{bmatrix},\quad F=\begin{bmatrix}\rho V\\ \rho Vu+\eta_x P\\ \rho Vv+\eta_y P\\ \rho Vw+\eta_z P\end{bmatrix},\quad G=\begin{bmatrix}\rho W\\ \rho Wu+\zeta_x P\\ \rho Wv+\zeta_y P\\ \rho Ww+\zeta_z P\end{bmatrix} \tag{3}$$

$$E_v=M\left[\frac{1}{J}(\xi_x^2+\xi_y^2+\xi_z^2)\frac{\partial Q}{\partial \xi}+\frac{1}{J}(\xi_x\eta_x+\xi_y\eta_y+\xi_z\eta_z)\frac{\partial Q}{\partial \eta}+\frac{1}{J}(\xi_x\zeta_x+\xi_y\zeta_y+\xi_z\zeta_z)\frac{\partial Q}{\partial \zeta}\right] \tag{4}$$

$$F_v=M\left[\frac{1}{J}(\xi_x\eta_x+\xi_y\eta_y+\xi_z\eta_z)\frac{\partial Q}{\partial \xi}+\frac{1}{J}(\eta_x^2+\eta_y^2+\eta_z^2)\frac{\partial Q}{\partial \eta}+\frac{1}{J}(\eta_x\zeta_x+\eta_y\zeta_y+\eta_z\zeta_z)\frac{\partial Q}{\partial \zeta}\right] \tag{5}$$

$$G_v=M\left[\frac{1}{J}(\xi_x\zeta_x+\xi_y\zeta_w+\xi_z\zeta_z)\frac{\partial Q}{\partial \xi}+\frac{1}{J}(\eta_x\zeta_x+\eta_y\zeta_y+\eta_z\zeta_z)\frac{\partial Q}{\partial \eta}+\frac{1}{J}(\zeta_x^2+\zeta_y^2+\zeta_z^2)\frac{\partial Q}{\partial \zeta}\right] \tag{6}$$

$$M=\begin{bmatrix}0 & 0 & 0 & 0\\ 0 & \mu & 0 & 0\\ 0 & 0 & \mu & 0\\ 0 & 0 & 0 & \mu\end{bmatrix},\quad J=\frac{\partial(\xi,\eta,\zeta)}{\partial(x,y,z)}=\begin{bmatrix}\xi_x\xi_y\xi_z\\ \eta_x\eta_y\eta_z\\ \zeta_x\zeta_y\zeta_z\end{bmatrix} \tag{7}$$

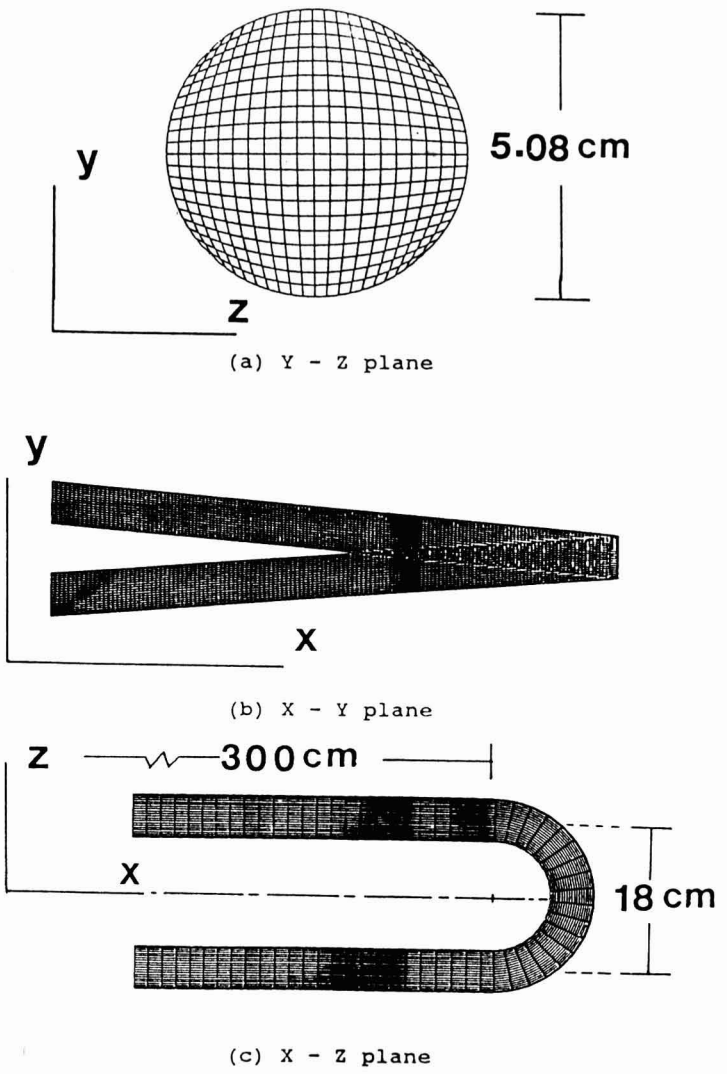

FIG. 1. DIMENSIONS, COORDINATES AND GRIDS OF THE HOLDING TUBE

where the variables u, v, w are the physical velocities, U, V, W the contravariant velocities, μ the viscosity of the fluid, and S_x, S_y, S_z the source terms. J is the Jacobian of the transformation and β the coefficient of artificial compressibility, which is widely used in solving incompressible flow to facilitate convergence (Merkle and Athavale 1987; Kwak *et al.* 1985; Yagley *et al.* 1992). The expression of β in Yagley *et al.* (1992) was used in the current model.

The initial and boundary conditions used in the numerical computation consisted of a specified fluid velocity profile (fully developed) at the inlet, with the corresponding pressure boundary condition determined from the initial velocity field, and a uniform pressure and relaxed velocity profile at the exit. On the tube wall, the traditional no-slip boundary condition was used for the fluid velocity, which was then used in the normal momentum equation to obtain the pressure at the wall.

Velocities and Trajectories of Particles

The particles suspended in a three-dimensional flow field could be expected to undergo translational and rotational motions in all three directions. Therefore, three linear and three angular momentum equations should be solved simultaneously to describe the motion of the particles. Since the Lagrangian frame of reference was used in the current model, the motion of each particle is governed by the individual particle dynamic equations (mass acceleration equations). The three linear dynamic equations are given by:

$$m\left(\frac{dV_{px}}{dt}\right)=\sum F_x \tag{8}$$

$$m\left(\frac{dV_{py}}{dt}\right)=\sum F_y \tag{9}$$

$$m\left(\frac{dV_{pz}}{dt}\right)=\sum F_z \tag{10}$$

where m is the mass of a single particle, V_{pk} and F_k (k = x,y,z) are particle velocities and forces acting on the particle in the x, y, z directions, respectively.

The rotational motions of the particles are caused by the imbalanced viscous shear forces acting on their surface, which result in local torques. The three angular dynamic equations can be written as:

$$I\left(\frac{d\Omega_x}{dt}\right)=\sum T_x \tag{11}$$

$$I\left(\frac{d\Omega_y}{dt}=\sum T_y\right) \tag{12}$$

$$I\left(\frac{d\Omega_z}{dt}\right)=\sum T_z \tag{13}$$

where I is the moment of inertia, which for a sphere has the value of (2/5)*m*a^2. T_k (for k = x, y, z) is the local torque.

The particles suspended in viscous fluid are also subjected to the following drag and lift forces (Sastry and Zuritz 1987).

(1) Saffman Lift Force (Saffman 1965, 1968)

$$F_s=6.46\rho_f a^2\left[\frac{\nu}{|K|}\right]^{1/2} K\times(V_p-V_f) \tag{14}$$

where K is the curl of fluid velocity, ν the kinematic viscosity, a is the radius of the particle, and V_p and V_f are the velocities of particle and fluid, respectively.

(2) Magnus Lift Force (Rubinow and Keller 1961)

$$F_{rk} = \pi\rho_f a^3\Omega \times (V_p - V_f) \tag{15}$$

where Ω is the angular velocity of the particle.

(3) Drag Force

$$F_d=\frac{1}{2}C_d\rho_f\pi a^2|V_f-V_p|(V_f-V_p) \tag{16}$$

where the drag coefficient (C_d) is satisfactorily described by Cliff and Gauvin (1971):

$$C_d = \frac{24}{Re_p}(1 + 0.15Re_p^{0.687});\ (1<Re_p<1000) \tag{17}$$

where

$$Re_p=\frac{\rho 2a|V_f-V_p|}{\mu} \tag{18}$$

(4) Buoyancy Force (acting only in the y-direction)

$$F_b=\left(\frac{4}{3}\right)\pi a^3(\rho_f-\rho_p)g \tag{19}$$

where g is the gravitational constant.

In this simulation, if a particle reaches the wall of the holding tube, no motion in the normal direction towards the wall is permitted, but motion in tangential and axial directions are allowed without restraint.

After substitution of the above force expressions into the linear momentum equations (8, 9 and 10), the final linear momentum equations for particles in viscous flow are obtained as:

$$m\frac{dv_p}{dt}=6.46\rho_f a^2\left[\frac{\nu}{|K|}\right]^{1/2}Kx(V_p-V_f)+\pi a^3\rho_f\Omega x(V_p-V_f) +\frac{1}{2}C_D\rho_f\pi a^2|V_f-V_p|(V_f-V_p)+\frac{4}{3}\pi a^3(\rho_f-\rho_p)g \tag{20}$$

In scalar form, the linear momentum equations are given as:

In the x-direction:

$$m\frac{du_p}{dt}=6.46\rho_f a^2\left[\frac{\nu}{|K|}\right]^{1/2}\left[\left[\frac{\partial u}{\partial z}-\frac{\partial w}{\partial x}\right]\cdot(w_p-w_f) -\left[\frac{\partial v}{\partial x}-\frac{\partial u}{\partial y}\right]\cdot(v_p-v_f)\right]+\pi\rho_f a^3[\Omega_y(w_p-w_f) -\Omega_z(v_p-v_f)]+\frac{1}{2}C_d\rho_f\pi a^2|u_f-u_p|(u_f-u_p) \tag{21}$$

In the y-direction:

$$m\frac{dv_p}{dt}=6.46\rho_f a^2\left[\frac{\nu}{|K|}\right]^{1/2}\left[\left[\frac{\partial v}{\partial x}-\frac{\partial u}{\partial y}\right]\cdot(u_p-u_f) -\left[\frac{\partial w}{\partial y}-\frac{\partial v}{\partial z}\right]\cdot(W_p-W_f)\right]+\pi\rho_f a^3[\Omega_z(u_p-u_f) -\Omega_x(W_p-W_f)]+\frac{1}{2}C_d\rho_f\pi a^2|v_f-v_p|(v_f-v_p) +(\frac{4}{3})\pi a^3(\rho_f-\rho_p)g \tag{22}$$

In the z-direction:

$$m\frac{dw_p}{dt}=6.46\rho_f a^2\left[\frac{\nu}{|K|}\right]^{1/2}\left[\left[\frac{\partial w}{\partial y}-\frac{\partial v}{\partial z}\right]\cdot(v_p-v_f) -\left[\frac{\partial u}{\partial z}-\frac{\partial w}{\partial x}\right]\cdot(u_p-u_f)\right]+\pi\rho_f a^3[\Omega_x(v_p-v_f) -\Omega_y(u_p-u_f)]+\frac{1}{2}C_d\rho_f\pi a^2|w_f-w_p|(w_f-w_p) \tag{23}$$

The first, second and third terms on the right hand side of Eq. 21, 22 and 23 are Saffman lift, Magnus lift and drag force, respectively. The fourth term on the right hand side of Eq. 22 is the gravitational force resulting from density differences.

The rigorous expression for the torque experienced by suspended particles in viscous fluid can be written as:

$$T = \int_A r \times (\tau \cdot n) dA \tag{24}$$

where A is the surface area of the spherical particle.

After proper arrangement, the three angular dynamic equations of the particles could be written as:

$$\frac{d\Omega_x}{dt} = \frac{15\mu}{\rho_p a^2} \left[\frac{\pi}{8} \left(\frac{\partial v}{\partial z} + \frac{\partial w}{\partial y} \right) - \Omega_x \right] \tag{25}$$

$$\frac{d\Omega_y}{dt} = \frac{15\mu}{\rho_p a^2} \left[\frac{\pi}{8} \left(\frac{\partial u}{\partial z} + \frac{\partial w}{\partial x} \right) - \Omega_y \right] \tag{26}$$

$$\frac{d\Omega_z}{dt} = \frac{15\mu}{\rho_p a^2} \left[\frac{\pi}{8} \left(\frac{\partial u}{\partial y} + \frac{\partial v}{\partial x} \right) - \Omega_z \right] \tag{27}$$

These linear and angular dynamic equations were solved iteratively along with the four equations of motion for the fluid phase. A compact fourth-order Runge-Kutta method was used to solve the equations.

Simulation Procedure

The equations of motion of the fluid phase (Eq. 1) were solved first without considering the particles' influence. With the computed information on the fluid field, particle velocities and trajectories in this flow field were calculated by solving the six dynamic equations for the particles (Eq. 21–23, 25–27). In order to account for the interaction between the fluid and the particles, source terms were calculated from the computed velocities and trajectories of the particles. The fluid equations of motion were then solved again with these source terms in place. This iterative procedure was continued until convergence between the solution of the two phases was achieved. A procedure flow-sheet is presented in Fig. 2 indicating this iteration process.

RESULTS AND DISCUSSION

Flow Field of Liquid and Solid Phases

In order to clearly describe the flow characteristics of both fluid and particles, the whole physical domain was divided into three sections: the first straight tube, the bend and the second straight tube.

For the two straight tube sections, the cross section locations (distance from the bend) were expressed in terms of the normalized distance s/2a ("s" is the distance from or to the bend, and "a" is the radius of the tube). At both the entrance to, and exit from the bend, s was defined as zero. Negative values were assigned to the upstream locations and positive values to the downstream locations. For the bend section, the cross section locations were expressed in terms of angles. A schematic diagram of this division is shown in Fig. 3.

Velocities and trajectories of particles were calculated at each time step. Based on the assumption of no particle-particle interactions, each particle path will only depend on the fluid flow field and its initial radial position on the inlet cross section of the tube. Therefore, we only need to trace one set of particles with different initial radial positions. In this study, nine particles with different radial positions were considered to arrive simultaneously at the inlet cross section of the tube at every time step; each particle having a velocity (V_p) equal to the stream line velocity (V_f) of the fluid passing through the particle's center. Based on the size and number of particles occupying the whole flow field, a 10% v/v particle loading was obtained.

First Straight Tube. In the first straight tube, one-dimensional (axial-direction) flow is dominant. Fig. 4 shows that the axial velocity contours of the fluid phase are symmetric about the center of the tube and that the particles had a negligible influence on the fluid velocity contours due to the small momentum exchanges taking place in this section. The particles maintained their initial symmetric radial positions unchanged up to the bend entrance, at which point their positions start shifting due to the bend influence [Fig. 4(f)].

Bend Section. At the bend entrance, a secondary flow started to develop resulting in two symmetric vortices perpendicular to the primary (axial) flow. As shown in Fig. 5, this secondary motion carries the fluid from the inner to the outer wall along the horizontal cross section plane of symmetry and back to the inner side following the pipe wall contours. The secondary motion can be explained in terms of the response of a viscous-fluid element to an imbalance between the centrifugal acceleration and the cross section pressure gradient developed due to the curvature of the tube. At the bend entrance, the fluid experiences an increased resistance and is forced to change its flow direction. This causes a substantial momentum loss which results in a rapid increase in pressure towards the outside wall. It is the presence of this strong cross section pressure gradient that helps to set up the secondary flow.

The presence of the particles altered the velocity profiles of the carrier fluid due to the large momentum transfer between the two phases. The centrifugal forces changed the radial positions and velocities of the particles. These changes, in turn, greatly affected the flow field of the fluid phase as illustrated by the secondary flow vector plots in the bend section shown in Fig. 5. The flow

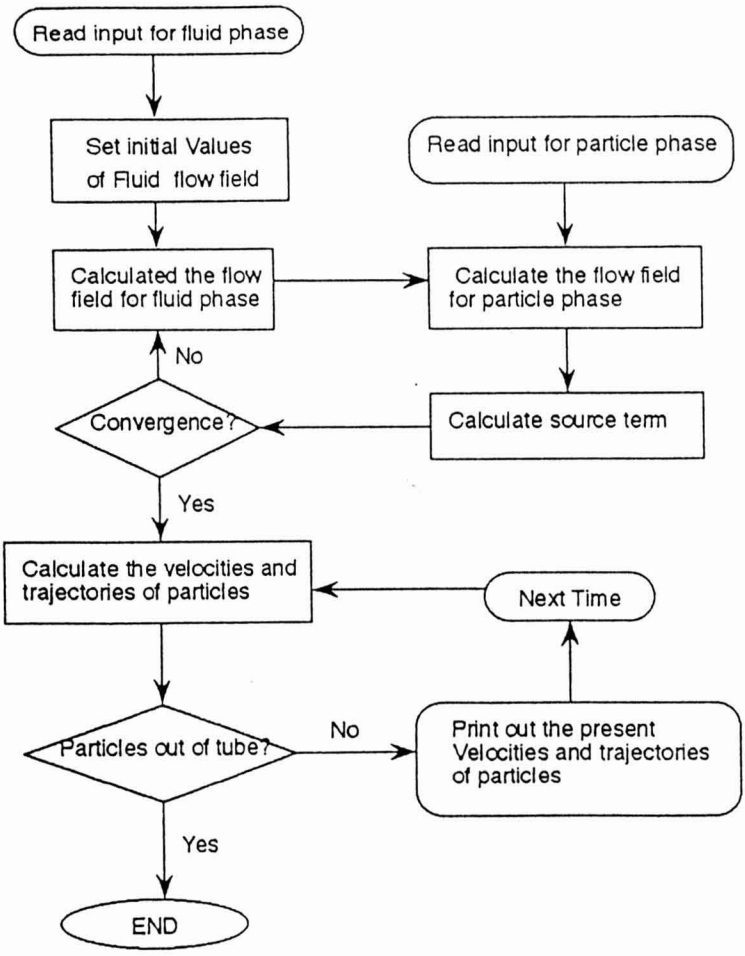

FIG. 2. ITERATION PROCEDURE IN THE SIMULATION

patterns shown in the figure are caused by the particles obstructing the fluid flow path (the fluid had to negotiate its way around the particles), and the mechanisms involved are quite complex. Due to the relative big particle size in the current situation, the inertia associated with these particles is also considerable. This inertia first exerted a retardation effect on the fluid flow, which resulted in the reduction in strength of the secondary flow near the bend inlet [Fig. 5 (a)–(b)]. Further down the bend, as the particles achieved enough acceleration, this retardation effect quickly disappeared. The accelerated particles, in turn, pushed the fluid around from the midsection to the bend exit as is shown in Fig. 5 (c)–(f). As a result, the particles extended the bend effect on the downstream fluid flow field.

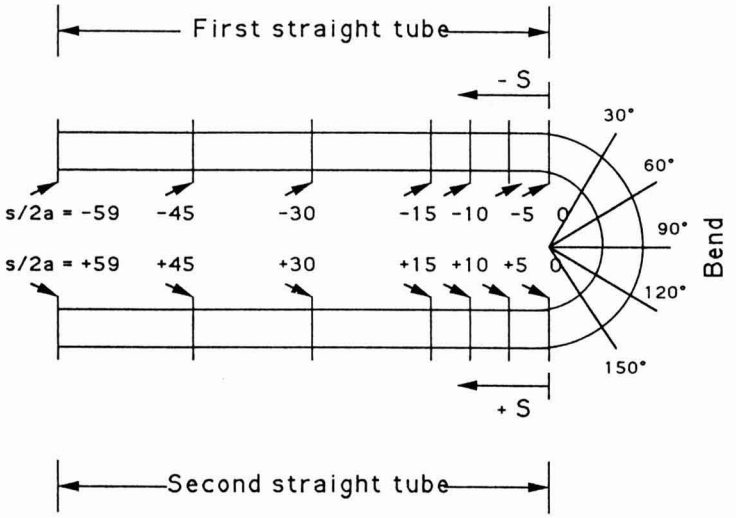

FIG. 3. SCHEMATIC DIAGRAM OF THE CROSS SECTION LOCATIONS ON THE HOLDING TUBE

The secondary flow shifted the maximum fluid axial velocity region towards the outer wall as can be seen in Fig. 6. The particles distorted even more these shifted velocity contours. A decrease of the radius of curvature of the bend would displace the fluid maximum velocity even closer to the outer wall (Fairbank and So 1987).

The secondary flow induced by centrifugal forces pushed the particles towards the outer wall [Fig. 7 (a)–(d)], and then back to the center region of the pipe as they approached the bend exit [Fig. 7 (e) and (f)]. Similar phenomena were observed by Toda and Ishikawa (1973) in their experimental studies on particulate two-phase flow. These phenomena will obviously affect the particle flow behavior and residence time, proving to be of considerable practical interest in holding tube flow.

An analysis of the equations describing laminar flow through curved tubes shows that two parameters characterize the flow: the radius ratio δ = a/R and the Reynolds number, Re; both expressed in terms of the Dean number, De = $\delta^{1/2}$Re (Berger *et al.* 1983). Where a is the radius of the tube and R is the mean radius of curvature. Since the Dean number can be considered as the ratio of the square root of the product of the inertia and centrifugal forces to the viscous force, it provides a measure of the intensity of the secondary flow (Fairbank and So 1987).

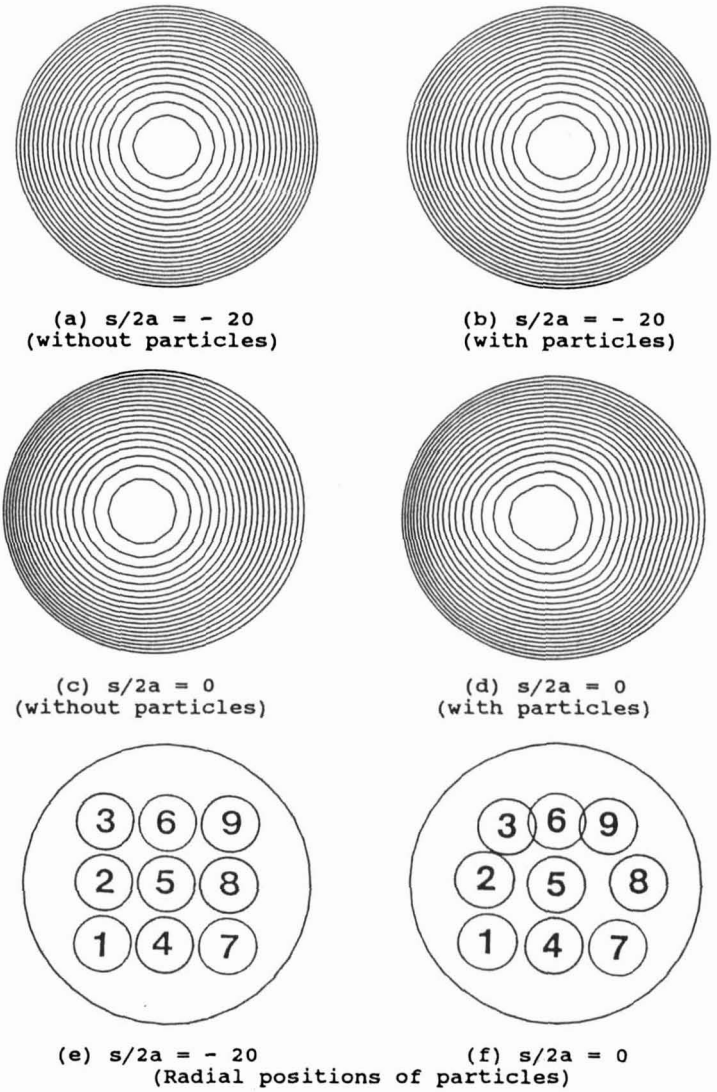

FIG. 4. FLUID AXIAL VELOCITY CONTOURS AND PARTICLE RADIAL POSITIONS IN THE FIRST STRAIGHT TUBE

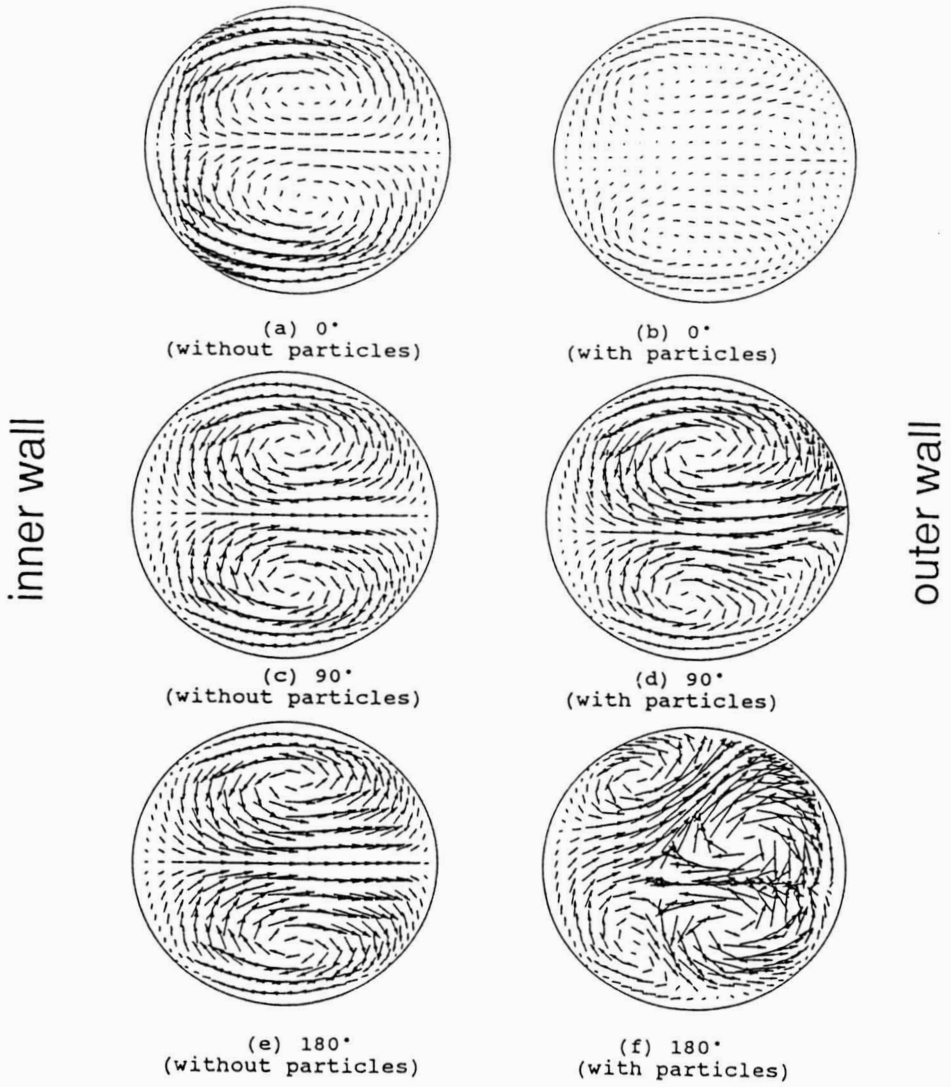

FIG. 5. SECONDARY FLOW DEVELOPED IN THE BEND AT THE INDICATED ANGLES

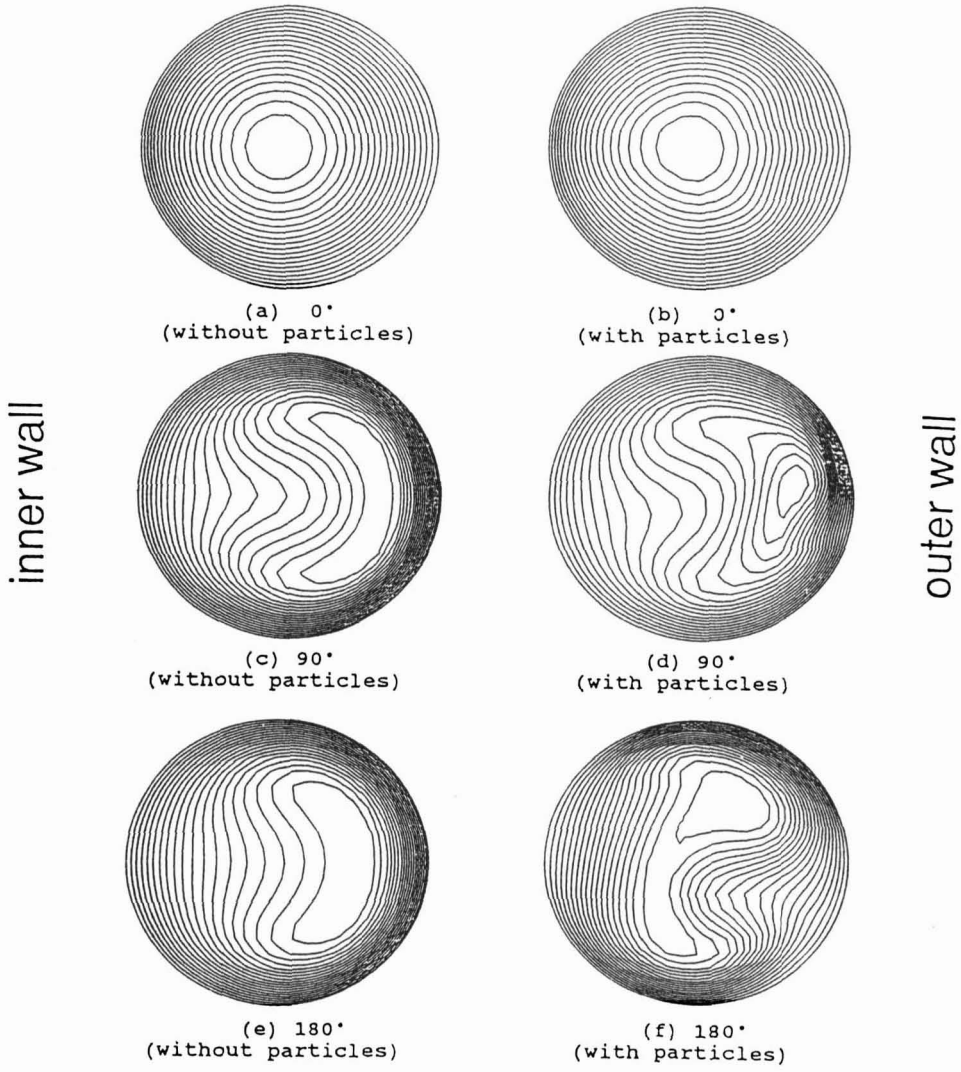

FIG. 6. FLUID AXIAL VELOCITY CONTOURS IN THE BEND AT THE INDICATED ANGLES

Second Straight Tube. Although the centrifugal forces are present only within the bend, the radial pressure gradient set up to balance them can propagate downstream away from the bend. The secondary flow vectors with and without the presence of the particles (Fig. 8) show that the particles extended the downstream bend effect. In the present simulation (with $\delta \approx 0.28$, $\mathrm{Re} \approx 152$, and $\mathrm{De} \approx 81$), the axial fluid velocity contours in the second straight

tube (Fig. 9) show that without particles, a fully developed fluid velocity profile was achieved at about s/2a = + 14, while with particles the fully developed flow field was not obtained until s/2a = + 29. Comparable results were found experimental by Fairbank and So (1987) working with air in a similar tube/bend arrangement. These secondary motions can persist for much longer distances downstream (up to 40 diameters) under high Dean number conditions (Ward-Smith 1980).

The velocities and radial positions of particles still kept changing well into second straight tube due to the persistence of the bend effect. The rate of these changes became slower towards the middle of the tube, and relatively stable conditions were achieved as the particles moved further downstream (Fig. 10). But, these "recovered" radial positions were no longer symmetric, as was the case in first straight tube.

Fluid and Particle Velocities. The influences of the particles on the fluid axial velocity profiles are shown in Fig. 11, 12 for selected cross sections of the bend and second straight tube, respectively. As seen in the figures, the particles caused a shift of the maximum velocity region from the outside wall towards the inside wall near the bend outlet and in the early stages of the second straight tube. This is because as most of the particles moved towards the outside wall in the bend, the particles forced the fluid flow towards the inner wall, gradually shifting the maximum fluid velocity region in that direction. As the particles moved downstream, they migrated towards the inner wall causing the fluid maximum velocity to shift in the opposite direction and then back towards the center of the tube, where fully developed flow recovery was attained when the secondary flow vanished and the radial positions of the particles became relative stable (s/2a = 29).

In the first straight tube the particle velocities, V_p, were slightly less than the fluid stream-line velocities, V_f, passing through the center of the particles. The velocity differences between the two phases became larger in the bend due to the large velocity changes occurring in this section, but these differences completely disappeared at the exit of the second tube. The velocities V_p and V_f at three cross sections are listed in Table 1. The results show that while some of the faster particles in the first straight tube became slower at the end of the second tube, some of the slower ones became faster.

For aseptic processing, the existence of secondary flow would probably improve the efficiency of the heat transfer process. Although heat transfer is not considered in the current study, one could reasonably expect that the secondary current induced by the bend curvature can create a strong mixing effect between the hot and the cold liquid. Variable density effects due to temperature gradients will further enhance the strength of this secondary motion because the heavier cold liquid will be subjected to a larger centrifugal force.

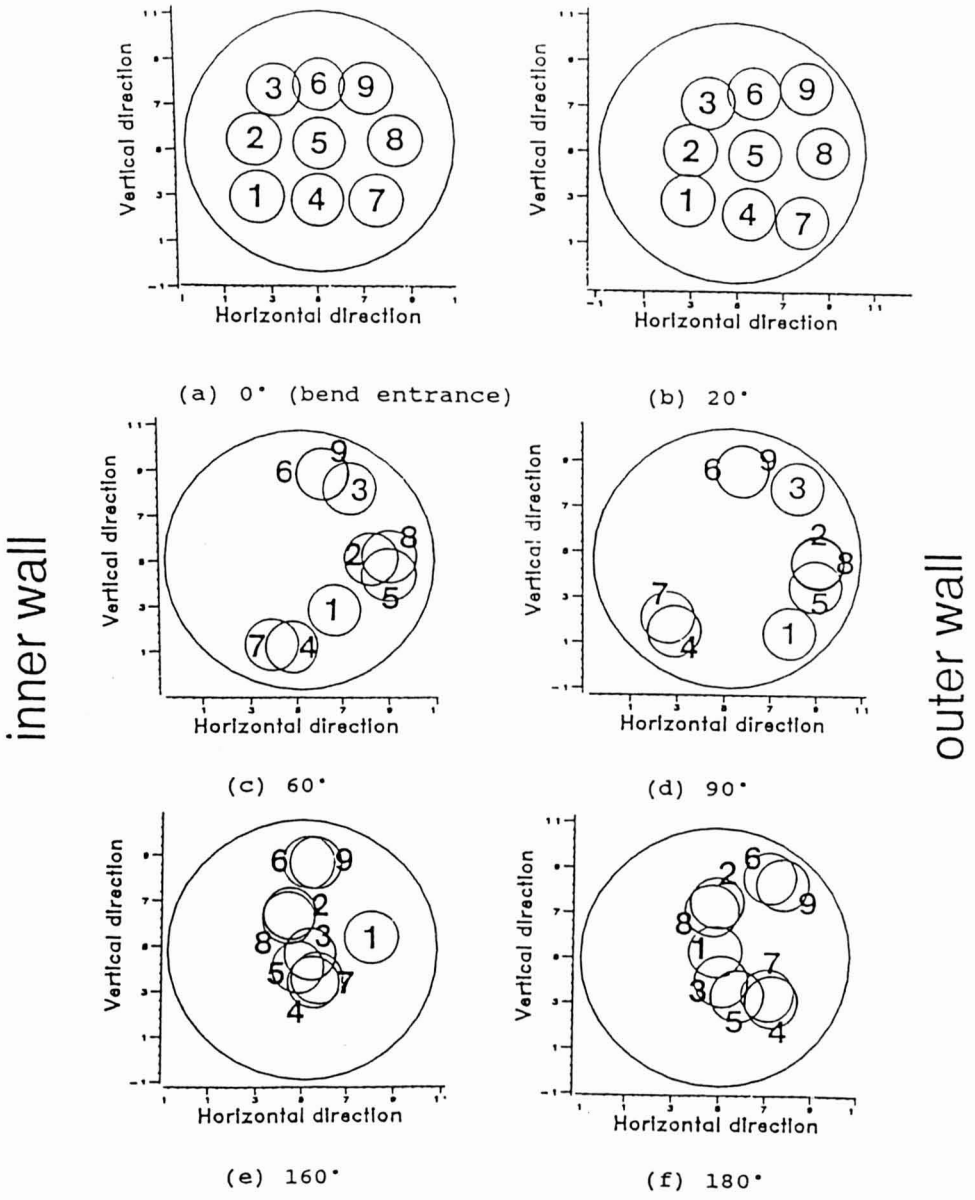

FIG. 7. RADIAL POSITIONS OF THE PARTICLES IN THE BEND

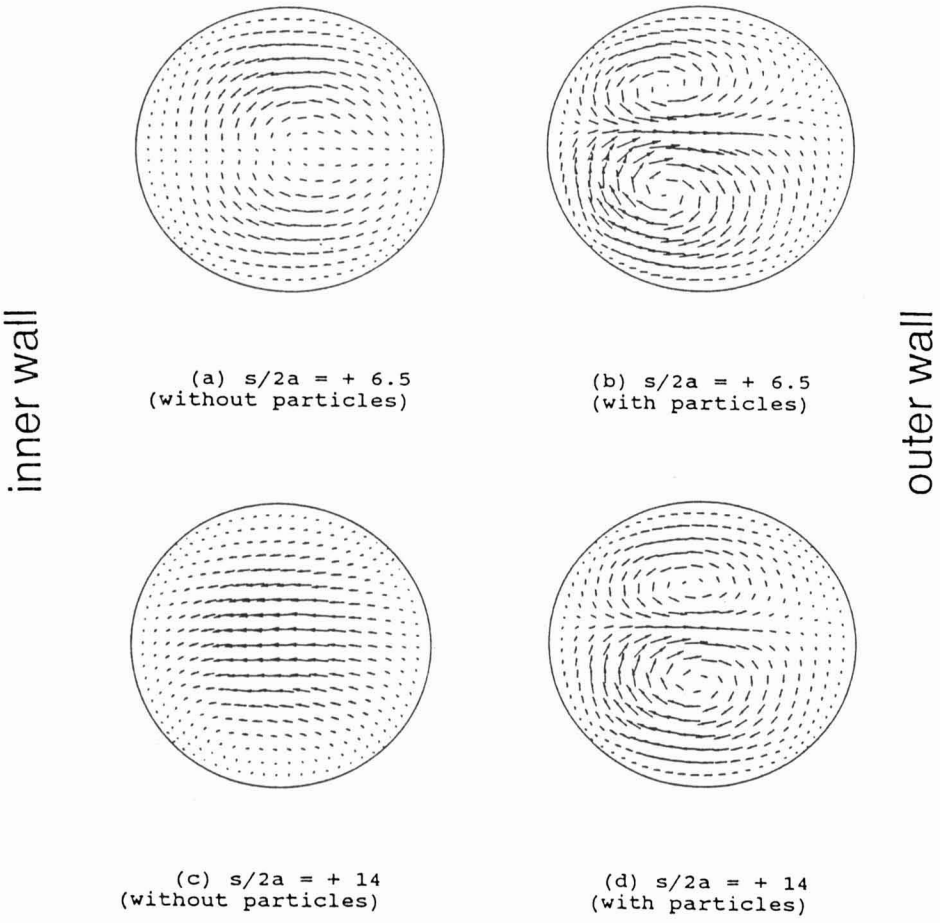

FIG. 8. SECONDARY FLOW DEVELOPED IN THE SECOND STRAIGHT TUBE

Residence Time Distributions and Average Velocities of Particles

The radial position and velocity (or residence time) changes experienced by the particles, resulting primarily from the bend effect, significantly affected their residence time distributions in the holding tube.

The residence times and average velocities of the particles at various cross sections (Fig. 13) are listed in Tables 2 and 3, respectively.

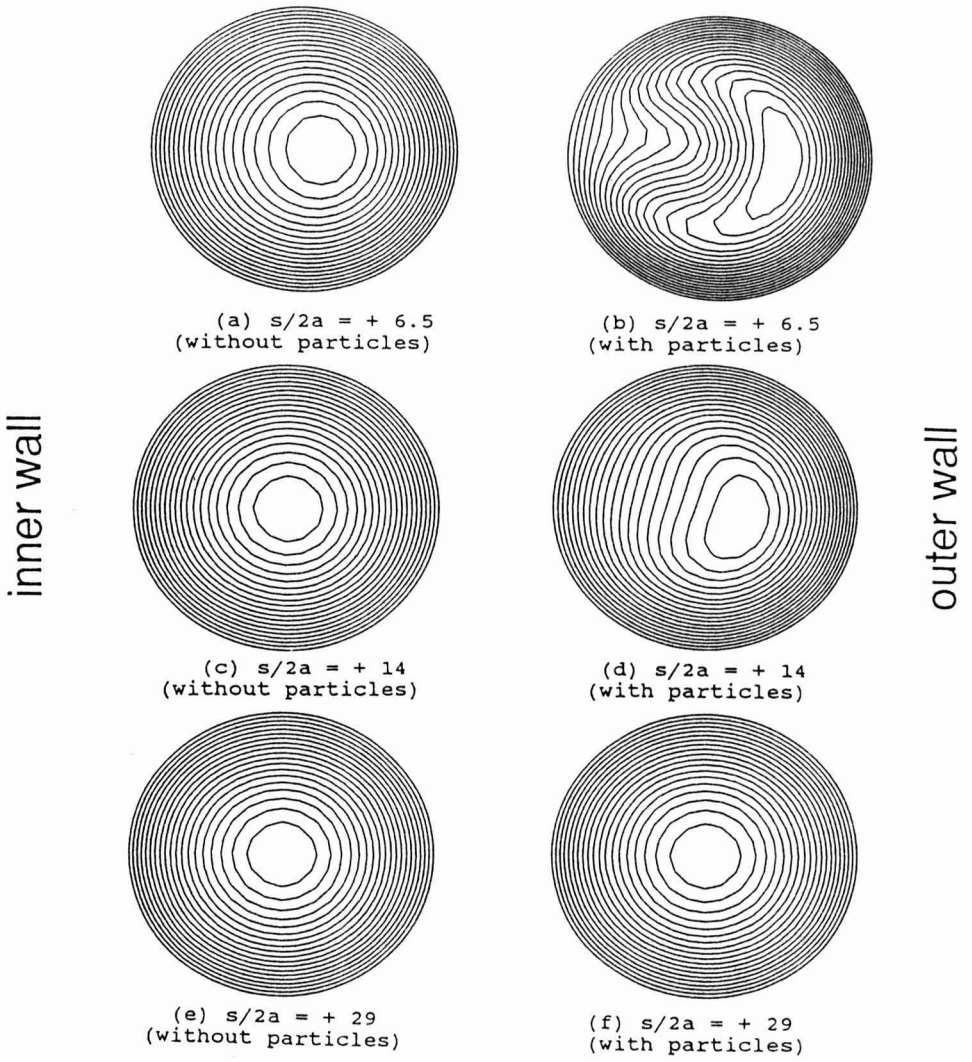

FIG. 9. FLUID AXIAL VELOCITY CONTOURS IN THE SECOND STRAIGHT TUBE

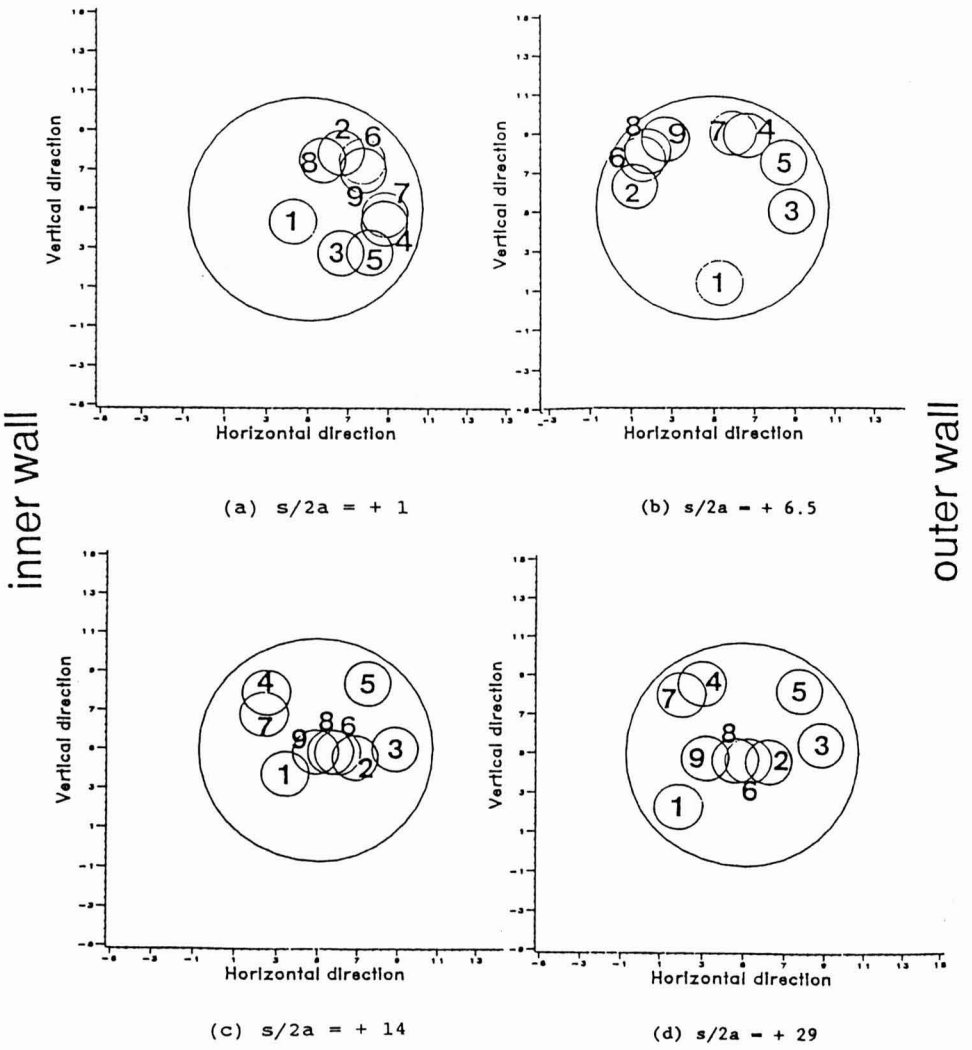

FIG. 10. PARTICLE RADIAL POSITIONS IN THE SECOND STRAIGHT TUBE

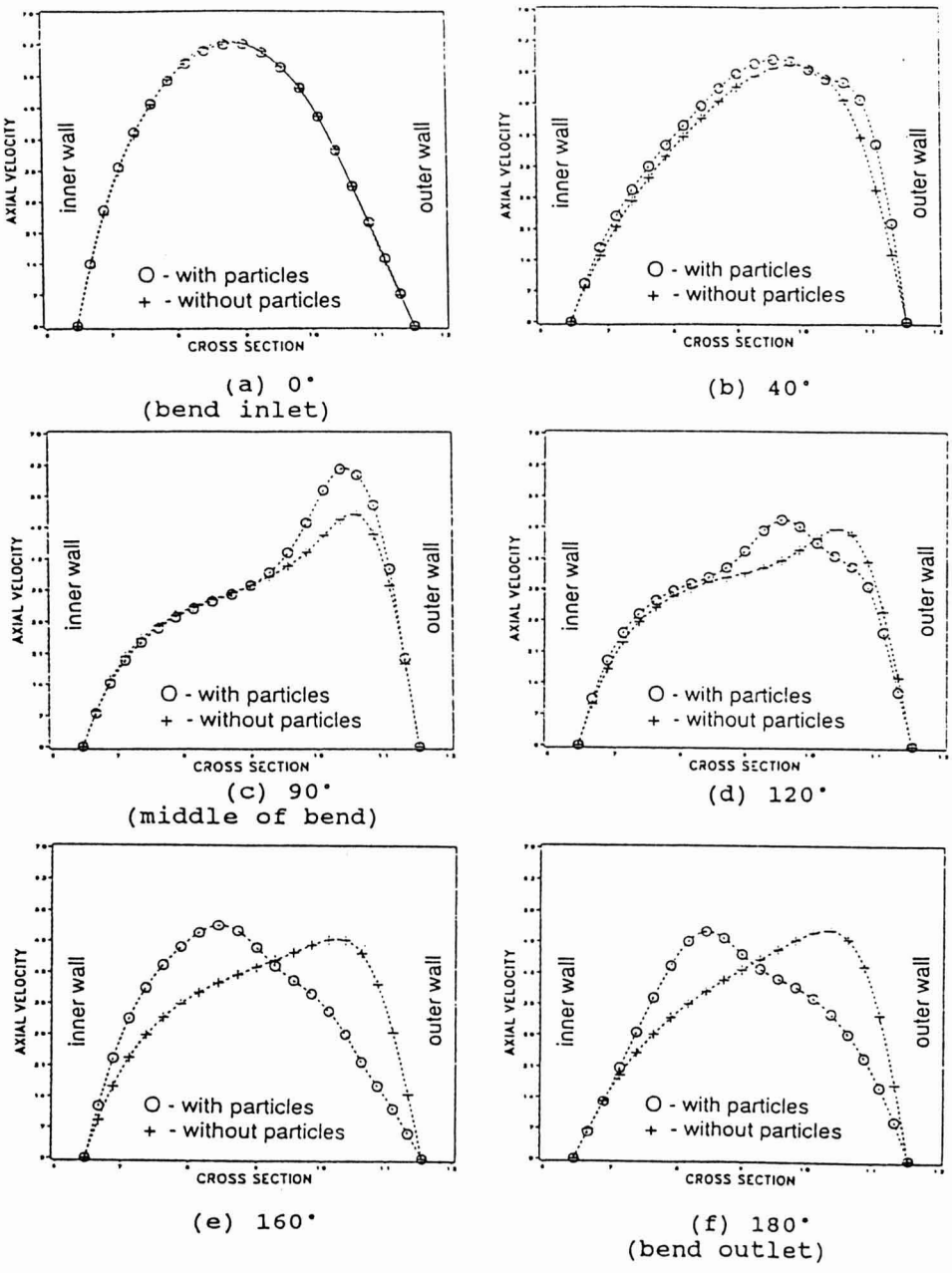

FIG. 11. THE INFLUENCE OF THE PARTICLES ON THE FLUID AXIAL VELOCITY PROFILES IN THE BEND

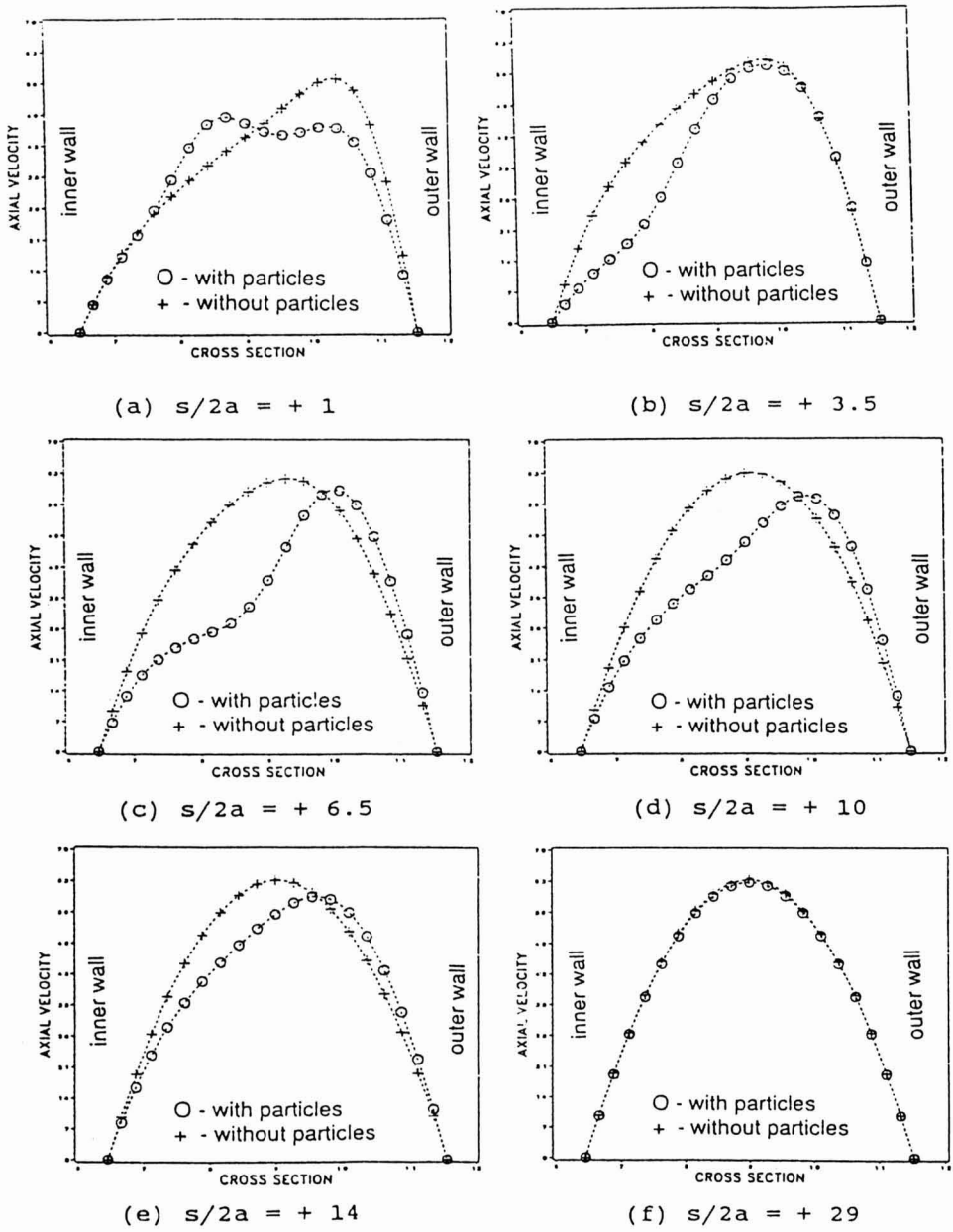

FIG. 12. THE INFLUENCE OF THE PARTICLES ON THE FLUID AXIAL VELOCITY PROFILES IN THE SECOND STRAIGHT TUBE

TABLE 1.
COMPARISON OF FLUID AND PARTICLE VELOCITY AT THE INDICATED CROSS SECTIONS (CM/S)

	At s/2a = −20		At Bend Exit		At Tube Exit	
#	Vp	Vf	Vp	Vf	Vp	Vf
1	24.90	25.06	39.84	44.85	51.01	51.03
2	38.62	38.86	46.06	48.17	52.09	52.10
3	35.09	35.30	49.29	52.41	22.23	22.23
4	43.26	43.45	49.80	52.35	27.87	27.85
5	62.74	62.95	50.99	53.84	22.28	22.28
6	43.98	44.18	26.19	24.34	59.95	59.95
7	29.60	29.76	50.53	53.12	36.65	36.66
8	37.76	38.00	45.59	47.68	61.68	61.68
9	35.32	35.52	21.01	19.14	62.92	62.92
mean	39.03	39.23	42.14	43.96	44.08	44.08

In the first straight tube, the particles crossed the inlet all at the same time, but with a parabolic velocity profile. This symmetric profile gave rise to a widening residence time distribution as they moved along this section. This effect can be seen in Table 2 by comparing the values of Max-Min between sections 1 and 2. When the particles flowed into the bend and early stages of the second straight tube, their radial positions alternated between high and low fluid velocity regions, resulting in an almost suppression of the axial dispersion of the particles as indicated by the Max-Min values in sections 2 to 5. But, as the particles reached a stable radial position in the section of the recovered quasi-parabolic profile of the fluid (after section 5), the axial dispersion started to increase again as can be seen by the Max-Min value in section 6. However, observing the development of the axial dispersion effect along the holding tube, it can be seen that from the inlet plane (Max-Min = 0) to section 2, the Max-Min grows to 5.17, while between sections 2 and 6 it only increases by 0.9 (from 5.17 to 6.07). From these numbers one can speculate that from section 6 onward (the inlet to the next 180° bend), the particles would experience a small axial dispersion effect, and that the Max-Min value would grow by about the same magnitude (0.9) between that point and the inlet of the third bend.

As shown in Table 1, the particle velocities were almost always less than the fluid streamline velocities passing through their center. On the other hand, the mean particle velocities shown in Table 3, were all — but one — larger than the average fluid velocity, which was 30 cm/s in the current simulation. The same result was found by Sandeep and Zuritz (1991) in their experimental study on residence time distributions of spherical particles in holding tube flow. Additionally, they found that the ratio of the mean-to-minimum particle residence time ranged between 1.06 and 1.16; in the present simulation, the

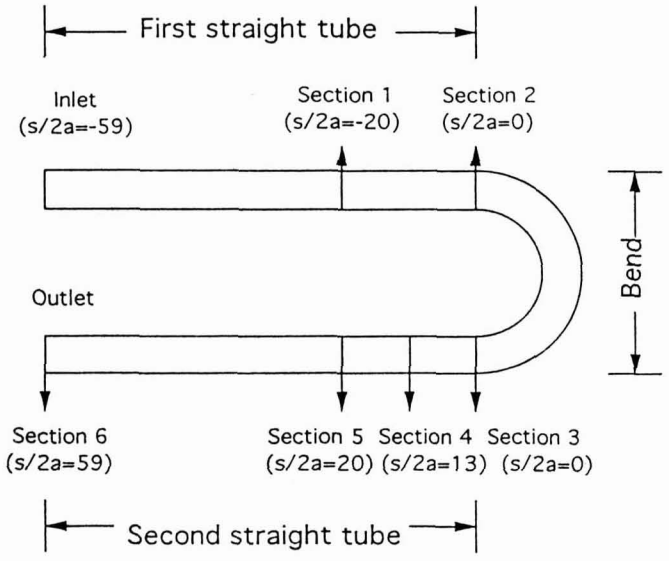

FIG. 13. CROSS SECTION LOCATIONS FOR THE DETERMINATION OF PARTICLE RESIDENCE TIMES

TABLE 2.
RESIDENCE TIMES OF PARTICLES AT VARIOUS CROSS SECTIONS[1](S)

Particle#	Sec. 1	Sec. 2	Sec. 3	Sec. 4	Sec. 5	Sec. 6
No. 1	6.37	9.92	10.88	14.38	16.61	18.64
No. 2	4.78	7.36	8.19	10.84	12.68	14.57
No. 3	5.59	8.25	9.26	12.74	17.29	21.67
No. 4	4.48	6.77	7.53	11.44	15.35	19.10
No. 5	3.16	4.75	5.59	9.20	13.74	18.15
No. 6	4.46	6.70	7.56	10.44	12.11	13.77
No. 7	6.12	9.21	10.12	14.00	16.99	19.84
No. 8	4.85	7.51	8.53	11.14	12.77	14.38
No. 9	5.61	8.27	9.28	12.30	13.93	15.52
mean	5.05	7.63	8.55	11.83	14.61	17.29
Max-Min	3.21	5.17	5.29	5.18	5.18	6.07
Change	101%	108%	94.6%	56.3%	42.8%	44.1%

[1]Cross sections are shown in Fig. 13.

TABLE 3.
AVERAGE PARTICLE VELOCITIES AT VARIOUS CROSS SECTION[1] (CM/S)

Sec #1	Sec #2	Sec #3	Sec #4	Sec #5	Sec #6
39.6	39.3	38.4	31.9	29.3	36.3

[1]Cross section locations are shown in Fig. 13.

ratio at section 6 (outlet) was 1.26. This small variation may be due to the difference in holding tube length, as they used four straight tubes and three 180° bends. However, an analysis of the variation of this ratio along the six sections shows that it decreases from 1.6 at section 1, to 1.2 at section 5 and then increases to only 1.26 in section 6. If there were two more bends and straight tubes, judging from the previous analysis, one would expect the ratio to fall within the experimentally determined range.

CONCLUSIONS AND RESEARCH NEEDS

Velocities of fluid, and particles trajectories and velocities have been quantitatively predicted under a particulate two-phase pipe flow situation. The simulation results indicated that the bend had a considerable influence on both fluid flow field and particle residence times in pipe flow. They also showed that the particles had a significant effect on the flow field and extended the bend effect on the downstream fluid flow field.

In the current model, the carrier medium is a Newtonian fluid. Furthermore, particle-particle interactions were neglected. The carrier fluids used in aseptic processing, however, are generally non-Newtonian fluids, and particle interactions can be very important, particularly when the particle loading is high. Both non-Newtonian fluid and particle-particle interactions are currently being incorporated in the model.

LIST OF SYMBOLS

Symbol	Meaning
a	Radius of particle (m)
C_d	Drag coefficient
F	Force (N)
F_b	Buoyancy force (N)

F_{rk}	Magnus lift force (N)
F_s	Saffman force (N)
g	Gravitational acceleration (m/s^2)
h_f	Solid-liquid interface heat transfer coefficient (W/m^2C)
I	Moment of inertia ($kg\ m^2$)
J	Jacobian matrix
K	Curl of fluid velocity (s^{-1})
m	Mass of one particle (kg)
P	Pressure (Pa)
r	Radius of holding tube (m)
Re	Reynolds number
RTDs	Residence time distributions (s)
S	Source term in fluid momentum equation
T	Torque (N m)
U, u	ξ or x direction velocity (m/s)
V, v	η or y direction velocity (m/s)
W, w	ζ or z direction velocity (m/s)

Greek Letters

β	Coefficient of artificial compressibility
Γ	Preconditioning matrix
ξ, η, ζ	Computational grid coordinate
μ	Coefficient of viscosity (Pa s)
ν	Kinematic viscosity (m^2/s)
ρ	Density (kg/m^3)
Σ	Summation
Ω	Angular velocity of particle (radians/s)

Subscripts

d	Drag
f	Fluid
p	Particle
x,y,z	Direction

REFERENCES

AUTON, T.R. 1973. The Dynamics of Bubbles, Drops and Particles in Motion in Liquids. Ph.D. dissertation, Cambridge Univ.

BERGER, S.A., TALBOT L. and YAO, L.S. 1983. Flow in curved pipes. Ann. Rev. Fluid Mech. *15*, 461–512.

BERLEMONT, A., DESJONQUERES, P. and GOUESBET, G. 1990. Particle lagrangian simulation in turbulent flows. Int. J. Multiphase Flow *16*(1), 19–34.

CLIFF, R. and GAUVIN, W. 1971. Motion of entrained particles in gas stream. Can. J. Chem. Eng. *49*, 439–50.

DURST, F., MILOJEVIC, D. and SCHONUNG, B. 1984. Eulerian and Lagrangian predictions of particulate two-phase flows: a numerical study. Appl. Math. Modelling *8*, 101–115.

DUTTA, B. and SASTRY, S.K. 1990a. Velocity Distributions of food particle suspensions in holding tube flow: experimental and modeling studies on average particle velocities. J. Food Sci. *55*(5), 1448–1453.

DUTTA, B. and SASTRY, S.K. 1990b. Velocity distributions of food particle suspensions in holding tube flow: distribution characteristics and fastest-particle velocities. J. Food Sci. *55*(6), 1703–1710.

FAIRBANK, J.A. and SO, R.M.C. 1987. Upstream and downstream influence of pipe curvature on the flow through a bend. Heat Fluid Flow *8*(3), 211–217.

KAIMAL, M.R. and DEVANATHAN, R. 1980. Motion of a viscous fluid with suspended particles in a curved tube. Int. J. Eng. Sci. *18*, 847–854.

KWAK, D., CHANG, J.L.C., SHANKS, S.P. and CHAKRAVARTHY, S.R. 1985. A three dimensional incompressible Navier-Stokes flow solver using primitive variables. AIAA J. *23*, 390–396.

LU, Q.Q., FONTAINE, J.R. and AUBERTIN, G. 1993. A Lagrangian model for solid particles in turbulent flows. Int. J. Multiphase Flow *19*(2), 347–367.

MERKLE, C.L. and ATHAVALE, M. 1987. Time-accurate unsteady incompressible flow algorithms based on artificial compressibility. AIAA 8th Computational Fluid Dynamics Conf., AIAA Paper 87–1137, June, Honolulu, HA.

OHASHI, H., SUGAWARA, T., KIFUCHI, K. and ISE, M. 1980. Average particle velocity in solid liquid two phase flow through vertical and horizontal tubes. J. Chem. Eng. Japan *13*(5), 343–349.

RUBINOW, S.I. and KELLER, J.B. 1961. The transverse force on a spinning sphere moving in a viscous liquid. J. Fluid Mech. *11*, 447–459.

SAFFMAN, P.G. 1965. The lift on a small sphere in slow shear flow. J. Fluid Mech. *22*, 385–400.

SAFFMAN, P.G. 1968. Corrigendum to the paper "The Lift on a Small Sphere in Slow Shear Flow". J. Fluid Mech. *31*, 624.

SANDEEP, K.P. and ZURITZ, C.A. 1991. Residence time distribution of multiple particles in non-Newtonian tube flow. ASAE Paper No. 91–549. Amer. Soc. of Agricultural Engineers, St. Joseph, MI.

SASTRY, S.K. and DUTTA, B. 1989. Modeling of flow of liquid-particle mixtures in tubes. ASAE Paper No. 89-6587. Amer. Soc. of Agricultural Engineers, St. Joseph, MI.

SASTRY, S.K., HESKITT, B.F. and BLAISDELL, J.L. 1989. Experimental and modeling studies on convective heat transfer at the particle-liquid interface in aseptic processing systems. Food Technol. Mar., 132–143.

SASTRY, S.K. and ZURITZ, C.A. 1987. A model for particle suspension flow in a tube. ASAE Paper No. 87-6537. Amer. Soc. of Agricultural Engineers, St. Joseph, MI.

TODA, M. and ISHIKAWA, T. 1973. On the particle velocities in solid liquid two phase flow through straight pipes and bends. J. Chem. Eng. Japan *6*(2), 140–146.

WARD-SMITH, A.J. 1980. *Internal Fluid Flow: The Fluid Dynamics of Flow in Pipes and Ducts*. Clarendon Press. Oxford.

YAGLEY, J., FENG, J. and MERKLE, C.L. 1992. The effect of aspect ratio on the effectiveness of combustor coolant passages. AIAA/SAE/ASME/ ASEE 28th Joint Propulsion Conference and Exhibit. AIAA-92-3153. July 6–8, Nashville, TN.

A SOLUTION TO THE EQUATIONS GOVERNING HEAT TRANSFER IN AGITATING LIQUID/PARTICULATE CANNED FOODS

NIKOLAOS G. STOFOROS[1] and RICHARD L. MERSON

Department of Food Science and Technology and
Department of Biological and Agricultural Engineering
University of California, Davis
Davis, CA 95616

Accepted for Publication July 20, 1994

ABSTRACT

A semi-analytical (concerning the particle temperature) semi-numerical (concerning the fluid temperature) solution to the differential equations governing heat transfer to axially rotating liquid/particulate canned foods was obtained using Duhamel's theorem and a numerical 4th-order Runge-Kutta scheme. This solution avoids some of the shortcomings of earlier solutions such as the requirement for constant heating medium temperature, the need for empirical formulas, or the use of unrealistic assumptions regarding the fluid temperature. The agreement between the proposed solution and limiting case analytical results was very good. A maximum fluid temperature difference of less than 2C was momentarily observed at the beginning of heating; differences between particle surface temperatures were even smaller. Comparison between predicted values and experimental data from the literature showed good agreement only as far as the fluid temperature was concerned; particle surface temperatures deviated significantly.

INTRODUCTION

Knowledge of the time-temperature profile for the food under processing is essential in evaluating the lethal effect of a heat treatment on microbial or quality factor destruction and, therefore, in designing a thermal process. For liquid/particulate food systems, prediction of heat transfer rates is restricted, at present, to film theory analysis. Heat transfer coefficients are incorporated into coupled differential equations describing energy balances on both liquid and particles (Merson and Wolcott 1986; Rao and Anantheswaran 1987; Stoforos 1988); provided that these heat transfer coefficients are known, the solution to

[1]Author Stoforos' present address: Thermopilon 5, 35100 Lamia, Greece.

Journal of Food Process Engineering **18** (1995) 165–185.

the differential equations gives the temperature profile for the processed liquid and particles. Solutions to these equations have been presented for fluid and particle temperatures under various heat treatments: for axially rotating liquid/particulate canned foods (Lenz and Lund 1978; Rumsey 1984; Lekwauwa and Hayakawa 1986), for continuous sterilization of liquid foods containing discrete particles in scraped-surface heat exchangers and holding tubes (de Ruyter and Brunet 1973; Manson and Cullen 1974; Hemmings and Kern 1979; Sastry 1986; Chandarana and Gavin 1989; Chang and Toledo 1989; Lee and Singh 1990; Armenante and Leskowicz 1990; Merson and Sawada 1991), or for particulate processing in fluidized beds (Chang and Wen 1966; Sawada and Merson 1986). Although much can be learned about processing of liquid/particulate canned foods by studying continuous processing of liquid/particulate systems, the following discussion is limited to references pertaining to in-container processing.

For axially rotating cans, Lenz and Lund (1978) developed a solution using Duhamel's theorem and a 4th-order Runge-Kutta numerical scheme. They decoupled the fluid and particle energy balance equations by first assuming that the fluid temperature was approximated by the expression for canned liquid without particles. Lekwauwa and Hayakawa (1986) introduced a statistically-described particle volume distribution. The temperature distribution for individual particles was obtained using Duhamel's theorem and empirical formulas describing the heat transfer problem to spherical, cylindrical or oblate spheroidal-shaped particles in a constant temperature fluid. The resulting equations were discretized and solved iteratively. In their numerical solution, they assumed that within each time step the fluid temperature was a linear function of time, the coefficients of these functions being determined iteratively such that the resulting particle and fluid temperatures satisfied the overall energy balance equation. Finally, for the same system, Rumsey (1984) has presented a finite difference numerical solution, assuming spherical particles. By discretizing the equations, he obtained an expression for the fluid temperature at a given time based on the average particle temperature at the previous time step. Particle temperatures were calculated from fluid temperature at the same time step, by dividing the spherical particle into ten concentric spherical shells. For each time step, he proceeded by first solving for the fluid temperature and then, using this solution, obtaining particle temperatures.

The objective of the current work is to present a solution to the differential equations governing the heat transfer to agitating liquid/particulate canned foods. It is a semi-analytical (concerning the particle temperature) semi-numerical (concerning the fluid temperature) solution and was obtained using Duhamel's theorem and a numerical 4th-order Runge-Kutta scheme.

Theory

The system under investigation is a fluid with dispersed particles in an axially rotating can completely surrounded by a heating medium (e.g., steam). The governing differential equations are derived from thermal energy balances on the liquid and solid (particle) phases. Major assumptions that characterize both the derivation and solution of the equations are: uniform fluid temperature, constant heat transfer coefficients, uniform initial temperatures for both particle and fluid, equal diameter spherical particles, and constant physical and thermal properties for both the fluid and particles. Neglecting the heat accumulated in the can walls, an energy balance on the can contents yields

$$U_o A_c (T_{st} - T_f) = m_f C_{pf} \frac{dT_f}{dt} + m_p C_{pp} \frac{d<T_p>}{dt} \tag{1}$$

For ε being the fraction of the effective can volume occupied by the particles, V_{ce} the effective can volume (total can volume minus headspace volume), and ρ_f and ρ_p the fluid and the particle density, respectively, Eq. (1) becomes

$$U_o A_c (T_{st} - T_f) = \rho_f V_{ce}(1 - \varepsilon) C_{pf} \frac{dT_f}{dt} + \rho_p V_{ce} \varepsilon C_{pp} \frac{d<T_p>}{dt} \tag{2}$$

Equation (2), subject to the initial condition

$$T_f(t = 0) = T_{fi} \tag{3}$$

constitutes the governing equation for the fluid temperature.

For each spherical particle, the governing differential equation for the temperature distribution is

$$\frac{\partial (r_p T_p)}{\partial t} = \alpha_p \frac{\partial^2 (r_p T_p)}{\partial r_p^2} \tag{4}$$

subject to the following initial and boundary conditions

$$T_p(r_p, t = 0) = T_{pi} \tag{5}$$

$$T_p(r_p = 0, t) = \text{finite} \tag{6}$$

$$k_p \frac{\partial T_p}{\partial r_p}\Big|_{r_p = R_p} = h_p(T_f - T_{ps}) \tag{7}$$

where T_{ps} is the particle surface temperature.

Provided that the heat transfer coefficients (U_o and h_p) are known, solution of Eq. (2) and (4), with the conditions imposed through Eq. (3), (5), (6) and (7), will give the temperature distribution for the fluid and particles. The two differential equations are coupled through the boundary condition at the particle surface, Eq. (7), so they should be solved simultaneously.

MATHEMATICAL PROCEDURE

Duhamel's theorem is a superposition method which provides solution to differential equations with time-dependent boundary conditions based on the solution of the same problem with constant boundary conditions. For the heat conduction problem in a spherical particle with convective boundary condition, Duhamel's theorem states (e.g., Carslaw and Jaeger 1959; Hildebrand 1976; Myers 1971):

If $U(r_p,t)$ represents the temperature at any position r_p and time t for a sphere with zero initial temperature, heated by a medium of unity temperature, then the solution to the same problem but for which the medium temperature is a function of time, $\Phi(t)$, is given by

$$V_p(r_p,t) = \int_{\lambda=0}^{\lambda=t} \Phi(\lambda) \frac{\partial}{\partial t}\big(U(r_p,t-\lambda)\big) d\lambda \tag{8}$$

For our problem, the solution for $U(r_p,t)$ is given by (Carslaw and Jaeger 1959)

$$U(r_p,t) = 1 - \frac{2BiR_p}{r_p} \sum_{n=1}^{\infty} \frac{\lambda_n^2 + (Bi-1)^2}{\lambda_n^2 + Bi(Bi-1)} \frac{\sin(\lambda_n)\sin(\lambda_n \frac{r_p}{R_p})}{\lambda_n^2} \exp\left(-\frac{\lambda_n^2 \alpha_p}{R_p^2} t\right) \tag{9}$$

where $\pm\lambda_n$, n = 1, 2,... are the roots of

$$\lambda_n \cot(\lambda_n) + Bi - 1 = 0 \tag{10}$$

and Bi is defined as

$$Bi = \frac{h_p R_p}{k_p} \tag{11}$$

Evaluating the derivative $\partial U(r_p, t-\lambda)/\partial t$ through Eq. (9), substituting the resulting expression into Eq. (8), and correcting for the initial particle temperature, T_{pi}, not being zero, the following equation is obtained for the particle temperature of our problem (Stoforos 1988).

$$T_p(r_p,t)=T_{pi}+\frac{2\alpha_p Bi}{r_p R_p}\sum_{n=1}^{\infty}\frac{\lambda_n^2+(Bi-1)^2}{\lambda_n^2+Bi(Bi-1)}\sin(\lambda_n)\sin(\lambda_n\frac{r_p}{R_p})$$
$$\int_{\lambda=0}^{\lambda=t}(T_f(\lambda)-T_{p_i})\exp(-\frac{\lambda_n^2\alpha_p}{R_p^2}(t-\lambda))d\lambda \tag{12}$$

In order to evaluate the integral appearing in Eq. (12), since $T_f(t)$ is still unknown, we assume that

$$T_f(\lambda) = T_f(t) \text{ for } 0 \le \lambda \le t$$

Hence,

$$\int_{\lambda=0}^{\lambda=t}(T_f(\lambda)-T_{pi})\exp(-\frac{\lambda_n^2\alpha_p}{R_p^2}(t-\lambda))d\lambda=$$
$$(T_f(t)-T_{pi})\frac{R_p^2}{\lambda_n^2\alpha_p}(1-\exp(-\frac{\lambda_n^2\alpha_p}{R_p^2}t)) \tag{13}$$

Substituting Eq. (13) into Eq. (12) and using the following identity

$$\frac{2BiR_p}{r_p}\sum_{n=1}^{\infty}\frac{\lambda_n^2+(Bi-1)^2}{\lambda_n^2+Bi(Bi-1)}\frac{\sin(\lambda_n)\sin(\lambda_n\frac{r_p}{R_p})}{\lambda_n^2}=1 \tag{14}$$

gives upon rearranging

$$T_p(r_p,t)=T_f(t)-(T_f(t)-T_{pi})\frac{2BiR_p}{r_p}\sum_{n=1}^{\infty}\frac{\lambda_n^2+(Bi-1)^2}{\lambda_n^2+Bi(Bi-1)}$$
$$\frac{\sin(\lambda_n)\sin(\lambda_n\frac{r_p}{R_p})}{\lambda_n^2}\exp(-\frac{\lambda_n^2\alpha_p}{R_p^2}t) \tag{15}$$

A short proof the validity of Eq. (14) can be obtained by setting $t = 0$ into Eq. (9) and noting that $U(r_p, t = 0) = 0$. Equation (15) is the exact solution for T_p only when $T_f(t)$ = constant. For all other cases, due to the assumed T_f function, Eq. (15) overestimates T_p.

The next step is to introduce Eq. (15) into Eq. (2) in order to eliminate $<T_p>$. For the average particle temperature, $<T_p>$, defined by

$$<T_p> = \frac{\int v_p T_p dv_p}{\int v_p dv_p} \tag{16}$$

for

$$v_p = \frac{4}{3}\pi R_p^3$$

and

$$dv_p = 4\pi r_p^2 dr_p$$

Eq. (16) reduces to

$$<T_p> = \frac{3}{R_p^3}\int_0^{Rp} T_p r_p^2 dr_p \tag{17}$$

Using Eq. (17), for T_p given by Eq. (15), the following expression for the average particle temperature is obtained

$$<T_p(t)> = T_f(t) - (T_f(t) - T_{p_i}) 6Bi^2 \sum_{n=1}^{\infty} \frac{\lambda_n^2 + (Bi-1)^2}{\lambda_n^2 + Bi(Bi-1)} \frac{\sin^2(\lambda_n)}{\lambda_n^4} \exp\left(-\frac{\lambda_n^2 \alpha_p}{R_p^2} t\right) \tag{18}$$

By defining

$$\sigma(t) = 6Bi^2 \sum_{n=1}^{\infty} \frac{\lambda_n^2 + (Bi-1)^2}{\lambda_n^2 + Bi(Bi-1)} \frac{\sin^2(\lambda_n)}{\lambda_n^4} \exp\left(-\frac{\lambda_n^2 \alpha_p}{R_p^2} t\right) \tag{19}$$

from Eq. (18), we obtain

$$\frac{d<T_p>}{dt} = (1-\sigma)\frac{dT_f}{dt} - (T_f - T_{pi})\frac{d\sigma}{dt} \tag{20}$$

Substituting Eq. (20) into Eq. (2) and rearranging yields

$$\frac{dT_f}{dt}\left[1+\frac{\rho_p\varepsilon C_{pp}}{\rho_f(1-\varepsilon)C_{pf}}(1-\sigma)\right]+T_f\left[\frac{U_oA_c}{\rho_fV_{ce}(1-\varepsilon)C_{pf}}-\frac{\rho_p\varepsilon C_{pp}}{\rho_f(1-\varepsilon)C_{pf}}\frac{d\sigma}{dt}\right]+ T_{p_i}\frac{\rho_p\varepsilon C_{pp}}{\rho_f(1-\varepsilon)C_{pf}}\frac{d\sigma}{dt}-T_{st}\frac{U_oA_c}{\rho_fV_{ce}(1-\varepsilon)C_{pf}}=0 \tag{21}$$

Equation (21) can be written as

$$C_1(t)\frac{dT_f}{dt}+C_2(t)T_f+C_3(t)T_{pi}+C_4T_{st}=0 \tag{22}$$

where the coefficients C_1 through C_4 correspond to the coefficients appearing in Eq. (21). Using Eq. (19) the above coefficients are given, explicitly, by the following expressions

$$C_1(t)=1+\frac{\rho_p\varepsilon C_{pp}}{\rho_f(1-\varepsilon)C_{pf}}\left[1-6Bi^2\sum_{n=1}^{\infty}\frac{\lambda_n^2+(Bi-1)^2}{\lambda_n^2+Bi(Bi-1)}\frac{\sin^2(\lambda_n)}{\lambda_n^4}\exp\left(-\frac{\lambda_n^2\alpha_p}{R_p^2}t\right)\right] \tag{23}$$

$$C_2(t)=\frac{U_oA_c}{\rho_fV_{ce}(1-\varepsilon)C_{pf}}+\frac{\rho_p\varepsilon C_{pp}}{\rho_f(1-\varepsilon)C_{pf}}\frac{6Bi^2\alpha_p}{R_p^2}\sum_{n=1}^{\infty}\frac{\lambda_n^2+(Bi-1)^2}{\lambda_n^2+Bi(Bi-1)}\frac{\sin^2(\lambda_n)}{\lambda_n^4}\exp\left(-\frac{\lambda_n^2\alpha_p}{R_p^2}t\right) \tag{24}$$

$$C_3(t)=\frac{\rho_p\varepsilon C_{pp}}{\rho_f(1-\varepsilon)C_{pf}}\frac{6Bi^2\alpha_p}{R_p^2}\sum_{n=1}^{\infty}\frac{\lambda_n^2+(Bi-1)^2}{\lambda_n^2+Bi(Bi-1)}\frac{\sin^2(\lambda_n)}{\lambda_n^2}\exp\left(-\frac{\lambda_n^2\alpha_p}{R_p^2}t\right) \tag{25}$$

and

$$C_4=-\frac{U_oA_c}{\rho_fV_{ce}(1-\varepsilon)C_{pf}} \tag{26}$$

Note that $C_3(t) = -(C_2(t) + C_4)$.

Equation (22), subject to the initial condition given by Eq. (3), was solved numerically for T_f using a 4th-order Runge-Kutta scheme. After the fluid temperatures were calculated, Eq. (12) was used to obtain the temperature of the

particle at any position and time. The integral appearing in Eq. (12) was evaluated using the trapezoidal rule. A problem concerning the convergence of Eq. (12) appears due to the numerical calculation of the integral. For $\lambda = t$, the exponential term drops out of the summation and the remaining series converges very slowly. To overcome this problem, the integral was divided into two parts; from $\lambda = 0$ to $\lambda = t - \Delta t$ and from $\lambda = t - \Delta t$ to $\lambda = t$, for Δt being the time step used for the numerical solution. By assuming

$$T_f(\lambda) = \frac{(T_f(t - \Delta t) + T_f(t))}{2} \quad \text{for } t - \Delta t \leq \lambda \leq t \tag{27}$$

then

$$\int_{\lambda=t-\Delta t}^{\lambda=t} (T_f(\lambda) - T_{pi}) \exp\left(-\frac{\lambda_n^2 \alpha_p}{R_p^2}(t-\lambda)\right) d\lambda = \frac{R_p^2}{\lambda_n^2 \alpha_p} \left[\frac{T_f(t-\Delta t) + T_f(t)}{2} - T_{pi}\right] \left(1 - \exp\left(-\frac{\lambda_n^2 \alpha_p}{R_p^2} \Delta t\right)\right) \tag{28}$$

Hence, due to Eq. (28) and the identity given by Eq. (14), from Eq. (12) we obtain

$$T_p(r_p, t) = \frac{T_f(t-\Delta t) + T_f(t)}{2} + \frac{2\alpha_p Bi}{r_p R_p} \sum_{n=1}^{\infty} \frac{\lambda_n^2 + (Bi-1)^2}{\lambda_n^2 + Bi(Bi-1)} \sin(\lambda_n) \sin\left(\lambda_n \frac{r_p}{R_p}\right) \int_{\lambda=0}^{\lambda=t-\Delta t} (T_f(\lambda) - T_{pi}) \exp\left(-\frac{\lambda_n^2 \alpha_p}{R_p^2}(t-\lambda)\right) d\lambda - \frac{2BiR_p}{r_p} \left[\frac{T_f(t-\Delta t) + T_f(t)}{2} - T_{pi}\right] \sum_{n=1}^{\infty} \frac{\lambda_n^2 + (Bi-1)^2}{\lambda_n^2 + Bi(Bi-1)} \frac{\sin(\lambda_n) \sin\left(\lambda_n \frac{r_p}{R_p}\right)}{\lambda_n^2} \exp\left(-\frac{\lambda_n^2 \alpha_p}{R_p^2} \Delta t\right) \tag{29}$$

Equation (29) was actually the equation used in the computer program to calculate the particle temperature. The error introduced due to the approximation made through Eq. (27) is of the same order as the error due to the numerical evaluation of the integral, and it diminishes at long times when the rate of change of the fluid temperature decreases.

A final topic in this section concerns the convergence of the series in Eq. (23) through Eq. (25). Using the 4th-order Runge-Kutta scheme to solve Eq. (22), it is necessary to calculate $C_1(t)$, $C_2(t)$, and $C_3(t)$ at $t = 0$. For $t = 0$, the

exponential term in Eq. (23) to (25) drops out, and as in the case just discussed, the series converges slowly. By the same reasoning used to arrive to Eq. (14), it can be shown that

$$2\mathrm{Bi}\sum_{n=1}^{\infty}\frac{\lambda_n^2+(\mathrm{Bi}-1)^2}{\lambda_n^2+\mathrm{Bi}(\mathrm{Bi}-1)}\frac{\sin^2(\lambda_n)}{\lambda_n^2}=1 \tag{30}$$

and

$$6\mathrm{Bi}^2\sum_{n=1}^{\infty}\frac{\lambda_n^2+(\mathrm{Bi}-1)^2}{\lambda_n^2+\mathrm{Bi}(\mathrm{Bi}-1)}\frac{\sin^2(\lambda_n)}{\lambda_n^4}=1 \tag{31}$$

Hence, for t = 0 using Eq. (30) and (31) in Eq. (23) and (24),

$$C_1(0)=1 \tag{32}$$

and

$$C_2(0)=\frac{U_oA_c}{\rho_f V_{ce}(1-\varepsilon)C_{pf}}+\frac{\rho_p\varepsilon C_{pp}}{\rho_f(1-\varepsilon)C_{pf}}3\mathrm{Bi}\frac{\alpha_p}{R_p^2} \tag{33}$$

$C_3(0)$ can be calculated as $C_3(0) = -(C_2(0) + C_4)$.

Using Eq. (29) for particle temperature calculations and Eq. (32) and (33) at t = 0 for fluid temperature calculations in the computer program, the series converged within 30 terms for the worst case (that is, for low thermal diffusivity spheres).

RESULTS AND DISCUSSION

Using the described mathematical procedure, fluid and particle surface temperature data were created for various cases and compared with predicted and experimental values from the literature. Furthermore, predicted and experimental particle surface temperatures were compared in terms of their effect on microbial destruction through the following equation (e.g. Ball and Olson 1957):

$$F_{T_{ref}}^{Z}=\int_0^t 10^{(T_{ps}(\lambda)-T_{ref})/z}d\lambda \tag{34}$$

Comparison with Analytical Data

Using Laplace transforms, Sawada and Merson (1986) obtained an analytical solution for fluidized bed sterilization of particulate foods in the limiting case of constant medium temperature, T_{st}, and equal initial temperatures for both liquid and particles (see also Sawada 1984). By redefining certain parameters, their solution can be used to predict fluid and particle temperature data for canned liquid/particulate foods (Stoforos 1988; Stoforos and Merson 1990). In Fig. 1 and 2 results obtained by the present method are compared with data created using Sawada and Merson's analytical solution. Fluid and particle surface temperatures are plotted for potato spheres (R_p = 0.0111 m) in deionized water, and for aluminum spheres (R_p = 0.0127 m) in silicone fluid (1.5 cst kinematic viscosity at 25C). For these and all subsequent figures, the values of V_{ce} = 0.00047 m^3 and A_c = 0.03565 m^2 were used, while the physical and thermal properties used (Table 1) were those reported by Hassan (1984). A 2.0 s time step was used with the numerical solution, T_{st} was assumed constant, at 100.0C, and initial temperatures of T_{pi} = T_{fi} = 28.5C were used.

For both cases, agreement between the present and the analytical solution was very good. For potato spheres in deionized water, maximum temperature differences between the analytical and the present solution occurred for the fluid at about 40 s where ΔT_f was 1.17C, and for the particle surface at about 60 s with maximum ΔT_{ps} of 0.54C. For aluminum spheres in silicone fluid,

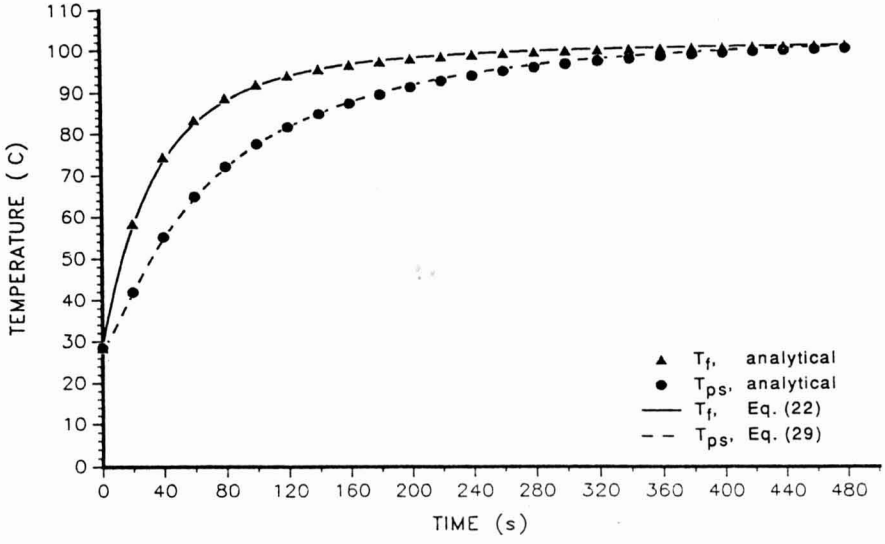

FIG. 1. COMPARISON WITH ANALYTICAL RESULTS (SAWADA 1984) FOR POTATO SPHERES IN DEIONIZED WATER
U_o = 1100 W/m²K, Bi = 5.1.

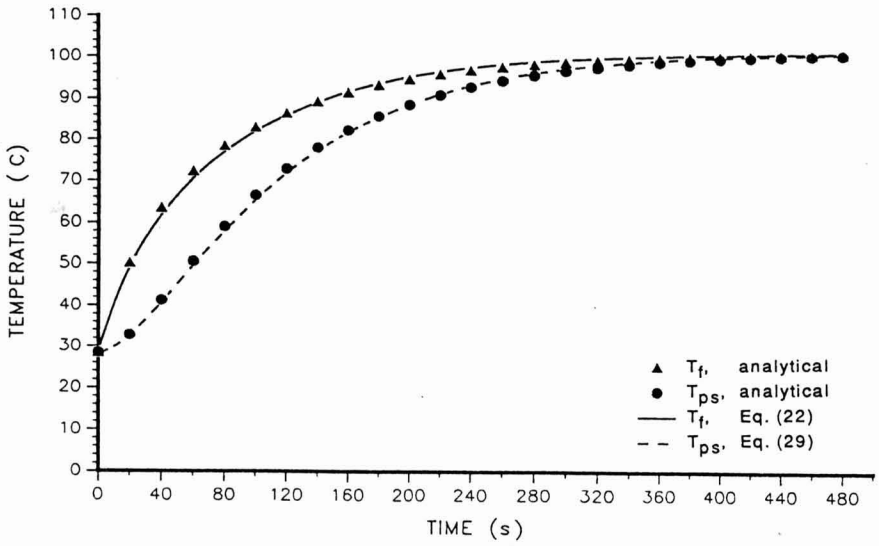

FIG. 2.COMPARISON WITH ANALYTICAL RESULTS (SAWADA 1984) FOR ALUMINUM SPHERES IN 1.5 cst SILICONE FLUID
U_o = 311.7 W/m²K, Bi = 0.0137.

TABLE 1.
THERMAL AND PHYSICAL PROPERTIES AND EXPERIMENTAL DESIGN PARAMETERS USED FOR SIMULATION

	Potato Spheres in Deionized Water	Aluminum Spheres in 1.5 cst Silicon Fluid
ρ_f (kg/m³)	981.1	850.5
C_{pf} (J/kgK)	4183	1770
ρp (kg/m³)	1063	2880
C_{pp}(J/kgK)	3517	896
k_p (W/mK)	0.62	204.3
α_p (m²/s)	1.66×10^{-7}	81.42×10^{-6}
R_p (m)	0.0111	0.0127
ε	0.29	0.20
N (rpm)	9.3	9.3

maximum ΔT_f of 1.80C was observed at about 60 s, and maximum ΔT_{ps} of 1.22C at 100 s. Due to the assumption in deriving Eq. (22) that $T_f(\lambda) = T_f(t)$, for $0 \leq \lambda \leq t$, it is expected that maximum temperature differences will occur at times close (but not equal) to the beginning of heating, where the rate of change of T_f is greatest. Times where maximum temperature differences occurred were later for the silicone fluid, which heated more slowly than water.

A common pattern can be identified in Fig. 1 and 2. Our method predicts initially lower T_f and T_{ps} values compared to analytical ones, but after some time, the temperatures predicted by our method are slightly higher than the analytical values. This can be explained by examining the $d<T_p>/dt$ term where $<T_p(t)>$ is our first estimate of the average particle temperature history, given by Eq. (18). Due to the assumed fluid temperature function, Eq. (18) overestimates $<T_p>$. This means that the predicted average particle temperature [from Eq. (18)] rises faster than the actual $<T_p>$ at the beginning of heating, but, due to the asymptotic nature of the temperature increase, after some time the predicted average particle temperature approaches the final $<T_p>$ earlier which results in a slower heating rate after that time. In order for Eq. (22) to be satisfied, T_f must behave in a complementary way. Therefore, our predicted fluid temperatures initially lag behind the analytical ones, but after some heating time, they tend to be higher than the analytical values.

Finally, since particle temperatures are evaluated by Eq. (29) and are directly dependent on T_f values, T_p data follow the same pattern as T_f data.

This reasoning leads to the conclusion that repeated iterations between Eq. (22) and (29) would provide a more accurate solution. This was indeed the case. One more iteration improved our results while further iterations left the values practically unchanged (fluid temperatures differed by less than 0.2C for the worst case). However, to include one more iteration to the solution we must use discrete $<T_p>$ data and solve Eq. (2) instead of Eq. (22). This results in a considerable increase in computation time and, considering the agreement of our method with analytical results, the iterations were not adopted.

Comparison with Lenz and Lund's Method

In Fig. 3, the ideas used to develop our procedure are compared with those used by Lenz and Lund (1978). A value of Bi = 0.0137, corresponding to the experimental findings of Hassan (1984), was used. The two fluid temperature curves presented in Fig. 3 are for the cases of fluid processed with and without particles. The lower T_f curve is obtained using Eq. (22) with U_o = 311.7 W/m^2K, and it is assumed to represent true T_f data for fluid processed with particles. Lenz and Lund used Eq. (12) to obtain particle temperatures, using T_f values obtained for the case of liquid processed without particles. In order to simulate their method, such fluid temperature data were obtained using Eq. (35), that is, assuming constant heating medium temperature

$$T_f(t)=T_{st}-(T_{st}-T_{fi})\exp(-\frac{hA_c}{m_fC_{pf}}t) \tag{35}$$

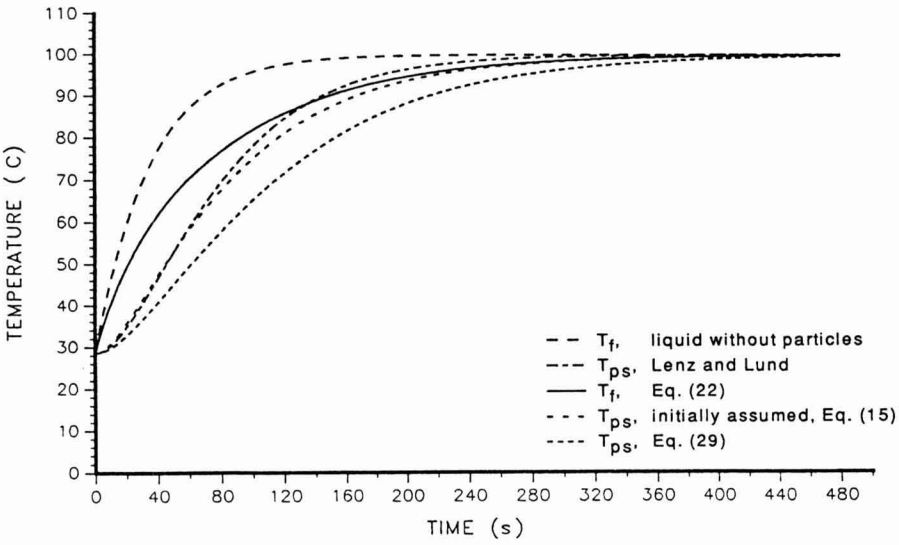

FIG. 3.COMPARISON WITH LENZ AND LUND'S (1978) METHOD FOR ALUMINUM SPHERES IN 1.5 cst SILICONE FLUID
T_{st} = 100C (constant), $T_{fi} = T_{pi}$ = 28.5C.

In order to use Eq. (35), the value of the heat transfer coefficient, h, must be known. Lenz and Lund (1978) reported higher heat transfer coefficients for the case of liquid processed without particles than with particles. From their data, h values for fluids without particles can be as much as three times higher than h values for fluids with particles. Therefore, a moderate value of h = 450 W/m^2K (about 1.5 times higher than U_o = 311.7 W/m^2K) was selected to create fluid temperature data associated with Lenz and Lund's method.

The importance of h should be emphasized, since, as will be shown later, this is the main parameter determining the accuracy of the Lenz and Lund method. Using the fluid temperature data created for h = 450 W/m^2K and Eq. (29) we created particle surface temperature data corresponding to Lenz and Lund's solution. Using the fluid temperature data created for U_o = 311.7 W/m^2K and Eq. (29) we created particle surface temperature data corresponding to our method. Particle surface temperatures were also created using Eq. (15) and the T_f values for U_o = 311.7 W/m^2K. These data correspond to our initially assumed $T_p(r_p,t)$ function. As Fig. 3 shows, even these T_{ps} data are more accurate than final T_{ps} predictions by Lenz and Lund. Hence, although we do not present the final solution for T_f obtained by Lenz and Lund's method, it is clear that it is less accurate than our solution, since their data are based on the previously discussed T_p curve.

Another interesting result that can be seen from Fig. 3 is that the T_{ps} values predicted by Lenz and Lund can be even higher than the true T_f data. This is, of course, due to using the assumed T_f curve for fluid without particles. It is clear that the accuracy of the Lenz and Lund method depends on the magnitude of the differences of fluid temperatures for fluid processed with and without particles. This is something that they cannot control during their solution. Lenz and Lund reported good agreement between predicted and experimental values for the temperature at the center of a plastic sphere. This is to be expected for their experimental conditions since they heated the monitored sphere in the absence of additional particles. Hence, fluid temperature values for liquid alone or liquid with the single plastic sphere should be practically identical. As is also true for our method, the accuracy of Lenz and Lund's method can be improved if the temperature solutions are used iteratively.

Comparison with Experimental Data

Using the present method and the heat transfer coefficients obtained experimentally by Hassan (1984) for potato spheres in deionized water, the temperature data presented in Fig. 4 were created. In contrast to Fig. 1, temperature data presented in Fig. 4 were obtained using discrete time-varying T_{st} data, the ones obtained experimentally by Hassan (1984). In addition, T_{fi} was different than T_{pi}. Predicted and experimental fluid temperatures (Hassan 1984)

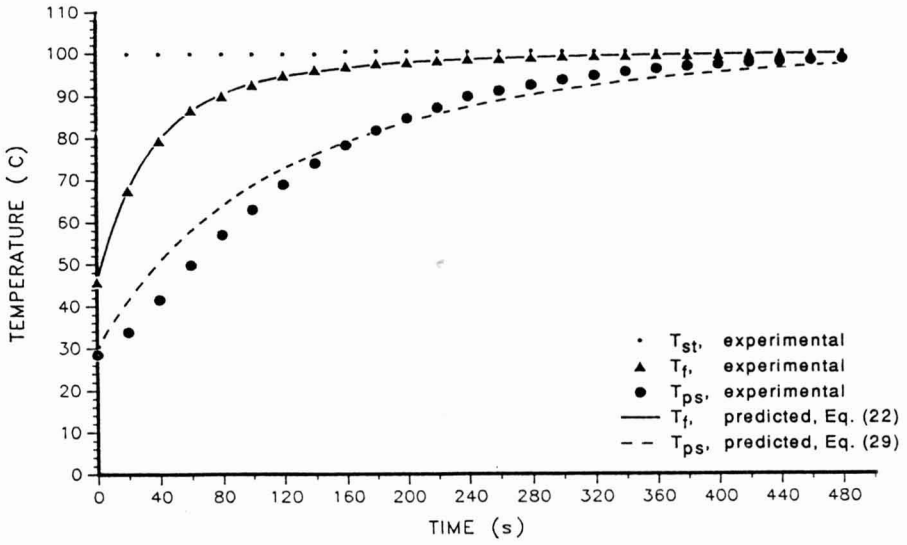

FIG. 4. COMPARISON WITH EXPERIMENTAL DATA (HASSAN 1984) FOR POTATO SPHERES IN DEIONIZED WATER
U_o = 1099 W/m^{2}K, Bi = 2.55, T_{fi} = 45.8C, T_{pi} = 28.5C.

were in good agreement. However, particle surface data deviated significantly. For the data presented in Fig. 4, the differences between predicted and experimental particle surface temperatures are shown in Fig. 5. The pattern of differences between predicted and experimental T_{ps} values was similar to the one observed by Rumsey (1984). Predicted values were higher than the experimental ones at the beginning of heating, but subsequently, they were lagging behind the experimental curve. The following two reasons were considered as possible explanation for this discrepancy. First, the experimental particle temperatures might be erroneous due to the experimental methodology followed (Stoforos 1988). The data obtained by Hassan (1984) by monitoring the surface temperature, through a thermocouple, of a particle restricted at the center of the can are not necessarily representative for the rest of the free moving particles (Merson and Stoforos 1990). Second, the use of average, constant, values for the heat transfer coefficients (in particular h_p) might not be appropriate (especially as measured at the fixed particle). By observing Fig. 5, we can conclude that a new, lower, value for the liquid-particle film heat transfer coefficient will fit better the experimental data at the beginning of heating; for example at 40 s. However, in order to fit the experimental data at subsequent times, e.g., at 60 s, this new value for h_p must be increased (since the difference between predicted and experimental data at 60 s is lower than the difference at 40 s). (Note an apparent deviation at 20 s which is a result of the imposed initial condition and the particular numerical Δt value used.) This reasoning suggests a time (temperature) dependant liquid-particle film heat transfer coefficient which gradually increases approaching a constant value, higher than the average

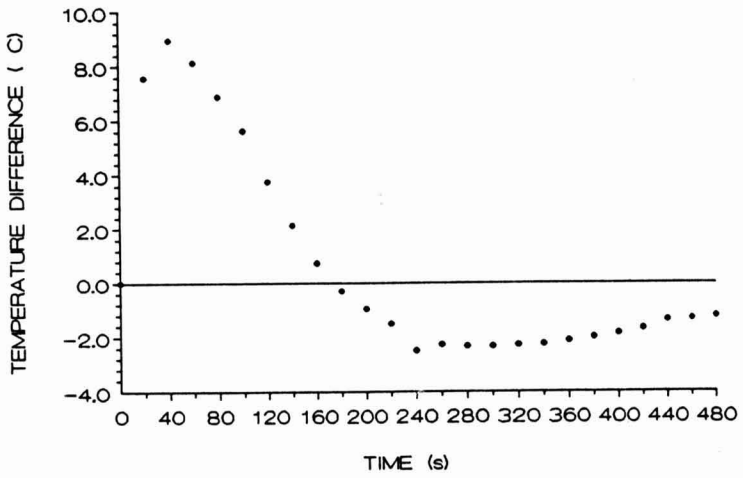

FIG. 5. PARTICLE SURFACE TEMPERATURE DIFFERENCES (PREDICTED MINUS EXPERIMENTAL VALUES) FOR POTATO SPHERES IN DEIONIZED WATER
U_o = 1099 W/m^{2}K, Bi = 2.55, T_{fi} = 45.8C, T_{pI} = 28.5C.

value calculated by Hassan (1984) and used with the model. This is not unrealistic, especially for the particular experimental data used here; for the particle fixed at the can center through a stiff thermocouple, and being so rotated at the constant can rotational speed, the relative fluid to particle velocity (a parameter directly affecting h_p) is expected to increase as the fluid viscosity decreases at increasing temperatures. Note however, that the above mentioned behavior for h_p is not necessarily the case for unrestricted, free moving, particles.

As expected, temperature differences were amplified when used to calculate process F values. Using Eq. (34) with the particle surface temperature data presented in Fig. 4 and for T_{ref} = 100C and z = 9C, the following F values, F = 1.06 min and F = 1.66 min, were calculated for the predicted and experimental temperatures, respectively.

Effect of Heat Transfer Coefficients on Fluid and Particle Temperatures

Equations (22) through (26) present the fluid temperature as a function of the Biot number (and, hence, of h_p). Therefore, in principle, we could use Eq. (22) together with experimental fluid temperature to predict h_p values, thus eliminating the need for obtaining ambiguous particle temperature data. However, despite concerted efforts, we were unable to calculate reliable h_p values when Eq. (22) was used for T_f predictions. The reason is that fluid temperature is not a strong function of h_p. Considering the accuracy of our solution, the error in T_f predictions introduced by our method is high relative to fluid temperature differences which result from varying the h_p value. Figure 6 shows predicted T_f data for the case of potato spheres in deionized water for various U_o and h_p values. Note that T_f is strongly dependent on U_o but only slightly on h_p. Differences of about 20% in h_p values result in differences in T_f values within the error introduced by our method. Hence, our method cannot be used to predict h_p values based only on T_f experimental data.

As would be expected, in contrast to fluid temperatures, particle surface temperatures are strongly dependent on h_p, as seen in Fig. 7. Therefore, provided that reliable experimental data for both fluid and particle surface temperatures exist, our method can be used to obtain heat transfer coefficients. For this method, only a few discrete T_f and T_p measurements are enough to estimate U_o and h_p values. For coefficient determination, our method overcomes weaknesses of other methods: The method used by Lenz and Lund (1978) is restricted to high thermal conductivity particles, while the method of Hassan (1984; Deniston *et al.* 1987) needs complete time-temperature histories for both fluid and particle surface. On the other hand, if our method is used to fit experimental T_f and T_p data for the heat transfer coefficients, the computer time requirement could be of concern.

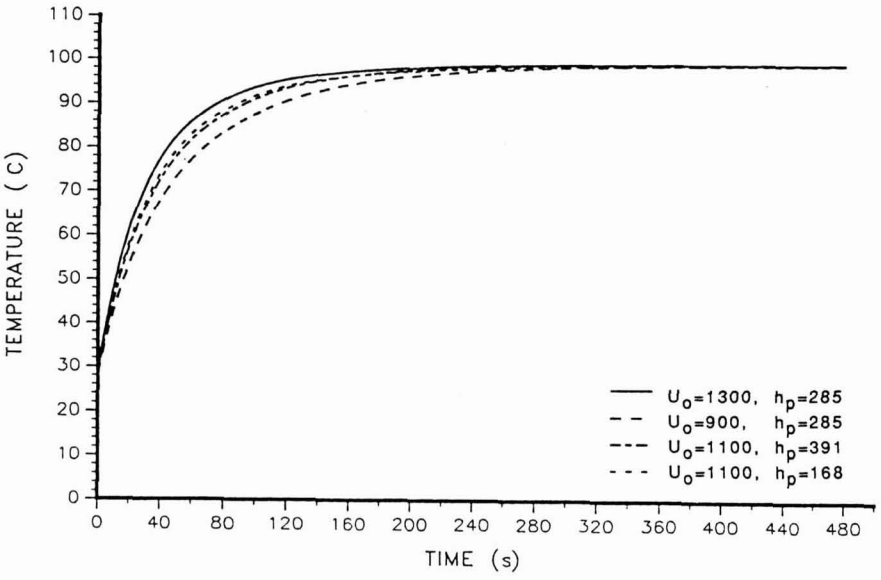

FIG. 6. EFFECT OF U_o AND h_p ON FLUID TEMPERATURE FOR POTATO SPHERES IN DEIONIZED WATER

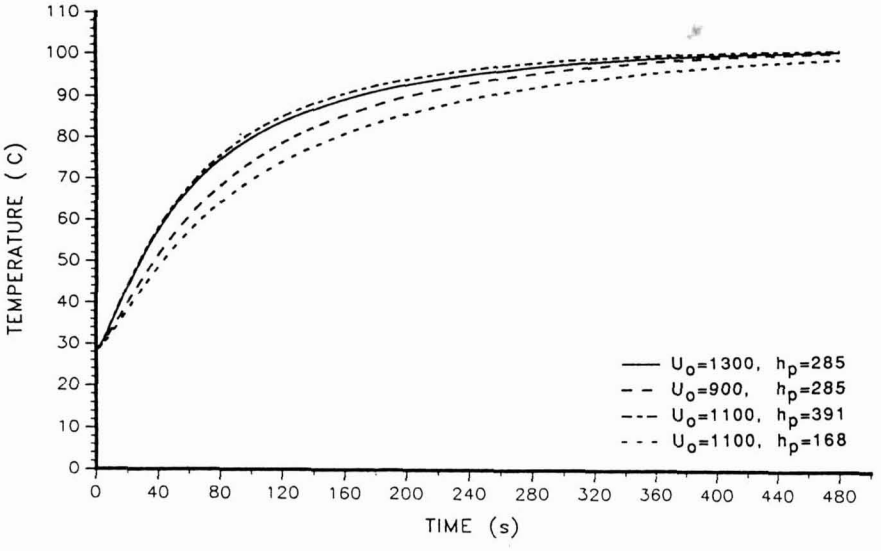

FIG. 7. EFFECT OF U_o AND h_p ON PARTICLE SURFACE TEMPERATURE FOR POTATO SPHERES IN DEIONIZED WATER

SUMMARY AND CONCLUSION

The proposed solution has been proven to give accurate predictions for fluid and particle temperatures for the case of thermal processing of axially rotated canned liquid/particulate food systems. Such temperature predictions, coupled with microbial and quality destruction data, are valuable to the food industry in designing thermal processes. With slight modification of the coefficients appearing in the governing equations, this method can be used to predict temperature data for the case of bulk heating of particulate foods in fluidized beds or other aseptic processes of liquid/particulate foods, under steady state conditions, provided that the liquid temperature is uniform in the radial direction. Time-dependent heating medium temperatures can be easily handled. To use the proposed method, the heat transfer coefficients U_0 and h_p must be known. Alternatively, the solution can be used to fit experimental fluid and particle data for the heat transfer coefficients.

NOMENCLATURE

A_c	Can surface area, m^2
Bi	Biot number, $Bi = h_p R_p/k_p$, dimensionless
C_{pf}	Specific heat of fluid, J/kgK
C_{pp}	Specific heat of particle, J/kgK
$C_1(t)$	Coefficient in Eq. (22) given by Eq. (23), dimensionless
$C_2(t)$	Coefficient in Eq. (22) given by Eq. (24), dimensionless
$C_3(t)$	Coefficient in Eq. (22) given by Eq. (25), dimensionless
C_4	Coefficient in Eq. (22) given by Eq. (26), dimensionless
F^z_{Tref}	(Or simply F) time at a constant reference temperature, T_{ref}, required to destroy a given percentage of microorganisms whose thermal resistance is characterized by z, s
h	Heat transfer coefficient, W/m^2K
h_p	Liquid-particle film heat transfer coefficient, W/m^2K
k_p	Thermal conductivity of particle, W/mk
m_f	Mass of fluid, kg
m_p	Mass of particles, kg
N	Can rotational speed, revolutions per minute
R_p	Particle radius, m
r_p	Particle radial distance, m
T_f	Fluid temperature, C
T_{fi}	Initial fluid temperature, C
T_p	Particle temperature, C
T_{pi}	Initial particle temperature, C
T_{ps}	Particle surface temperature, C

T_{ref} Reference temperature, C
T_{st} Heating medium temperature, C
t Heating time, s
U_o Overall heat transfer coefficient, W/m^2K
$U(r_p,t)$ Particle temperature, (see Eq. (8)), C
V_{ce} Effective can volume, m^3
$V_p(r_p,t)$ Particle temperature, Eq. (8), C
v_p Particle volume, m^3
z Temperature interval required for the time required to destroy a certain percentage of microorganisms to traverse a logarithmic cycle, C

Greek Letters

α_p Thermal diffusivity of particle, $\alpha_p = k_p/\rho pC_{pp}$, m^2/s
ε Volume fraction occupied by the particles, dimensionless
λ Dummy time variable, s
λ_n Nth eigenvalue, given by Eq. (10), dimensionless
ρ_f Fluid density, kg/m^3
ρ_p Particle density, kg/m^3
σ Function defined by Eq. (19), dimensionless
$\Phi(t)$ Time-dependent heating medium temperature, see Eq. (8), C

Symbols

$< >$ Volume average
Δ Increment

REFERENCES

ARMENANTE, P.M. and LESKOWICZ, M.A. 1990. Design of continuous sterilization systems for fermentation media containing suspended solids. Biotechnol. Prog. *6*, 292–306.

BALL, C.O. and OLSON, F.C.W. 1957. *Sterilization in Food Technology. Theory, Practice, and Calculations*, McGraw-Hill Book Co., New York.

CARSLAW, H.S. and JAEGER, J.C. 1959. *Conduction of Heat in Solids*, 2nd Ed., Clarendon Press, Oxford, England.

CHANDARANA, D.I. and GAVIN, A. III, 1989. Establishing thermal processes for heterogeneous foods to be processed aseptically: A theoretical comparison of process development methods. J. Food Sci. *54*(1), 198–204.

CHANG, S.Y. and TOLEDO, R.T. 1989. Heat transfer and simulated sterilization of particulate solids in a continuously flowing system. J. Food Sci. *54*(4), 1017–1023, 1030.

CHANG, T.M. and WEN, C.Y. 1966. Fluid-to-particle heat transfer in air-fluidized beds. Chem. Eng. Prog. Symp. Ser. No. 67, *62*, 111–117.

DENISTON, M.F., HASSAN, B.H. and MERSON, R.L. 1987. Heat transfer coefficients to liquids with food particles in axially rotating cans. J. Food Sci. *52*, 962–966, 979.

DE RUYTER, P.W. and BRUNET, R. 1973. Estimation of process conditions for continuous sterilization of foods containing particulates. Food Technol. *27*(7), 44–51.

HASSAN, B.H. 1984. Heat transfer coefficients for particles in liquid in axially rotating cans. Ph.D. thesis, Dept. of Agricultural Engineering, Univ. of California, Davis, CA.

HEMMINGS J.W. and KERN, J. 1979. The non-adiabatic calorimeter problem and its application to transfer processes in suspensions of solids. Int. J. Heat Mass Transfer *22*, 99–109.

HILDEBRAND, F.B. 1976. *Advanced Calculus for Applications*, 2nd Ed., Prentice-Hall, Englewood Cliffs, NJ.

LEE, J.H. and SINGH, R.K. 1990. Determination of lethality and processing time in a continuous sterilization system containing particulates. J. Food Eng. *11*, 67–92.

LEKWAUWA, A.N. and HAYAKAWA, K. 1986. Computerized model for the prediction of thermal responses of packaged solid liquid food mixture undergoing thermal processes. J. Food Sci. *51*(4), 1042–1049, 1056.

LENZ, M.K. and LUND, D.B. 1978. The lethality-Fourier number method. Heating rate variations and lethality confidence intervals for forced-convection heated foods in containers. J. Food Proc. Eng. *2*, 227–271.

MANSON, J.E. and CULLEN, J.F. 1974. Thermal process simulation for aseptic processing of foods containing discrete particulate matter. J. Food Sci. *39*, 1084–1089.

MERSON, R.L. and SAWADA, H. 1991. An analytical solution for modeling heat-hold-cool sterilization of particulate-containing foods. Presented at the Conf. of Food Engineering: Advances and Technologies, Mar. 10–12, Chicago, IL.

MERSON, R. L. and STOFOROS, N.G. 1990. Motion of spherical particles in axially rotating cans. Effect on liquid-particle heat transfer. In *Engineering and Food, Vol. 2, Preservation Processes and Related Techniques*, (W.E.L. Spiess and H. Schubert, eds.) pp. 60–69, Elsevier Applied Science Publishers, Essex, England.

MERSON, R. L. and WOLCOTT, T.K. 1986. Recent developments in thermal process design. In *Food Engineering and Process Applications*, (M. LeMaguer and P. Jelen, eds.), Vol. 1, pp. 501–520, Elsevier Science Publishing Co., New York.

MYERS, G. 1971. *Analytical Methods in Conduction Heat Transfer*, McGraw-Hill Book Co., New York.

RAO, M.A. and ANANTHESWARAN, R.C. 1987. Convective heat transfer to fluid foods in cans. In *Advances in Food Research*, (C.O. Chichester, E.M. Mrak and B.S. Schweigert, eds.), Vol. 32, pp. 39–84, Academic Press, New York.

RUMSEY, T.R. 1984. Modeling heat transfer in cans containing liquid and particles. Paper #84-6515 presented at the Winter Meeting of ASAE, New Orleans, LA.

SASTRY, S.K. 1986. Mathematical evaluation of process schedules for aseptic processing of low-acid foods containing discrete particulates. J. Food Sci. *51*(5), 1323–1328, 1332.

SAWADA, H. 1984. Estimation of process conditions for bulk sterilization of particulate foods in water fluidized beds. M.S. thesis, Dept. of Food Science and Technology, Univ. of California, Davis, CA.

SAWADA, H. and MERSON, R.L. 1986. Estimation of process conditions for bulk sterilization of particulate foods in water-fluidized beds. In *Food Engineering and Process Applications*, (M. LeMaguer and P. Jelen, eds.), Vol. 1, pp. 569–581, Elsevier Science Publishing Co., New York.

STOFOROS, N.G. 1988. Heat transfer in axially rotating canned liquid/particulate food systems. Ph.D. thesis, Dept. of Agricultural Engineering, Univ. of California, Davis, CA.

STOFOROS, N.G. and MERSON, R.L. 1990. Estimating heat transfer coefficients in liquid/particulate canned foods using only liquid temperature data. J. Food Sci. *55*(2), 478–483, 521.

KINETICS OF OSMOTIC DEHYDRATION OF COCONUT

N.K. RASTOGI and K.S.M.S. RAGHAVARAO[1]

Department of Food Engineering
Central Food Technological Research Institute
Mysore-570013, India

Accepted for Publication July 20, 1994

ABSTRACT

Osmotic dehydration rates were determined for coconut over a range of osmotic solution concentration (40–70°B) and temperature (25–45C). A semi-empirical relation for kinetics of osmotic dehydration has been proposed, which indicates the moisture diffusion as a function of concentration of osmotic solution and its temperature. Good agreement was observed between the observed and predicted values (correlation coefficient 0.90). The effective diffusion coefficients of water in coconut during osmotic dehydration were estimated and also the activation energy of the osmotic dehydration process of coconut was found as 1.75×10^4 *J/kg-mole.*

INTRODUCTION

The process of osmosis can be used to remove water from a dilute solution retained within a semipermeable membrane by surrounding it with a more concentrated solution, water diffuses through the membrane from the dilute to the concentrated solution until an equilibrium is reached. The solute is unable to diffuse through membrane in the reverse direction or can do so only very slowly, so that the net result of this process is a transfer of water to a concentrated solution. However, when the processing time is quite high considerable diffusion of the osmotic solute from the solution in the reverse direction was observed (Ponting 1973).

Osmotic dehydration is a dynamic process in which water and acid (if available in the food material) diffuse into the concentrated osmotic solution rapidly in the beginning and at a relatively slow rate later while the solute diffusion to the food material is relatively slow in the beginning and increases with increasing immersion time (Ponting 1973).

[1]Corresponding author.

Journal of Food Process Engineering **18** (1995) 187–197.

In general, osmotic dehydration is used in upstream processing for partial dehydration of plant or animal foods such as fruits, vegetables, fish, etc., before they are subjected to further processing viz: freezing (Ponting 1973), freeze drying (Hawkes and Flink 1978), vacuum drying (Dixon and Jen 1977), air drying (Nanjundaswamy *et al.* 1978).

However, the purpose of the present work is entirely different. When coconut is cut along the major axis, it results in two pieces of elliptical shape. The shells have an export market as they are used as ice-cream bowls, and are biodegradable. Here the aim is to exploit osmotic dehydration for the separation of the coconut kernel from the shell, a task which otherwise needs tedious manual labor. The kernel is used for further processing with improved taste imparted by an osmotic agent.

The other major application is to reduce the water activity of many food materials so that microbial growth will be inhibited to a large extent. Since most of the food contains large amounts of water, it is cost intensive to ship, pack and store (Rao 1977, Biswal and Le Maguer 1989). Osmotic dehydration has been identified and implemented as one of the energy efficient methods of partial dehydration, since there is no need for an energy intensive phase change (Bolin *et al.* 1983). Moreover, as the feed is not subjected to a high temperature during osmotic dehydration, the heat damage to color and flavor is minimal.

In order to make the osmotic dehydration step a economically feasible one, the osmotic solution needs to be reconcentrated by some means either evaporation or addition of fresh osmotic reagent. It should be noted that in the present case, the extent of dehydration required for the separation of kernel from the shell is not as high as the other cases (only 30% of the water present in the coconut). This makes the reconcentration step an economically viable one. Further, it has been observed that repeated reconcentration is not having any countereffect on the product characteristics.

Many salts and saccharides (mono, di and poly) are used as osmotic agents. Basically the resulting osmotic solution should be harmless, of low water activity and of acceptable taste. Among salts, sodium chloride was found to be an excellent osmotic agent (Lerici *et al.* 1985), but its application is limited because of the salty taste it imparts to the food (Hawkes and Flink 1978). Sucrose, among saccarides, has been widely used as an osmotic agent due to several advantages it offers. Sucrose prevents food discolorization to a large extent by enzymic oxidative browning by its inhibitive capacity towards polyphenol oxidase enzyme (Ponting 1973). Further, it imparts good taste to the food material. Sucrose being a disaccharide, has lower diffusivity when compared with other osmotic agents (Chandrasekhran and King 1972), so less of it will be absorbed by the food material, making it an ideal choice as osmotic agent.

In general, the rate of osmotic dehydration is a function of concentration and temperature of osmotic solution, immersion time, solution to food ratio and

specific surface area. Hence a systematic study of the effect of most of these parameters on the kinetics of osmotic dehydration was conducted. Semiempirical model equation has been proposed for the diffusional water loss.

PREVIOUS WORK

Many authors (Farkas and Lazar 1969; Convey *et al.* 1983; Rahman *et al.* 1990) have investigated the effect of temperature and solute concentration on the kinetics of osmotic dehydration of different food materials. No information is available in the literature regarding osmotic dehydration of coconut and its advantages. Out of the available information for the other food material, very little information is available regarding the mathematical modelling or kinetics of osmotic dehydration. Most of the available information is in the form of empirical relations.

Farkas and Lazar (1969), suggested an empirical equation relating concentration of osmotic solution, its temperature, immersion time and weight loss. Contreras and Smyrl (1981), incorporated the effect of pH on weight loss during osmotic dehydration. Conway *et al.* (1983), proposed a model based on Fick's second law of diffusion. Andreotti *et al.* (1983), and Rahman and Lamb (1990), have given empirical equations for weight loss as a function of time, in which it was shown that weight loss in osmotic dehydration is proportional to square root of the immersion time.

THEORETICAL CONSIDERATIONS

The following equation for osmotic dehydration is written assuming an exponential approach to equilibrium, (Zugarramurdi and Lupin 1977)

$$-dM/dt = K_T(M-M_e) \quad (1)$$

where dM/dt is rate of osmotic dehydration, M is moisture content at any time t, Me is equilibrium moisture content and K_T is defined as an osmotic dehydration rate constant. The negative sign accounts for the fact that M is decreasing with time.

The general equation for mass transfer is given by

$$dC/dt = k.a(C^* - C) \quad (2)$$

where C and C* are the concentration at time 't' and at equilibrium, respectively, and k.a is the overall mass transfer coefficient. On comparison of Eq. 1 and 2, it can be noticed that K_T is similar to the overall mass transfer coefficient (k.a), where 'a' is specific area and 'k' is the individual mass transfer coefficient. For diffusion through solids, k in turn can be expressed as D_e/L_c, where

D_e is effective diffusion coefficient and L_c is characteristic length. Hence K_T can be expressed as

$$K_T = (D_e.a)/L_c \quad (3)$$

where D_e is effective diffusion coefficient of water in coconut, 'a' the specific area per unit volume and L_c the characteristic length (in the present case it is the thickness of the coconut piece). For similar effective diffusion coefficients in coconuts of different sizes and shapes, the rate of water removal due to osmotic dehydration will largely depend upon the factor a/L_c. Similar analysis for different situations is given by Tanaka and Yoshida (1984), Zugarramurdi and Lupin (1980), Heldman and Singh (1980) and Treybal (1968).

The dependence of 'De' on temperature is assumed to follow the Arrhenius equation

$$D_e = D_0 Exp(-A/RT) \quad (4)$$

where D_0 is a constant, A is the activation energy and R is the gas constant. It should be noted that in the above equation D_0 is dependent on the concentration of the osmotic solution, specific area and characteristic length, which was found empirically by a regression method.

$$D_0.a/L_c = 6.9B+202.66 \quad (5)$$

Substituting the value of the D_0 in Eq.(4), the value of D_e can be obtained. The value of K_T for different sizes and shapes can be obtained from Eq. (3). Solution of differential Eq. (1) can be written, with initial condition t = 0, M = M_0, as

$$M = M_e[1 - Exp(-D_e.a/L_c)t] + M_0 Exp(-D_e.a/L_c) \quad (6)$$

Theoretically, the moisture content at any time can be obtained by substituting the values of initial and equilibrium moisture contents and osmotic dehydration rate constant.

MATERIALS AND METHODS

Mature coconuts were taken from the local market. The shell of the coconut was manually removed. From the coconut kernel, thus obtained, six circular pieces of the diameter 25 mm and of thickness 7mm were cut. Sucrose syrup was used as an osmotic agent. A ratio of food/syrup 1:5 by weight was used.

Experiments were carried out by changing the concentration of syrup and temperature, from 40–70°B and 25–45°C, respectively. Four cans, each containing 400g sucrose solution of different concentration (viz: 40, 50, 60, 70°B, were kept in a constant temperature water bath. Weighed and numbered (1–6) pieces of the coconut were kept in each of the cans. At intervals of one

hour, pieces were taken out in serial order, rinsed in a stream of water and surface water was removed with tissue paper. Water present after osmotic dehydration was determined by taking the difference of the weight of a piece of coconut after osmotic dehydration (Y) and the weight of dry solid (Z). After osmotic dehydration the pieces were kept in oven at 100–110C in order to find out total solids (Z). The same exercise was repeated for different combinations of concentration of osmotic solution and its temperature. Each experiment was performed in triplicate and the average value was taken. The moisture content M (kg of water / kg of dry solid) was calculated with the assumption that no diffusion of solid is taking place either from coconut to the osmotic solution or from solution to the coconut. The correction factor to account for the variation in the initial weight of each sample (of same size) is incorporated in the calculations. The moisture content is calculated as

$$M \text{ (kg of water / kg of dry solid)} = (Y-Z)/Z \qquad (7)$$

RESULTS AND DISCUSSION

The moisture content (M) at various immersion times during the course of osmotic dehydration was experimentally determined over a range of temperature (25–35C) and concentration of osmotic solution (40–70°B). A typical plot of variation of moisture content with immersion time for 70°B and 35C is shown in Fig. 1. The rate of change of moisture content ($-dM/dt$) is deduced at different moisture levels from similar plots, as that shown in Fig. 1, over the entire range of temperature and concentration of osmotic solution. A typical plot of rate of change of moisture content, thus obtained, versus average moisture content is shown in Fig. 2. The slope of line gives the osmotic dehydration rate constant (K_T) and equilibrium moisture content (M_e) is inferred from the intercept. Fig. 3 shows that the dependence of effective diffusion coefficient (D_e) on temperature, follows the relationship given by Arrhenius (Eq. 4). The slope of the straight line (in Fig. 3) is used to determine the activation energy of the osmotic dehydration process and it is found to be 1.75×10^4 J/kg-mole in the present case. However, it was observed that the factor $(D_0.a)/L_c$ in turn depends on the concentration of osmotic solution. Hence by regression method a relationship between $(D_0.a)/L_c$ and concentration was obtained as shown in Eq. 5. A comparison between experimental and theoretical values of effective diffusion coefficient is shown in Fig. 4 and can be observed that agreement is very good. The order of the magnitude of the values of D_e is same as those reported in literature (Auzara *et al.* 1992; Favetto *et al.*1981, Beristain *et al.*

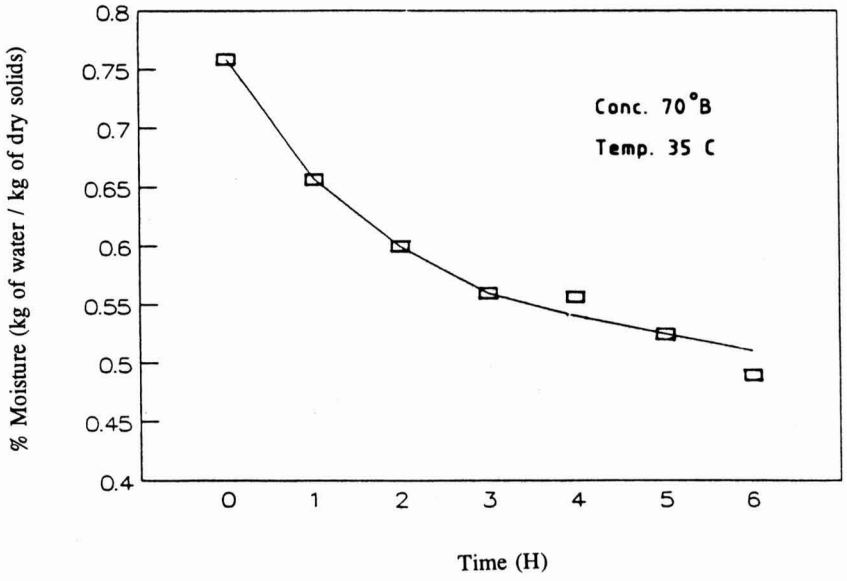

FIG. 1. VARIATION OF MOISTURE CONTENT WITH TIME

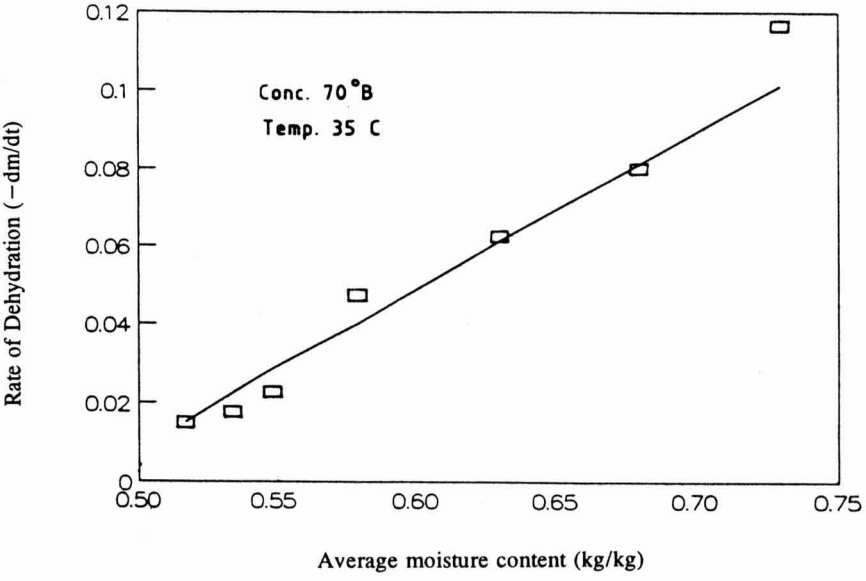

FIG. 2. RATE OF DEHYDRATION VERSUS AVERAGE MOISTURE CONTENT

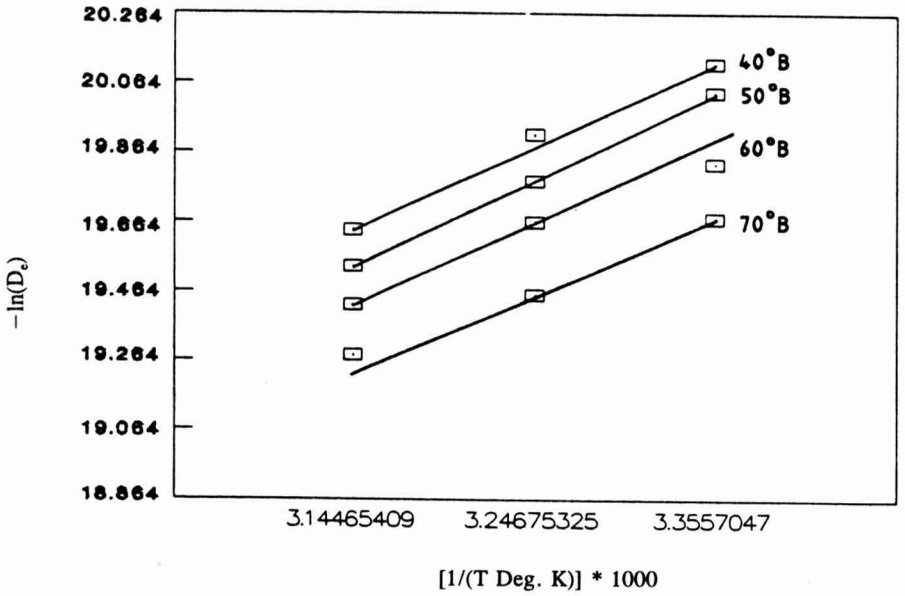

FIG. 3. ARRHENIUS PLOT

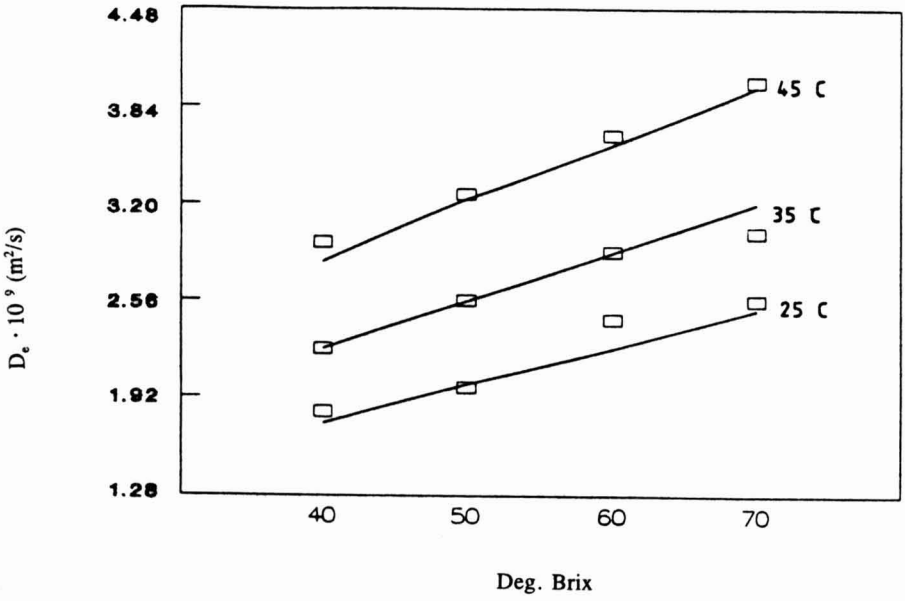

FIG. 4. EFFECT OF CONCENTRATION ON D_e

1990). However, the values of D_e obtained in the present study are slightly lower than those reported for food materials such as pineapple and beef which can be appreciated by the fact that coconut has relatively less porous structure.

Theoretically, the moisture content at any given immersion time was calculated from Eq. 6 by substituting the values of D_e (which in turn is obtained from Eq. 4 and 5), specific area, characteristic length, initial and equilibrium moisture contents. Figure 5 shows a typical plot for comparison of theoretical values of moisture content, thus obtained with experimental ones, at 70°B and 35C. It is clear from the figure that the proposed relation fits the experimental results fairly well (correlation coefficient O.95).

By observing similar plots prepared for other process conditions, it appeared that the discrepancy of experimental data from the curve of the proposed relation (Eq. 6) is relatively more at higher temperatures for any given concentration of osmotic solution (correlation coefficient 0.90). The probable reason could be the impairment of the selectivity of the cell membrane at higher temperatures. Further, at any given concentration and temperature, there is a little discrepancy of the experimental values from theoretical ones towards the end of the osmotic dehydration process. Perhaps the assumption that no diffusion of solid is taking place in either way may not be as valid towards the end of the osmotic dehydration process.

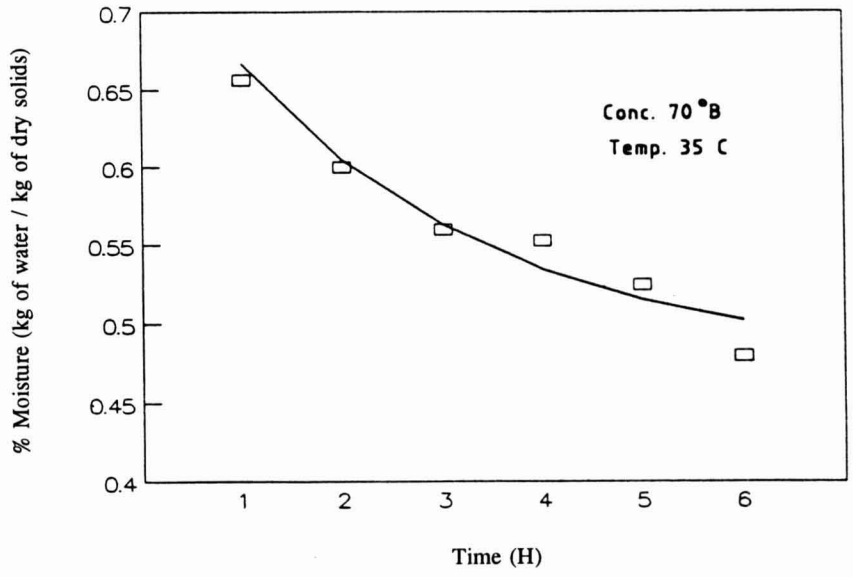

FIG. 5. COMPARISON OF EXPERIMENTAL VALUES WITH THEORETICAL ONES

CONCLUSIONS

Osmotic dehydration was found to be a successful method to aid the removal of coconut kernel without much difficulty. The moisture content at any given immersion time during the course of osmotic dehydration can be predicted from the proposed model equation in order to optimize the process conditions. Effective diffusion coefficients of water in coconut obtained from the proposed model are similar to those reported in the literature.

ACKNOWLEDGMENT

Authors would like to thank Mr. A. Ramesh, Head, Department of Food Engineering, for his active encouragement.

NOMENCLATURE

a Specific area, m^2/m^3.
A Activation Energy, J / kg-mole
B Concentration of osmotic solution, degree Brix
C Concentration at time 't', kg-mole/m^3
C* Equilibrium concentration, kg-mole/m^3
D_0 Constant
D_e Effective diffusion coefficient at any temperature T, m^2/s
k Individual mass transfer coefficient, m/s
K_T Osmotic dehydration rate constant at any temperature T, h^{-1}
L_c Characteristic length, m
M_0 Initial moisture content of coconut piece on dry basis, kg of water / kg of dry solid
M Moisture content of coconut at any time 't', kg of water / kg of dry solid
M_e Equilibrium moisture content on dry basis, kg of water / kg of dry solid
R Gas constant, 8.314×10^3 J/kg-mole °K
t Immersion time of coconut in osmotic solution, h
T Temperature of osmotic solution, °K
Y Weight of coconut after osmotic dehydration, kg
Z Weight of dry solids, kg

REFERENCES

ANDREOTTI, R., TOMASICCHIO, M. and MACCHIAVELLI, L. 1983. Disidratazione parziale della frutta per osmosi. Ind. Conserve *58*, 90–94.

AZUARA, E., CORTES, R., GARCIA, H.S. and BERISTAIN, C.I. 1992. Kinetic model for osmotic dehydration and its relationship with Fick's second law. Int. J. Food Sci. Technol. *27*,409–418.

BERISTAIN, C.I., AZUARA, E., CORTES, R. and GARCIA, H.S. 1990. Mass transfer during osmotic dehydration of pineapple rings. Int. J. Food Sci.Technol. *25*, 576–582.

BISWAL, R.N. and LE MAGUR, M. 1989. Mass transfer in plant material in contact with aqueous solution of ethanol and sodium chloride: equilibrium data. J. Food Process Engineering *11*, 159–176.

BOLIN, H.R., HUXOLL, C.C., JACKSON, R. and NG, K.C. 1983. Effect of osmotic agent and concentration on food quality. J. Food Sci. *48*, 202–205.

CHANDRASEKHRAN, S.K. and KING, J.C. 1972. Multicomponent diffusion and vapour liquid equilibria of dilute organic component in aqueous sugar solution. AIChE J. *18*(3), 517–522.

CONTRERAS, J.E. and SMYRL, T.G. 1981. An evaluation of osmotic concentration of apple ring using corn syrup solid solutions. Can. Inst. Food Sci. Technol. J. *14*, 310–314.

CONWAY, J., CASTAIGNE, F., PICAROIFT, G. and VOVAN, X. 1983. Mass transfer consideration in the osmotic dehydration of apples. Can. Inst. Food Sci. Technol. J. *16*, 25–29.

DIXON, G.M. and JEN, J.J. 1977. Changes of sugar and acid of osmovac dried apple slices. J. Food Sci. *42*, 1126–1131.

FARKAS, D.F. and LAZAR, M.E. 1969. Osmotic dehydration of apple pieces. Effect of temperature and syrup concentration on rates. Food Technol. *23*, 688–690.

FAVETTO, G., CHIRIFE, J. and BARTHOLOMAI, G.B. 1981. A study of water activity lowering in meat during immersion cooking in the Sodium-chloride-glycerol solutions. I. Equilibrium considerations and diffusional analysis of solute uptake. J Food. Technol. *16*, 609–619.

HAWKES, J. and FLINK, J.M. 1978. Osmotic concentration of fruit slices prior to freeze dehydration. J. Food Processing Preservation *2*, 265–284.

HELDMAN, D.R. and SINGH, R.P. 1980. *Food Process Engineering*, p. 21, Van Nostrand Reinhold/AVI, New York.

LERICI, C.L., PINNAVAIA, G., DALLA ROSA, M. and BARTOLUCCI, L. 1985. Osmotic dehydration of fruit: Influence of osmotic agents on drying behaviour and product quality. J. Food Sci. 50, 1217–1219.

NANJUNDASWAMY, A.M., RADHAKRISHNAIAH SETTY, G., BALACHANDRAN, C., SAROJA, S. and MURTHY REDDY, K.B.S. 1978. Studies on development of new categories of dehydrated product from indigenious fruits. Indian Food Packer *22*, 91–93.

PONTING, J.D. 1973. Osmotic dehydration of fruits. Recent modifications and applications. Proc. Biochem. *8* (12), 18–20.

PONTING, J.D., WALTERS, G.G., FORREY, R.R., JACKSON, R. and STANLEY, W.L. 1966. Osmotic dehydration of food. Food Technol. *20*, 125–128.

RAHMAN, M.S. and LAMB, J. 1990. Osmotic dehydration of pineapple. J. Food Sci. Technol. *27*, 150–152.

RAO, M.A. 1977. Energy consumption in refrigerated canned and frozen peas. J. Food Proc. Eng. *1*, 149–165.

TANAKA, H. and YOSHIDA, K. 1984. Heat and mass transfer mechanism in a grain storage silo. In *Engineering and Food: Vol. I*, (B.M. McKenna, ed.) p. 92. Elsevier Appl. Sci. Publ., New York.

TREYBAL, R.E. 1966. Mass Transfer Operations, p. 79, McGraw Hill Book Co., New York.

ZUGARRAMURDI, A. and LUPIN, H.M. 1977. Studies on anchovy salting. 2. Dynamics of the process. Lat. Am. J. Chem. Eng. Appl. Chem. *7*, 25–30.

ZUGARRAMURDI, A. and LUPIN, H.M. 1980. A model to explain observed behaviour on fish salting. J. Food Sci. *45*, 1305–1311, 1317.

MODELING FREQUENCY DISTRIBUTION OF STEADY-STATE O_2 PARTIAL PRESSURES IN MODIFIED-ATMOSPHERE PACKAGES

P.C. TALASILA and A.C. CAMERON[1]

Department of Horticulture
Michigan State University
East Lansing, MI 48824-1325

Accepted for Publication July 20, 1994

ABSTRACT

A mathematical model was developed to predict the frequency distribution of steady-state O_2 partial pressures in modified-atmosphere packages of fresh and minimally processed fruits and vegetables. Variation in O_2 uptake was predicted to have relatively larger influence on the package O_2 distribution than variation in film permeability to O_2. The model also predicted that the range of O_2 partial pressures in the packages would be larger for the products with lower $K_{1/2}$ (a constant in product O_2 uptake equation) values. The percent deviation of package O_2 partial pressures from $[O_2]_{med}$ increased with $[O_2]_{med}$ up to about 3 kPa and gradually decreased thereafter. Package O_2 distribution was symmetrical at higher $[O_2]_{med}$ but became gradually asymmetrical with decreasing $[O_2]_{med}$ from 6 kPa. The model was used to predict target $[O_2]_{med}$ for the design of modified-atmosphere packages for different probability levels of having package O_2 being equal to or less than a minimum tolerable level of the product.

INTRODUCTION

The application of modified-atmosphere packaging (MAP) technique for extending the storage life of fresh and minimally processed produce has been rapidly expanding (Crothers 1992; Zind 1992). MAP provides an economical and practical way to provide beneficial O_2 and CO_2 levels for products marketed in small quantities.

A procedure based on Fick's law of gas diffusion has been suggested to design MA packages (Beaudry *et al.* 1992; Cameron *et al.* 1989; Deily and Rizvi 1981; Hayakawa *et al.* 1975; Henig and Gilbert 1975; Kader *et al.* 1989; Talasila *et al.* 1992). In this procedure, product O_2 uptake and CO_2 production

[1]Corresponding author, Tel: (517) 355-6671.

Journal of Food Process Engineering **18** (1995) 199–217.

rates are matched with the film permeability to O_2 and CO_2, respectively, to obtain target O_2 and CO_2 concentrations.

In an ideal situation, all the packages should have the target gas levels at steady-state. However, in practice, the actual O_2 and CO_2 levels in the packages deviate from the target levels because of the natural product-to-product variation in O_2 uptake and CO_2 production rates and film-to-film variation in gas permeability to O_2 and CO_2 (see Beaudry *et al.* 1992). Since O_2 concentrations slightly below their beneficial level could be injurious for some fruits and vegetables (Kader 1989; Saltveit 1989), it is important to consider the variation in package O_2 levels when designing MA packages.

There has been very little discussion in the literature on the variation of gas levels in MA packages. Talasila *et al.* (1992) derived an equation to determine the magnitude of variation in the package O_2 and CO_2 partial pressures for the special case of constant respiration rate. However, to our knowledge, a detailed analysis of the problem has not been reported.

The specific objectives of this work were to (1) develop a mathematical model to predict the frequency distribution of steady-state package O_2 partial pressures for a given frequency distribution in product O_2 uptake and/or film permeability to O_2 (2) study the influence of various parameters on the frequency distribution of package O_2, and (3) develop an approach for designing MA packages that reduces the probability of developing injurious O_2 partial pressures.

MODEL DEVELOPMENT

Graphical Analysis

In a modified-atmosphere package, a steady-state O_2 partial pressure is obtained when the rate of O_2 permeating through the packaging film due to partial pressure difference between inside and outside is equal to the rate of O_2 uptake by the product. This concept is illustrated for a product with a specific O_2 uptake, a film of given permeability to O_2 and an outside O_2 partial pressure of 21 kPa in Fig. 1A. A deviation in O_2 uptake and film permeability to O_2 from the respective expected values creates an O_2 partial pressure that differs from the targeted value. The exact O_2 partial pressure created will depend on the magnitude of the deviation in O_2 uptake and film permeability to O_2 in that particular package. For instance, a $\pm$ 10% variation in O_2 uptake and film permeability to O_2 could create a range of package O_2 partial pressures from 1 to 4 kPa (Fig. 1B). In this example, the packages were designed for a target steady-state O_2 partial pressure of 2 kPa.

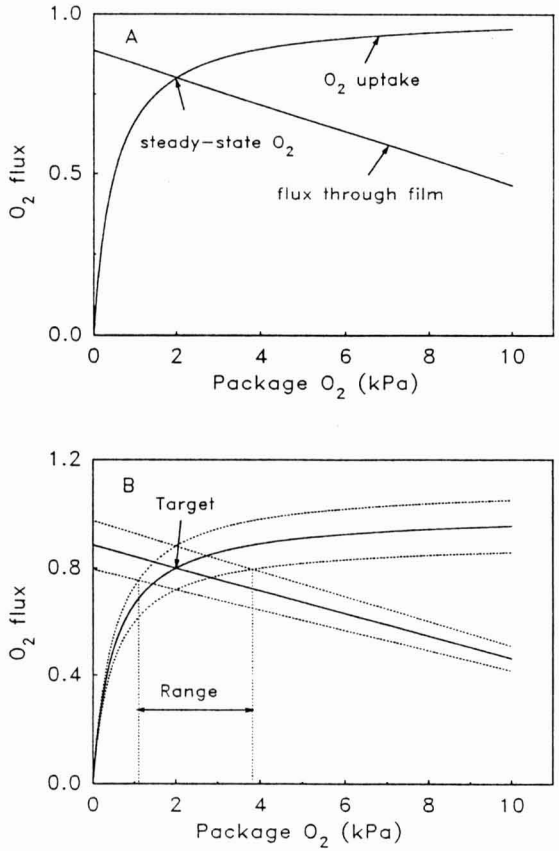

FIG. 1. ILLUSTRATION OF THE ATTAINMENT OF STEADY-STATE O_2 PARTIAL PRESSURE (A) AND THE OCCURRENCE OF PACKAGE O_2 DISTRIBUTION WHEN THERE IS A VARIATION IN PRODUCT O_2 UPTAKE AND FILM PERMEABILITY TO O_2 (B) IN A MODIFIED-ATMOSPHERE PACKAGE

A $\pm$ 10% variation in both O_2 uptake and film permeability to O_2 will create a range of O_2 partial pressures varying from 1 to 4 kPa in the packages that are originally designed to obtain 2 kPa at steady-state.

Derivation of the Model

The following assumptions were made for the development of the mathematical model:

(1) Product O_2 uptake and film permeability to O_2 follow normal distributions.
(2) Product O_2 uptake can be described using a Michaelis-Menten-type equation.
(3) The ratio of O_2 uptake of a product to the mean O_2 uptake of the population to which the product belongs is constant at all levels of package O_2 partial

pressure. This assumption implies that the coefficient of variation of product O_2 uptake has the same magnitude at all package O_2 partial pressures.

Assumptions 1 and 3 have been validated for cut broccoli at OC (Talasila *et al.* 1994) and assumption 2 was shown to be valid for several fresh products including blueberries (Cameron *et al.* 1994; Song *et al.* 1992), raspberries (Joles *et al.* 1994), and cut broccoli (Hagger *et al.* 1992; Lee *et al.* 1991; Talasila *et al.* 1994).

The concept of creation of steady-state O_2 partial pressure in MA packages in mathematical form can be described as follows (Cameron *et al.* 1989):

$$R_{O_2}W = \frac{P_{O_2}A}{\Delta x}([O_2]_{atm}-[O_2]_{pkg}) \quad (1)$$

where R_{O_2} is the O_2 uptake of the products in a package (see Nomenclature); W is the mass of the product in the package; P_{O_2} is the O_2 permeability; A is the surface area; Δx is the thickness of the film; $[O_2]_{atm}$ is the O_2 partial pressure outside the package; and $[O_2]_{pkg}$ is the steady-state package O_2 partial pressure.

If R_{O_2} and P_{O_2} are equal to the mean values of their respective populations, $[O_2]_{pkg}$ will be equal to the median of the package O_2 population:

$$\bar{R}_{O_2}W=\frac{\bar{P}_{O_2}A}{\Delta x}([O_2]_{atm}-[O_2]_{med}) \quad (2)$$

where $\bar{R}_{O_2}$ is the mean O_2 uptake, $\bar{P}_{O_2}$ is the mean film permeability to O_2 and $[O_2]_{med}$ is the median steady-state package O_2 partial pressure.

Package specifications are usually determined using Eq. (2) for a target O_2 partial pressure equal to $[O_2]_{med}$. In an ideal case of no variation in O_2 uptake and film permeability to O_2, all the packages should have $[O_2]_{pkg}$ equal to $[O_2]_{med}$ at steady-state.

If product O_2 uptake follows Michaelis-Menten-type equation (See Cameron *et al.* 1994; Hagger *et al.* 1992; Lee *et al.* 1991; Song *et al.* 1992), it may be expressed as a function of package O_2 partial pressure as:

$$\bar{R}_{O_2}=\frac{R_{O_2}^{max}\cdot[O_2]_{med}}{K_{1/2}+[O_2]_{med}} \quad (3)$$

where $K_{1/2}$ and $R_{O_2}^{max}$ are constants specific to a product. If R_{O_2} of products in a package is 'X' times $\bar{R}_{O_2}$ at all the O_2 partial pressures (see assumption 3), then from Fig. 1B:

$$R_{O_2} = X \frac{R_{O_2}^{max} \cdot [O_2]_{pkg}}{K_{1/2} + [O_2]_{pkg}} \quad (4)$$

and if P_{O_2} is 'Y' times $\bar{P}_{O_2}$:

$$P_{O_2} = Y \cdot \bar{P}_{O_2} \quad (5)$$

Note that RHS of Eq. (4) contains $[O_2]_{pkg}$ and not $[O_2]_{med}$. This becomes clear from the following analysis of Fig. 1B. If the O_2 uptake of products in a package is represented by the top dotted line of the O_2 uptake distribution and the O_2 flux through that package is represented by the bottom dotted line of the 'O_2 flux through film' distribution in Fig. 1B, the x and y coordinates of the point of intersection of the two curves will give $[O_2]_{pkg}$ and corresponding $\bar{R}_{O_2}$ of the products in that package, respectively. This R_{O_2} is 'x' times $\bar{R}_{O_2}$ corresponding to the same $[O_2]_{pkg}$.

Substituting Eq. (2), (3), (4), and (5) into Eq. (1) yields following relationship between $[O_2]_{pkg}$ and other variables

$$X \cdot \frac{[O_2]_{pkg}}{K_{1/2} + [O_2]_{pkg}} = Y \cdot \frac{[O_2]_{med}}{K_{1/2} + [O_2]_{med}} \cdot \frac{([O_2]_{atm} - [O_2]_{pkg})}{([O_2]_{atm} - [O_2]_{med})} \quad (6)$$

which when rearranged gives a quadratic equation in $[O_2]_{pkg}$. Only one of the solutions of the quadratic equation yields positive values for $[O_2]_{pkg}$:

$$[O_2]_{pkg} = \frac{1}{2} \cdot \left[-K_{1/2} + [O_2]_{atm} - \frac{X}{Y} \cdot (K_{1/2} + [O_2]_{med}) \cdot \frac{([O_2]_{atm} - [O_2]_{med})}{[O_2]_{med}} \right] +$$

$$\frac{1}{2} \cdot \left[\sqrt{\left[K_{1/2} - [O_2]_{atm} + \frac{X}{Y}(K_{1/2}[O_2]_{med}) \cdot \frac{([O_2]_{atm} - [O_2]_{med})}{[O_2]_{med}} \right]^2 + 4 \cdot K_{1/2} \cdot [O_2]_{atm}} \right] \quad (7)$$

Equation (7) will reduce to the model presented by Talasila *et al.* (1992) for the simplified case of constant O_2 uptake.

Note that $[O_2]_{pkg}$ in Eq. (7) is independent of the magnitudes of R_{O_2} and P_{O_2}. $[O_2]_{pkg}$ can be predicted from Eq. (7) for a given $[O_2]_{med}$, $K_{1/2}$, $[O_2]_{atm}$, X and Y. For example, if O_2 uptake of the products in an individual package is 1.2 times the mean O_2 uptake (X = 1.2) and film permeability to O_2 is 0.9 times the mean permeability (Y = 0.9), the steady- state O_2 partial pressure in that package ($[O_2]_{pkg}$) will be $\approx$0.4 kPa if the packages were designed for an O_2 partial pressure ($[O_2]_{med}$) of 1 kPa at steady- state. For this example, a $K_{1/2}$ of 0.25 kPa and an $[O_2]_{atm}$ of 21 kPa were assumed.

If R_{O_2} and P_{O_2} are normally distributed, then both X and Y will be normally

distributed. Let $f_1(x)$ and $f_2(y)$ be the probability density functions of X and Y, respectively. Since X and Y are independent, the distribution function for $[O_2]_{pkg}$, F(s), can be given as (see Parzen 1960):

$$F(s)=P[\ [O_2]_{pkg} \leq s] \ = \ \int\int_{([x,y]\ :\ g[x,y] \leq s)} f_1(x)f_2(y)dxdy \tag{8}$$

where s, x, and y are any real values that can be assumed by $[O_2]_{pkg}$, X, and Y, respectively and P is the probability function for $[O_2]_{pkg}$. Function 'g' is given by Eq. [7]:

$$[O_2]_{pkg} \ = \ g(x,y) \tag{9}$$

The inequality, $g(x,y) \leq s$, can be used to obtain the integration limits for x (see Parzen 1960). With proper integration limits for x and y, F(s) can be written as:

$$F(s)=\int_{-\infty}^{\infty} dy \qquad \int_{\frac{y}{4sb}(c-4s^2-4as)}^{\infty} dx f_1(x)f_2(y) \tag{10}$$

where

$$a=K_{1/2}-[O_2]_{atm}$$

$$b=\frac{(K_{1/2}+[O_2]_{med})([O_2]_{atm}-[O_2]_{med})}{[O_2]_{med}}$$

$$c=4K_{1/2}[O_2]_{atm}$$

With the change of variable from x to x′ as

$$x=\frac{y(c-4x'^2-4ax')}{4x'b} \tag{11}$$

in Eq. (10), F(s) becomes

$$F(s) \ = \ \int_{-\infty}^{\infty} dy \int_{-\infty}^{s} \frac{y}{b}\left(\frac{c}{4x'^2}+1\right) \cdot f_1\left(\frac{y[c-4x'^2-4ax']}{4x'b}\right) \cdot f_2(y)dx' \tag{12}$$

The probability density function for $[O_2]_{pkg}$, f(s), can be obtained by differentiating F(s) with respect to s:

$$f(s)=\frac{d}{ds}F(s)=\int_{-\infty}^{\infty} dy \frac{y}{b}\left(\frac{c}{4s^2}+1\right) f_1\left(\frac{y}{4sb}[c-4s^2-4as]\right) f_2(y) \tag{13}$$

The probability density functions, $f_1(x)$ and $f_2(y)$, for normal distribution are (Parzen 1960):

$$f_1(x) = \frac{1}{\sqrt{(2\pi)\sigma_X}} \exp\left[-\frac{(x-m_X)^2}{2\sigma_X^2}\right] \tag{14}$$

$$f_2(y) = \frac{1}{\sqrt{(2\pi)\sigma_y}} \exp\left[-\frac{(y-m_y)^2}{2\sigma_y^2}\right] \tag{15}$$

where m_X, σ_X and m_Y, σ_Y are the means and standard deviations of X and Y distributions, respectively. From the definitions of X and Y, both m_X and m_Y can be calculated as equal to 1 and σ_X and σ_Y as equal to the respective coefficients of variations (in decimal) of R_{O_2} and P_{O_2} distributions. Substituting Eq. (14) and (15) with the proper values of m_X, m_Y, σ_X, and σ_Y into Eq. (13) yields

$$f(s) = \frac{1}{2\pi\frac{CV_R}{100}\frac{CV_P}{100}} \int_{-\infty}^{\infty} dy \frac{y}{b}\left[\frac{c}{4s^2}+1\right] \exp\left[-\frac{\left[\frac{y}{4sb}[c-4s^2-4as]-1\right]^2}{2(CV_R/100)^2}\right] \exp\left[-\frac{(y-1)^2}{2(CV_P/100)^2}\right] \tag{16}$$

Equation (16) cannot be directly solved by any known integration methods. Numerical integration may be used to obtain probability densities of $[O_2]_{pkg}$ for various values of s. From this information, the density function of $[O_2]_{pkg}$, F(s), can be determined by numerical integration of the following equation:

$$F(s) = \int_{-\infty}^{s} f(s)ds \tag{17}$$

With the knowledge of coefficients of variation of O_2 uptake (CV_R) and film permeability to O_2 (CV_p), $K_{1/2}$, and $[O_2]_{atm}$, the distribution of $[O_2]_{pkg}$ can be calculated by using Eq. (17) for any given $[O_2]_{med}$. Valuable information, such as the probability of having $[O_2]_{pkg}$ below a certain level (F(s) or $P([O_2]_{pkg} \leq s)$) and the interval of $[O_2]_{pkg}$ with a certain probability level, can be directly obtained from the $[O_2]_{pkg}$ distribution. Alternatively, the required target $[O_2]_{med}$ for designing MA packages for a given probability of having $[O_2]_{pkg}$ equal to or less than a certain minimum level ($P([O_2]_{pkg} \leq s)$) can be predicted using a

'trial and error' or some other root finding method.

For the simple case of having variation in either O_2 uptake or film permeability to O_2, target $[O_2]_{med}$ can be directly predicted by mathematical manipulation of Eq. (7). The following equation was obtained by assuming no variation in film permeability to O_2 (i.e., Y = 1):

$$[O_2]_{med} = \frac{1}{2} \cdot \left[-K_{1/2} + [O_2]_{atm} - \frac{(K_{1/2} + [O_2]_{pkg})([O_2]_{atm} - [O_2]_{pkg})}{X \cdot [O_2]_{pkg}} \right] + \frac{1}{2} \left[\sqrt{\left[K_{1/2} - [O_2]_{atm} + \frac{(K_{1/2} + [O_2]_{pkg})([O_2]_{atm} - [O_2]_{pkg})}{X \cdot [O_2]_{pkg}} \right]^2 + 4 \cdot K_{1/2} \cdot [O_2]_{atm}} \right] \quad (18)$$

A relationship similar to Eq. (18) may be developed for the special case of no variation in O_2 uptake.

The X value in Eq. (18) for a given probability level (P) can be obtained from the corresponding standard normal deviate (z) using the following relationship deduced from the definitions of z (Steel and Torrie 1960) and X:

$$X = 1 + z\frac{CV_R}{100} \quad (19)$$

z values corresponding to a given P can be obtained by solving the density function for normal distribution using numerical integration (see Table 1 for typical z values).

For using the developed model for designing MA packages, accurate estimates of CV_R and CV_P are essential. CV_R depends on the mass of the product in the package (W). The following theoretical relationship (Steel and Torrie 1960) may be used to derive the relationship between W and CV_R:

$$\sigma_{\bar{R}} = \frac{\sigma_R}{\sqrt{n}} \quad (20)$$

where $\sigma_{\bar{R}}$ is the standard deviation of the means of several O_2 uptake populations, σ_R is the standard deviation of any one O_2 uptake population, and n is the number of individual products in any one population.

For the case of modified-atmosphere packaging, the products in each package may be assumed to constitute a population and the overall O_2 uptake of the products in the package may be assumed to be equal to the mean of the population. Then, $\sigma_{\bar{R}}$, σ_R, and n in Eq. (20) can be taken as standard deviation of product O_2 uptakes among the packages, standard deviation of O_2 uptake among the products in a package, and number of products in each package, respectively.

Assuming σ_R to be a constant for any specific product and the total product mass in a package is directly proportional to the number of products in the package, the following relationship may be derived between W and CV_R:

$$CV_R\sqrt{W} = K \tag{21}$$

where K is a constant. With the knowledge of mass of the product and the corresponding CV of O_2 uptake, CV for any other mass can be calculated from Eq. (21).

Talasila *et al.* (1994) used the developed mathematical model to predict the probabilities of $[O_2]_{pkg}$ being equal to or less than different given O_2 levels in cut broccoli packages at 0C and reported that the predicted probabilities agreed very closely with the experimental results.

ANALYSIS OF THE MODEL

Effect of O_2 Uptake and Film Permeability on Package O_2 Distribution

Package O_2 distribution is not influenced by the magnitudes of product O_2 uptake (R_{O_2}) or film permeability to O_2 (P_{O_2}) according to Eq. (16). However, the distribution depends on $K_{1/2}$ and on coefficients of variation of R_{O_2} (CV_R) and P_{O_2} (CV_p).

Figure 2 shows the effect of CV_R, CV_P, and $K_{1/2}$ on $[O_2]_{pkg}$ distribution. A probability interval of 0.01% (or a confidence interval of 99.99%) was used for calculating $[O_2]_{pkg}$ range. For an $[O_2]_{med}$ of 2 kPa and a $K_{1/2}$ of 0.25 kPa, $[O_2]_{pkg}$ was predicted to vary from 0.65 to 5.20 kPa when there is a 5% variation in R_{O_2} and P_{O_2}. A change in CV_R from 5% to 10% increased the range of $[O_2]_{pkg}$ from 0.65–5.20 kPa to 0.45–7.50 kPa. The range of $[O_2]_{pkg}$ also increased with a change in CV_p from 5% to 10%, however, the change was not as high as that caused by the similar increase in CV_R. A 10% variation in both R_{O_2} and P_{O_2} was predicted to cause the $[O_2]_{pkg}$ to vary from 0.25 to 8.50 kPa.

The range of $[O_2]_{pkg}$ was smaller for higher $K_{1/2}$ values (Fig. 2). For example, for a 5% variation in R_{O_2} and P_{O_2}, the range of $[O_2]_{pkg}$ was only 1.40–2.85 kPa for a $K_{1/2}$ of 5 kPa as compared to 0.65–5.20 kPa for 0.25 kPa. Also, for a $K_{1/2}$ of 5 kPa, there was not as significant a change in the range of $[O_2]_{pkg}$ as for 0.25 kPa with increase in variations in R_{O_2} and P_{O_2} from 5 to 10%.

Effect of $[O_2]_{med}$ on Package O_2 Distribution

The model predicted an increase in the range of $[O_2]_{pkg}$ with an increase in $[O_2]_{med}$ between 1 and 6 kPa (Fig. 3). For a $K_{1/2}$ of 0.25 kPa, the distribution of $[O_2]_{pkg}$ was symmetrical for an $[O_2]_{med}$ of 6 kPa, and it became gradually asymmetrical as $[O_2]_{med}$ changed from 6 kPa to 1 kPa. The range of $[O_2]_{pkg}$ was generally smaller for a $K_{1/2}$ of 5 kPa at any $[O_2]_{med}$ (Fig. 3). Also for this case,

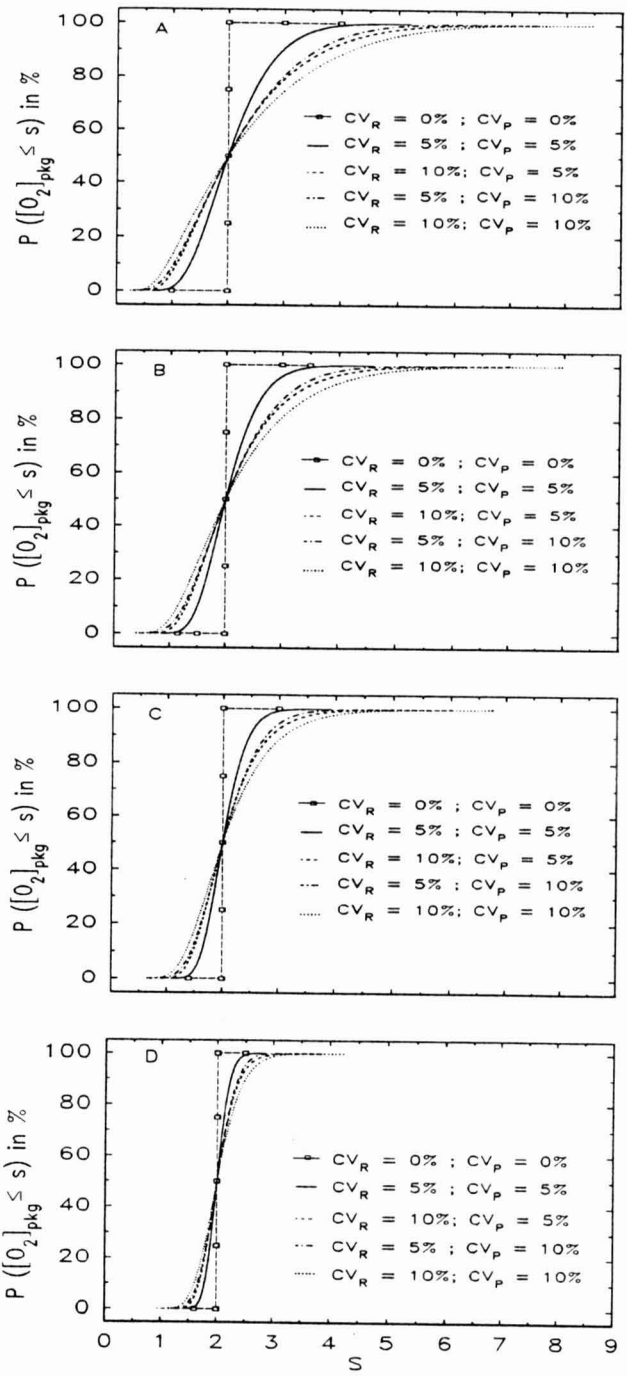

FIG. 2. FREQUENCY DISTRIBUTION OF O_2 PARTIAL PRESSURES IN THE PACKAGES THAT ARE DESIGNED TO OBTAIN AN $[O_2]_{med}$ OF 2 kPa AT STEADY-STATE FOR $K_{1/2}$ VALUES OF 0.25 kPa (A), 0.50 kPa (B), 1.00 kPa (C), AND 5.00 KPA (D) AND FOR COMBINATIONS OF 0% CV_R AND 0% CV_P (-□-); 5% CV_R AND 5% CV_P (—); 10% CV_R AND 5% CV_P (---); 5% CV_R AND 10% CV_P (— · —) AND 10% CV_R AND 10% CV_P (····)

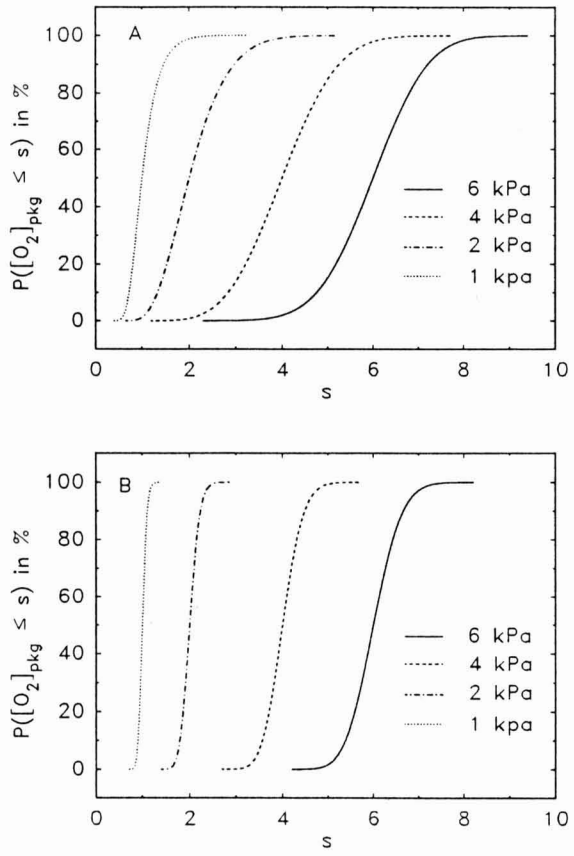

FIG. 3. FREQUENCY DISTRIBUTION OF O_2 PARTIAL PRESSURES IN THE PACKAGES THAT ARE DESIGNED TO OBTAIN $[O_2]_{med}$ OF 6 kPa (—), 4 kPa (---), 2 kPa (— · —) AND 1 kPa (····) AT STEADY-STATE FOR $K_{1/2}$ VALUES OF 0.25 kPa (A) AND 5.00 kPa (B) AND FOR A COMBINATION OF 5% CV_R AND 5% CV_P

$[O_2]_{pkg}$ distribution was close to symmetrical for all the $[O_2]_{med}$ between 1 and 6 kPa. The change in shape of the $[O_2]_{pkg}$ distribution with $[O_2]_{med}$ and $K_{1/2}$ value is due to the change in the shape of the product O_2 uptake curve for different $K_{1/2}$ values. Small $K_{1/2}$ values indicate a constant O_2 uptake from an $[O_2]_{pkg}$ level of 21 kPa to a very low value depending on the magnitude of the $K_{1/2}$ and a rapid decrease in O_2 uptake from there to zero level (see Cameron *et al.*

1994). For the case of small $K_{1/2}$ and low $[O_2]_{med}$, the distribution becomes asymmetrical as the change in $[O_2]_{pkg}$ is minimal even with a large variation in O_2 uptake.

Equations (18) and (19) were used to predict $[O_2]_{med}$ for different $[O_2]_{pkg}$ and P values. z values corresponding to different P levels were obtained from Table 1. The percent deviation, which was calculated as $((([O_2]_{med} - [O_2]_{pkg})/[O_2]_{med} \times 100))$, was as high as 58% for an $[O_2]_{med}$ of 3 kPa and a P of 0.001% (Fig. 4A). Percent deviation gives the difference between $[O_2]_{med}$ and $[O_2]_{pkg}$, the chance of occurrence of package O_2 levels equal to or lower than $[O_2]_{pkg}$ being P, expressed as a percentage of $[O_2]_{med}$. Percent deviation increased with $[O_2]_{med}$ between 0 and $\approx$ 3 kPa and gradually decreased there after (Fig. 4). An increase in P decreased the percent deviation. A change in $K_{1/2}$ from 0.25 kPa to 5.0 kPa significantly reduced the percent deviation.

Effect of Mass of the Product in the Package on CV_R

The CV of O_2 uptake may be reduced by increasing the mass of the product in each package. This will in turn decrease the range of package O_2 partial pressures. An analysis of Eq. (21) revealed that the CV_R can be decreased rapidly by increasing the product mass only up to a certain level (Fig. 5). Afterwards, the reduction in CV_R with increase in product mass is minimal.

TABLE 1.
CALCULATED z VALUES CORRESPONDING TO A GIVEN PROBABILITY LEVEL (P) FROM NUMERICAL INTEGRATION OF THE NORMAL DISTRIBUTION DENSITY FUNCTION

Probability (P)	z value
50	0.00
2	2.05
1	2.33
0.2	2.88
0.1	3.09
0.02	3.54
0.01	3.72
0.002	4.11
0.001	4.27
0.0002	4.62
0.0001	4.77

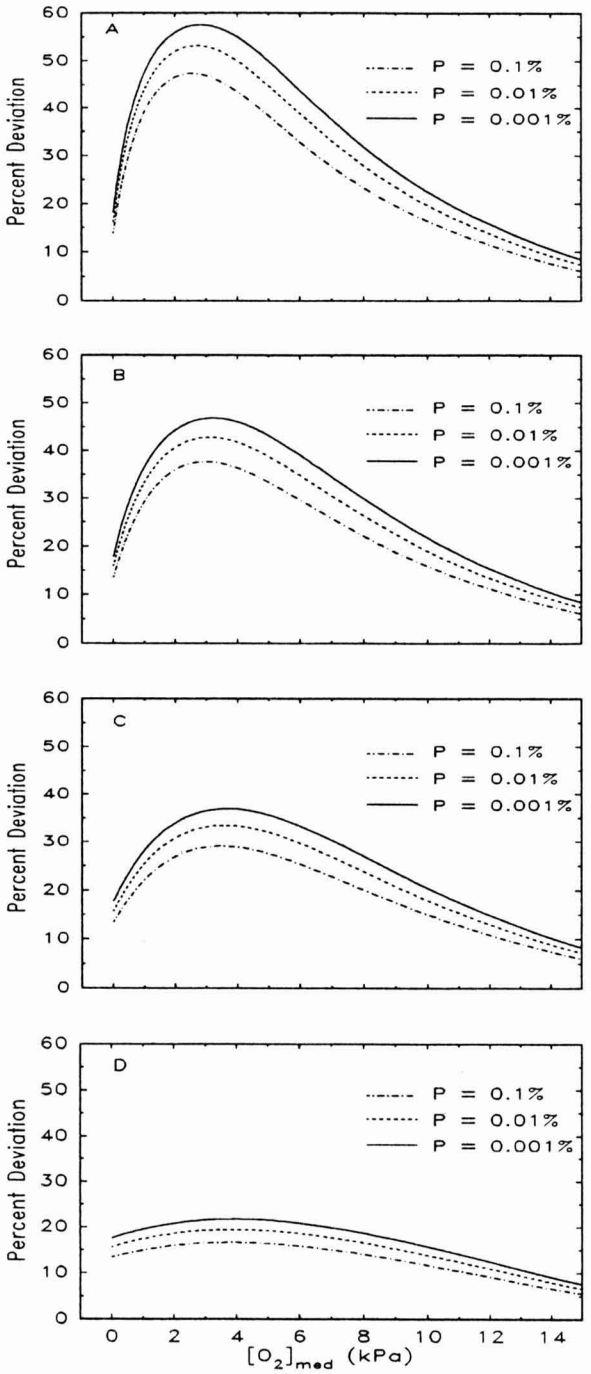

FIG. 4. PERCENT DEVIATION (CALCULATED AS $([O_2]_{med} - [O_2]_{pkg})/[O_2]_{med} \times 100$) AS A FUNCTION OF $[O_2]_{med}$ FOR $K_{1/2}$ VALUES OF 0.25 kPa (A), 0.50 kPa (B), 1.00 kPa (C), AND 5.00 kPa (D) AND FOR 0.001% (—), 0.01% (---), AND 0.1% (— · —) PROBABILITY

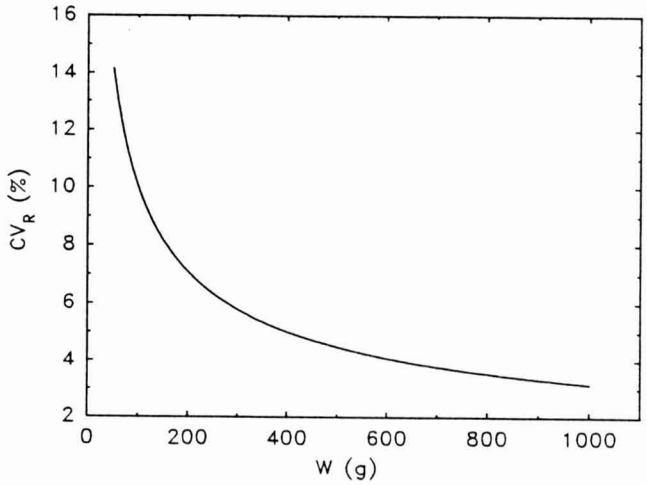

FIG. 5. RELATIONSHIP BETWEEN COEFFICIENT OF VARIATION OF O_2 UPTAKE (CV_R) AND MASS OF THE PRODUCT IN THE PACKAGE (W) BASED ON EQ. (21) FOR A K VALUE OF 100

Prediction of Target $[O_2]_{med}$ Levels for MA Package Design

A 'trial and error' solution with Eq. (16) and (17) was used to predict the required target $[O_2]_{med}$ for a given probability of having $[O_2]_{pkg}$ equal to or less than a certain minimum level ($P([O_2]_{pkg} \leq s)$). The model predicted that in order to have a 0.01% probability of having $[O_2]_{pkg} \leq 1.0$ kPa, the target $[O_2]_{med}$ should be ≥ 3.25 kPa. In this example, a $K_{1/2}$ of 0.25 kPa and a 5% CV in O_2 uptake and film permeability to O_2 were assumed.

Eq. (18) was used to predict the target $[O_2]_{med}$ for the simplified case of negligible variation in film permeability to O_2 for various probabilities of having $[O_2]_{pkg} \leq 1$ kPa and for a $K_{1/2}$ of 0.25 kPa (Table 2). Lower probabilities mandate considerably higher target $[O_2]_{med}$. An increase in coefficient of variation of O_2 uptake from 2.5% to 10% significantly increased the target $[O_2]_{med}$ for the package design.

DISCUSSION

An approach has been suggested in this paper to design packages based on a given low O_2 limit and a given probability of having package O_2 less than or equal to the low O_2 limit. A lower probability mandates higher target $[O_2]_{med}$, which will in turn require the usage of films with higher permeability to O_2 for a given mass of the product.

TABLE 2.
TARGET $[O_2]_{med}$ FOR A $K_{1/2}$ OF 0.25 kPa AND FOR VARIOUS CV_R AND PROBABILITIES OF HAVING $[O_2]_{pkg} \leq 1$ kPa

	CV_R		
Probability %	2.5%	5%	10%
		kPa	
0.1	1.36	1.86	3.20
0.01	1.45	2.10	3.81
0.001	1.53	2.32	4.34

The lower O_2 limit will be different for different fruits and vegetables and needs to be established empirically. Depending on the type of fruit or vegetable, the lower O_2 limit may be determined based on RQ break point (Beaudry *et al.* 1992; Cameron *et al.* 1994; Joles *et al.* 1994), which is an indicator of the start of the fermentative respiration process, or on other physiological or pathological limitations for the storage of the product. The lower O_2 limit increases with product temperature and storage duration (Beaudry *et al.* 1992; Ke *et al.* 1991a,b).

When the proposed approach is used, it is possible that steady-state O_2 partial pressures in some of the packages will be above the optimum level recommended for the product. For example, for a product with a $K_{1/2}$ of 0.25 kPa, there is a 10% probability that the steady-state O_2 partial pressures in packages designed to obtain a median O_2 partial pressure of 2 kPa will be above 3 kPa (Fig. 3A). An attempt to decrease the number of packages that are exposed to O_2 partial pressures above 3 kPa by decreasing the target $[O_2]_{med}$ increases the probability of exposing the packages to O_2 levels below a minimum tolerable limit. A compromise has to be made between the risk of exposing some packages to O_2 partial pressures above the optimum level to exposing the packages to O_2 partial pressures below the minimum tolerable limit.

The model predicted that the range of $[O_2]_{pkg}$ will be smaller for products with higher $K_{1/2}$ values (Fig. 2 and 3). Products such as blueberries (Cameron *et al.* 1994) and raspberries (Joles *et al.* 1994) have $K_{1/2}$ values considerably higher (0.80 kPa for blueberries and 5.6 kPa for raspberries at 0C) than for cut broccoli (0.25 kPa at 0C, Talasila *et al.* 1994). Therefore, for the same variation in O_2 uptake and film permeability, the range of package O_2 partial pressures in blueberry and raspberry packages will be considerably smaller than for the cut broccoli packages. However, variation in O_2 partial pressures inside the product is expected to be a function of K_m and not $K_{1/2}$. $K_{1/2}$ used in

developing the current model is not a true K_m for any underlying enzymatic reaction of the respiration activity in the product. It is generally assumed that the K_m for cytochrome oxidase is lower than 0.1 kPa and remains constant for all products, whereas $K_{1/2}$ is influenced by several factors, especially product skin resistance to O_2 diffusion relative to the rate of O_2 uptake. This explains why $K_{1/2}$ increased for blueberries from 0.80 kPa at 0C to 5.80 kPa at 20C (Cameron *et al.* 1994). While increasing the $K_{1/2}$ reduces variability in package O_2 partial pressures, the variability in O_2 partial pressures inside the product remains largely constant since K_m is constant for any product and does not change with $K_{1/2}$.

This study considered only product-to-product variation in O_2 uptake and package-to-package variation in film permeability. However, it is well known that variation in product respiration rate exists between harvests. Variation also exists in permeability of the film of the same type but from different sources (Doyon *et al.* 1991). If perforated films are used for product packaging, it is possible that the number of perforations per unit area of the film and the cross-sectional area of the perforations will vary. This will add to the variations considered in this study and will hence increase the range of the package O_2 levels.

Only the situations where products are injured by reduced O_2 levels were considered in the current study. There are some other situations where fruits and vegetables are injured by high CO_2 partial pressures (Kader 1989; Saltveit 1989). For these situations, an approach similar to the one developed in this paper may be used to design the packages based on the high CO_2 limit and the associated probability level. In certain cases where consideration of both O_2 and CO_2 partial pressures in the package is important, prediction of probability levels of the gases would not be as easy.

The results predicted by the model indicate that even a small variation in O_2 uptake and film permeability to O_2 could create a large variation in steady-state package O_2 partial pressures. This variation is in addition to the variation caused by any temperature changes that will occur during the distribution and marketing of the produce. It is well known that even a small change in temperature can substantially vary the gas levels inside the packages. Unless these possible variations, namely, natural variation in product respiration rate, film permeability, and variation in temperature, are taken into consideration when designing packages, the MA packaging technique may not be consistently beneficial.

NOMENCLATURE

A	Film surface area of the package (cm^2)
CV_p	Coefficient of variation of the distribution of P_{O_2} (%)

CV_R	Coefficient of variation of the distribution of R_{O_2} (%)
F	Distribution of $[O_2]_{pkg}$
f	Probability density of $[O_2]_{pkg}$
f_1	Probability density of X
f_2	Probability density of Y
g	Function representing the relationship among X,Y, and $[O_2]_{pkg}$
K	A constant relating CV_R and W in Eq. (21)
$K_{1/2}$	A constant in Michaelis-Menten-type equation of O_2 uptake as a function of package O_2 partial pressure (kPa)
K_m	A true Michaelis-Menten constant indicative of an enzymatic reaction of respiration process in the product (kPa)
m_X	Mean of the distribution of X
m_Y	Mean of the distribution of Y
n	Number of individual products in any one O_2 uptake population
$[O_2]_{atm}$	O_2 partial pressure outside the package (kPa)
$[O_2]_{med}$	Median steady-state package O_2 partial pressure (kPa)
$[O_2]_{pkg}$	Steady-state O_2 partial pressure in a package (kPa)
P	Probability of $[O_2]_{pkg}$
P_{O_2}	Film permeability to O_2 ($mmol \cdot cm \cdot cm^{-2} \cdot h^{-1} \cdot kPa^{-1}$)
$\bar{P}_{O_2}$	Mean of the film permeability to O_2 distribution ($mmol \cdot cm \cdot cm^{-2} \cdot h^{-1} \cdot kPa^{-1}$)
R_{O_2}	O_2 uptake of the product in a package ($mmol \cdot kg^{-1} \cdot h^{-1}$)
$\bar{R}_{O_2}$	Mean of the O_2 uptake distribution ($mmol \cdot kg^{-1} \cdot h^{-1}$)
$R_{O_2}^{max}$	A constant in Michaelis-Menten-type equation of O_2 uptake as a function of package O_2 partial pressure ($mmol \cdot kg^{-1} \cdot h^{-1}$)
s	Any real value that can be assumed by $[O_2]_{pkg}$
X	Fraction $R_{O_2} / \bar{R}_{O_2}$
x	Any real value that can be assumed by X
Y	Fraction $P_{O_2} / \bar{P}_{O_2}$
y	Any real value that can be assumed by Y
W	Mass of the product in a package (kg)
z	Standard normal deviate
Δx	Thickness of the packaging film (cm)
σ_R	Standard deviation of O_2 uptake among individual products in any one O_2 uptake population ($mmol \cdot kg^{-1} \cdot h^{-1}$)
$\sigma_{\bar{R}}$	Standard deviation of the mean O_2 uptake among several O_2 uptake populations ($mmol \cdot kg^{-1} \cdot h^{-1}$)
σ_X	Standard deviation of the distribution of X
σ_Y	Standard deviation of the distribution of Y

REFERENCES

BEAUDRY, R.M., CAMERON, A.C., SHIRAZI, A. and DOSTAL-LANGE, D.L. 1992. Modified-atmosphere packaging of blueberry fruit: Effect of temperature on package O_2 and CO_2. J. Amer. Soc. Hort. Sci. *117*, 436–441.

CAMERON, A.C., BEAUDRY, R.M., BANKS, N.H. and YELANICH, M.V. 1994. Modified-atmosphere packaging of blueberry fruit: Modeling respiration and package oxygen partial pressure as a function of temperature. J. Amer. Soc. Hort. Sci. *119*, 534-539.

CAMERON, A.C., BOYLAN-PETT, W. and LEE, J. 1989. Design of modified atmosphere packaging systems: Modelling oxygen concentrations within sealed packages of tomato fruits. J. Food Sci. *54*, 1413–1416, 1421.

CROTHERS, D. 1992. Packaging technology extends reach of precuts. Produce Bus. Aug., 33–36.

DEILY, K.R. and RIZVI, S.S.H. 1981. Optimization of parameters for packaging of fresh peaches in polymeric films. J. Food Proc. Eng. *5*, 23–41.

DOYON, G., GAGNON, J., TOUPIN, C. and CASTAIGNE, F. 1991. Gas transmission properties of polyvinyl chloride (PVC) films studied under subambient and ambient conditions of modified atmosphere packaging applications. Packag. Technol. Sci. *4*, 157–165.

HAGGER, P.E., LEE, D.S. and YAM, K.L. 1992. Application of an enzyme kinetics based respiration model to closed system experiments for fresh produce. J. Food Proc. Eng. *15*, 143–157.

HAYAKAWA, K., HENIG, Y.S. and GILBERT, S.G. 1975. Formulae for predicting gas exchange of fresh produce in polymeric films. J. Food Sci. *40*, 186–191.

HENIG, Y.S. and GILBERT, S.G. 1975. Computer analysis of variables affecting respiration and quality of produce packaged in polymeric films. J. Food Sci. *40*, 186–191.

JOLES, D.W., CAMERON, A.C., SHIRAZI, A., PETRACEK, P.D. and BEAUDRY, R.M. 1994. Modified-atmosphere packaging of 'Heritage' red raspberry fruit: The respiratory response to reduced oxygen, enhanced carbon dioxide and temperature. J. Amer. Soc. Hort. Sci. *119*, 540-544.

KADER, A.A. 1989. A summary of CA requirements and recommendations for fruits other than pome fruits. In *Proc. V Intl. Controlled Atmosphere Res. Conf.*, (J.K. Fellman, ed.) pp. 303–328, Wenatchee, WA.

KADER, A.A., ZAGORY, D. and KERBEL, E.L. 1989. Modified atmosphere packaging of fruits and vegetables. Crit. Rev. Food Sci. Nutr. *28*, 1–30.

KE, D., GOLDSTEIN, L., O'MAHONY, M. and KADER, A.A. 1991a. Effects of short-term exposure to low O_2 and high CO_2 atmospheres on quality attributes of strawberries. J. Food Sci. *56*, 50–54.

KE, D., RODRIGUEZ-SINOBAS, L. and KADER, A.A. 1991b. Physiology and prediction of fruit tolerance to low-oxygen atmospheres. J. Amer. Soc. Hort. Sci. *116*(2), 253–260.

LEE, D.S., HAGGER, P.E., LEE, J. and YAM, K.L. 1991. Model for fresh produce respiration in modified atmospheres based on principles of enzyme kinetics. J. Food Sci. *56*, 1580–1585.

PARZEN, E. 1960. *Modern Probability Theory and Its Applications*, John Wiley & Sons, New York.

SALTVEIT, M.E., Jr. 1989. A summary of requirements and recommendations for the controlled and modified atmosphere storage of harvested vegetables. In *Proc. V Intl. Controlled Atmosphere Res. Conf.*, (J.K. Fellman, ed.) pp. 329–352, Wenatchee, WA.

SONG, Y., KIM, H.K. and YAM, K.L. 1992. Respiration rate of blueberry in modified atmosphere at various temperatures. J. Amer. Soc. Hort. Sci. *117*, 925–929.

STEEL, R.G.D. and TORRIE, J.H. 1960. *Principles and Procedures of Statistics*, McGraw-Hill Book Co., New York.

TALASILA, P.C., CAMERON, A.C. and JOLES, D.W. 1994. Frequency distribution of steady-state O_2 partial pressures in modified-atmosphere packages of cut broccoli. J. Amer. Soc. Hort. Sci. (In Press).

TALASILA, P.C., CHAU, K.V. and BRECHT, J.K. 1992. Design of modified atmosphere packages for fresh fruits and vegetables. ASAE paper No. 92-6020, Amer. Soc. Ag. Eng., St. Joseph, MI.

ZIND, T. 1992. Embracing atmosphere packaging. The Packer, Nov. 7, 10B.

ON UPSCALING A CURD PARTICLE MODEL TO BATCH PROCESSING SCALE

J.C. AKKERMAN[1], M. DE GEE[2] and J. SCHENK[3,4]

[1] *Department of Dairy Science and Food Physics*
[2] *Department of Mathematics*
[3] *Department of Physics*
Wageningen Agricultural University
Wageningen, The Netherlands

Accepted for Publication August 15, 1994

ABSTRACT

Drainage of curd is the separation of solid curd grains and whey, an essential process step in making cheese. It is difficult to model this process by use of current consolidation theories, mainly because of the considerable loss of whey by the curd grains themselves during the expulsion of whey from pores between the curd grains. As an alternative we have studied a model that takes the expression of a single curd grain as a starting point. By analyzing experimental results of a column filled with uniform curd grains drained in radial direction while being under axial external pressure, we study the question to which extent this model might be used to predict the change of porosity with time. It appeared that the model gives reasonable results at low external pressures. At high external pressures the model proves to be inadequate. In the intermediate pressure range the model predicts too fast an expression of the curd grains, although a liquid pressure gradient between the center and the outside of the curd column could not be detected. This suggests the existence of isolated pores, or a geometric limitation of the deformation of curd grains in a curd bed.

INTRODUCTION

Cheese is one of the main dairy products. Though many different varieties of cheese are produced, the basic principle of the manufacture is always the same. It starts with clotting of the milk, i.e., the transformation of the liquid milk into a gel. Clotting can be accomplished either by adding rennet (an

[4] Retired.

[5] Correspondence should be sent to: Dr. M. de Gee, Department of Mathematics WAU, Dreijenlaan 4, 6703 HA Wageningen, The Netherlands, Fax: (0)8370-83554, Phone: (0)8370-84385.

Journal of Food Process Engineering **18** (1995) 219–231.

enzyme) to the cheese milk or by acidification of the milk. Subsequently, the gel is cut into pieces. Whey, i.e., an aqueous solution of lactose, proteins and salt, is expelled from the pieces. This process is called syneresis. The process is usually enhanced by stirring and heating of the curd/whey mixture. Finally, fairly rigid curd grains and a large amount of whey are obtained. The whey and curd are separated in a process called drainage of curd. It leads to the formation of a coherent mass of curd grains, that is subsequently salted and ripened. Drainage is therefore an essential step in the cheese-making process. Improvement of the current drainage process is of importance as it may increase yields and reduce sanitation costs and quality failures (Akkerman *et al.* 1994a).

Most current qualitative theories for the expulsion of liquid from a particle-liquid mixture by squeezing or compaction are (modified) Terzaghi models (Leclerc and Rebouillat 1985; Shirato *et al.* 1986). This model is shown symbolically in Fig. 1. In this model the time dependent behavior of the particle-liquid mixture is caused by restriction of the liquid flow, and there is no expulsion of liquid from the particles. In the drainage of curd, however, a part of the expelled whey originates from within the curd grains. Moreover, during the drainage bonds are formed between the curd particles, so called fusion (Akkerman *et al.* 1993). These two features are not present in the Terzaghi model.

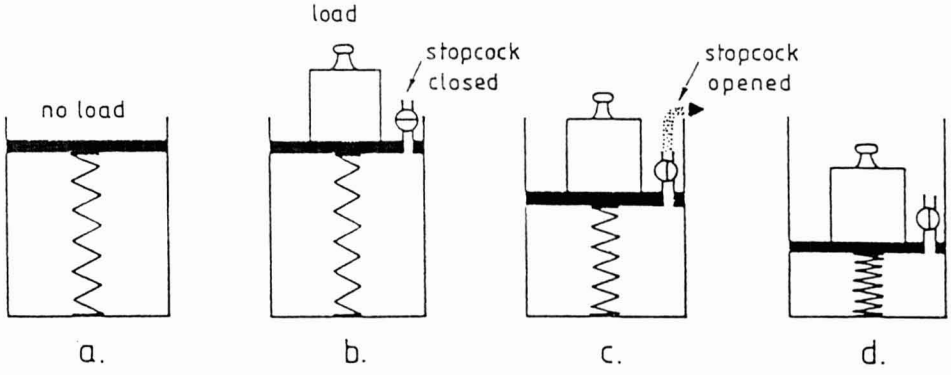

FIG. 1. THE TERZAGHI MODEL, EXPLAINED BY A FRICTIONLESS PISTON IN A CYLINDER FILLED WITH AN INCOMPRESSIBLE LIQUID, A SPRING, A STOPCOCK AND A LOAD

In (a) a spring is immersed in a cylinder filled with water. In (b) a load is applied. The piston cannot descend and the liquid pressure is equal to the applied pressure. In (c) the stopcock is opened, water escapes and the piston sinks. At (d) the spring carries the total load (Leclerc and Rebouillat 1985).

Kerkhof (1979) has applied the Terzaghi theory to the drainage of curd. Comparison of experiments and model calculations led him to the conclusion that an entirely new type of model was needed. To this end, Kerkhof introduced the so-called relaxation and expression of particles (R.E.P.) model. Compaction due to decreasing porosity and to decreasing curd volume are distinguished in this model and have different time constants. The mathematical relations of the decrease in free whey volume and in curd volume were derived from compression experiments. In these compression experiments it was assumed that after a certain time the compaction of the curd bed was caused by the whey expulsion from the curd grains only; the free whey content was assumed to be constant from then on. This model was used to predict uniaxial drainage behavior of thin layers of curd. Kerkhof compared his R.E.P. model calculations with experimental results. Although the predicted values did not exactly match the experimental ones, he ascertained that in general lines the model was in harmony with his experimental results. Kerkhof concluded therefore, that the time needed to deform and express curd grains is essential in the process of draining curd.

Kerkhof considered his approach as a tentative pilot study. Application of the model to factory conditions, involving thicker layers of curd, was not possible in the form at that time. Furthermore, for the relationships on particle level, e.g., fusion and whey expulsion, only rough estimates were available.

In this paper we try to obtain a better understanding of the fundamental properties of the curd drainage process. Experiments on well-defined curd grains have resulted in a model that describes the expulsion of whey out of a single curd grain under pressure. Using this model as a basis for a model for batch drainage we investigate to what extent the behavior of a single curd grain is significant for the behavior of a large collection of grains.

THE MODEL FOR A SINGLE CURD GRAIN

Drainage of curd is not an isolated process, as its outcome depends strongly on the preceding curd preparation and the subsequent shaping and pressing. In practice, curd grains exhibit considerable spread in size, shape and liquid content. Study of the drainage therefore requires a well-controlled curd preparation and to that end a new technique was developed. It enables the production of almost identical cube shaped curd grains. The basic features of the new apparatus are: the clotted milk is cut into uniform cubes by two wire grids, and the cubes are so gently stirred, that serious damage of the cubes is prevented. The latter feature is realized by subsequently pumping an amount of whey and large air bubbles through openings in the bottom of the cheese vat (see Fig. 2). A complete description of the apparatus is given by Akkerman *et al.* (1994a).

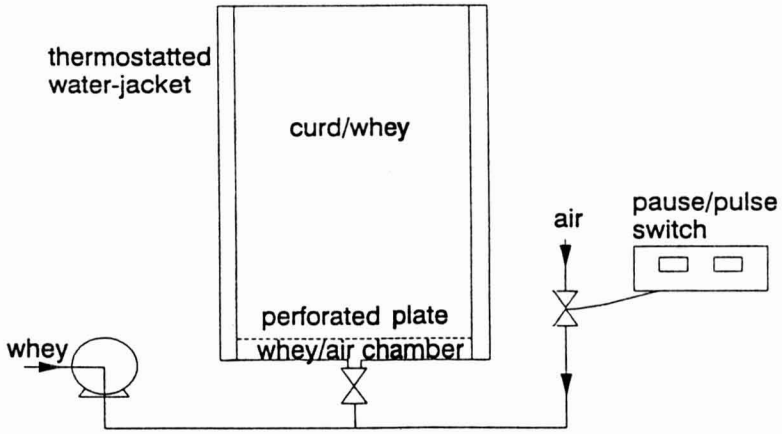

FIG. 2. DIAGRAM OF THE CHEESE VAT USED TO PREPARE CUBE SIZED CURD GRAINS

At the start the whey/air distribution chamber is filled with whey, its openings at the top temporarily closed to avoid mixing of whey and milk. After the clotting the gel is cut by wire frames (not shown).

The volume of the curd grains is characterized by their relative remaining volume i(t), that is the actual volume of a curd grain as a fraction of its volume before syneresis. The uniform curd grains are used to study the expression and deformation of a single curd grain in a uniaxial compression setup (Akkerman *et al.* 1994a). From these experiments Akkerman *et al.* (1994a) derived an empirical equation for the relative remaining volume of a single curd grain:

$$\frac{i(t)-i(\infty)}{i(0)-i(\infty)} = \exp(-kp_m\sqrt{t}) \qquad (1)$$

where

$i(t)$ = relative remaining volume at time t (−),
$i(\infty)$ = relative remaining volume at infinity (−) (≈ 0.10),
k = constant ($\approx 4.10^{-5}$ Pa^{-1} $s^{-1/2}$),
p_m = pressure on the curd grain (Pa),
t = time (s).

UPSCALING THE MODEL TO CURD BATCHES

Our aim is to use the model for the expression and deformation of a single curd grain as a tool to predict the change in porosity of a curd/whey mixture in a column that is being compressed. To that end the compaction and liquid pressure in a curd/whey mixture in a drainage column were studied in a setup as depicted in Fig. 3.

It turns out that in the upscaling two physical quantities play important roles: the pressure and the porosity. The total exerted pressure on the curd/whey mixture is taken to be equal to the external pressure, as the apparent weight of the (submerged) curd grains is relatively small. The exerted pressure can then be decomposed into three partial pressures (Schwartzberg 1983):

$$p_t = p_m + p_f + p_w \tag{2}$$

where

p_t = total exerted pressure (Pa),
p_m = pressure on the curd mass (Pa),
p_f = liquid pressure (Pa),
p_w = pressure loss due to adherence and friction to the wall (Pa).

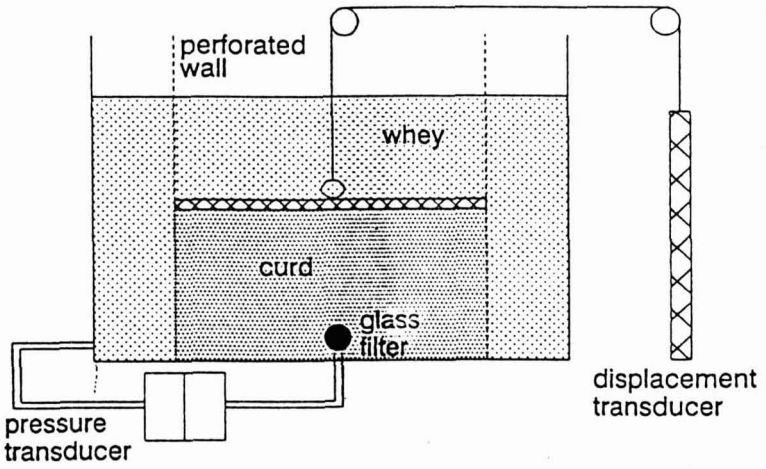

FIG. 3. A SCHEMATIC DRAWING OF THE MEASUREMENT OF THE LIQUID PRESSURE AND COMPACTION OF A CURD/WHEY MIXTURE IN A CYLINDRICAL DRAINAGE COLUMN
The external pressure was exerted by applying a weight.

It appeared that at relatively low external pressure (less than 1000 Pa), the overall liquid pressure difference between the center and the outside of the column was below the detection level. Therefore we assumed the contribution of the liquid pressure p_f, to be zero.

A significant part of the pressure exerted upon the curd grains in the drainage column is lost due to adherence and friction of the curd mass to the wall. The magnitude of this pressure loss, p_w, depends on the height within the column, that is, on the distance from the plane where the external pressure is applied. However, to simplify the equations a linear average of the pressure loss between top and bottom of the vessel was taken as an approximation that is independent of the height within the column. In this way an average value for p_w is taken according to experimental data (Akkerman *et al.* 1994b):

$$p_w = \frac{k_1 h p_t^{2.5}}{R} \tag{3}$$

where

k_1 = constant ($\approx 6.10^{-6}$ $Pa^{-1.5}$),
h = distance between top and bottom of the curd bed (m),
R = radius of the column (m).

The whey-filled pores between the curd grains, which were assumed to be uniformly distributed over the curd bed, do not carry a significant part of the pressure. The external pressure, in fact force per m^2, is carried by a smaller cross-sectional area of curd grains, hence the stress upon the curd grains can be (locally) higher than the overall pressure. Because of the statistical properties of porosity, the volumetric porosity of the curd/whey mixture equals the areal porosity; the Delesse principle (Weibel 1979). Since $p_f = 0$ this leads to the following average local stress p_m' upon the curd grains:

$$p_m' = \frac{p_t - p_w}{1 - \varepsilon} \tag{4}$$

where

p_m' = average local stress upon the curd grain (Pa),
ε = (volumetric) porosity (-).

The decrease of the volume of uniform curd grains can be derived from the expression of a single curd grain [i(0) is expressed as a volume fraction]. It has to be noted that during the expression of a single curd grain a considerable broadening of the grains occurs, which is taken into account by averaging the applied stress between two subsequent intervals in time in Eq. 1. If the increase

in cross-sectional area of curd grains in a batch may be supposed to be identical to that of a single grain, then the volume of the curd grains can simply be deduced:

$$\frac{V_g(t)-V_g(\infty)}{v_g(0)-V_g(\infty)}=\exp(-kp_m'\sqrt{t}) \tag{5}$$

where

$V_g(t)$ = remaining volume of the curd grains at time t,
$V_g(\infty)$ = remaining volume of the curd grains at infinity (≈ 0.10),
k = constant ($\approx 4.10^{-5}$ Pa^{-1} $s^{-1/2}$).

EXPERIMENTAL DESIGN

The upscaled model was designed to calculate the volume of the curd mass as a function of time. However, to use the model in this way the porosity ε of the curd/whey mixture must be known. In practice it turns out that it is extremely difficult to obtain good measurements for ε. Some measurements may be obtained using the optical fiber method described by Akkerman *et al.* (1992); however, this measurement procedure is not yet developed well enough to obtain a densely spaced (in time and space) set of reliable data. Therefore we have applied the upscaled model in a reversed way: using volume data of the curd/whey mixture we have tried to calculate its porosity.

The volume of the curd column is composed of the volume of the pores and the volume of the curd grains. If the volume of the curd grains can be predicted and the volume of the curd/whey mixture is measured, then the porosity may be calculated. The volume of the curd/whey mixture can be derived from the height measurements (Fig. 3). At the start of an experiment it is difficult to determine the height accurately, as the top of the curd bed is uneven. The porosity at the start of an experiment cannot be measured and is to a certain extent a matter of definition. To avoid these complications, the porosity was taken at 30 s at a value of 0.15. The latter value was obtained by Akkerman *et al.* (1994b) from experiments at an external pressure of 530 Pa. The volume of curd grains can then be calculated [where t is taken at 30 s, and $V_g(30) = i(0)$].

The average local stress upon the curd grains depends on the porosity, which varies in time. By taking an initial estimate for this porosity, the average local stress upon the curd grains can be calculated (Eq. 4). The volume of the curd grains follows then from a time dependent version of Eq. 5:

$$\frac{\tilde{V}_g(t_k)-V_g(\infty)}{V_g(t_{k-1})-V_g(\infty)}=\exp\left(-kp_m'(\sqrt{t_k}-\sqrt{t_{k-1}})\right) \quad (6)$$

where

p_m' = average of the local pressure on the curd grains over the interval $[t,t+\Delta t]$, depending on the value of the porosity,

$V_g(t)$ = remaining volume of the curd grains at time t,

$\tilde{V}_g(t+\Delta t)$ = approximated remaining volume of the curd grains at time $t+\Delta t$.

The approximated remaining volume $\tilde{V}_g(t+\Delta t)$ of the curd is then compared with the measured volume of the curd/whey mixture, and a new value for the porosity is calculated. This procedure is repeated until convergence of $\tilde{V}_g(t+\Delta t)$ to a limit $V_g(t+\Delta t)$ is obtained. A flow chart of the calculation scheme is given in Fig. 4.

RESULTS

The calculated porosity as a function of time at various external pressures together with some results of porosity measurements collected by Akkerman *et al.* (1994b) are given in Fig. 5.

At external pressures below 400 Pa, the calculated porosity decreased monotonically during a period of at least 900 s. The predicted porosity depends to a large extent on the estimated initial porosity, but presumably this value hardly affects the calculated monotonic decrease in porosity as a function of time. As the measured porosity at an external pressure of 530 Pa decreased monotonically, it is very likely that the porosity at external pressures below this value will also decrease monotonically. The above reasoning applies if the behavior of a single curd grain is a reasonable model for the expression of a column of these curd grains.

At external pressures in the range 400–1000 Pa the calculated porosity increased after an initial decrease. This happened at a still earlier stage for a higher external pressure. A significant increase of porosity is unrealistic (Kerkhof 1979). The calculated increase of porosity is an indication for an overestimation of the calculated speed of curd drainage. In reality, the expression of curd grains in a column may well be less than is the case for a single curd grain; this may be due to the limited possibilities for deformation of grains in the curd column and/or the locally retarded flow of whey. With respect to the latter, it has to be noted that the dimensions of the curd grains will be generally not small compared to the dimensions of the drainage system. In such a system, it is likely that a few interconnected openings transport a major part

of the whey flow; hence, in such a "channel" an overall liquid pressure between the center and the outside may be virtually absent, whereas elsewhere in the curd bed the permeability may be quite small (see Fig. 6).

At high external pressure levels (greater than 1000 Pa) the pressure on the liquid plays an important role, but in our relatively simple model this quantity is not taken into account; it leads to an overestimation of the stress upon the curd and thus to an overestimated decrease of the volume of the curd grains.

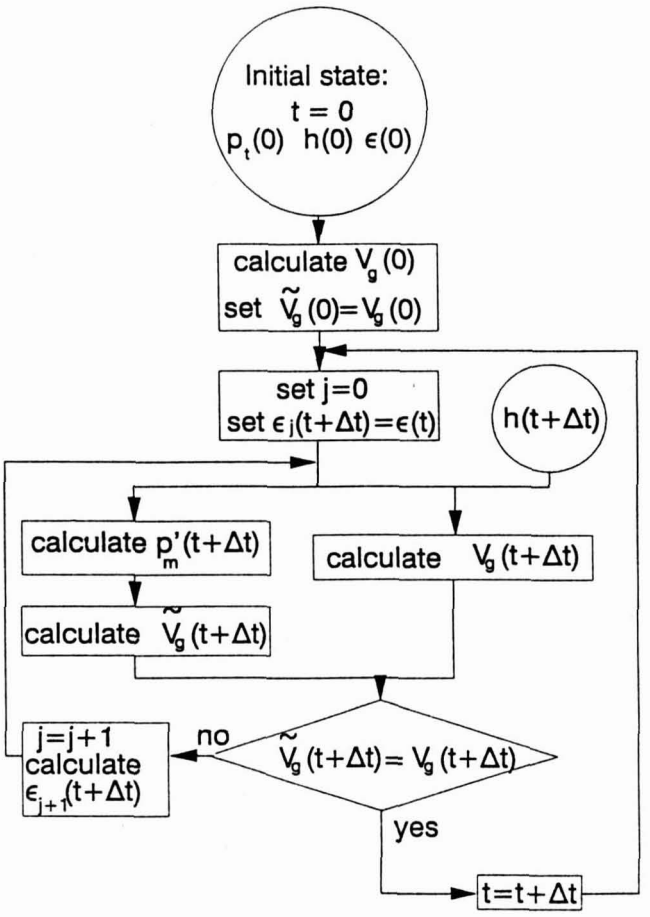

FIG. 4. THE SCHEME TO CALCULATE THE POROSITY $\varepsilon(t)$ FROM MEASUREMENT OF THE HEIGHT OF A CURD COLUMN h(t) AND THE VOLUME OF THE CURD GRAINS $V_g(t)$

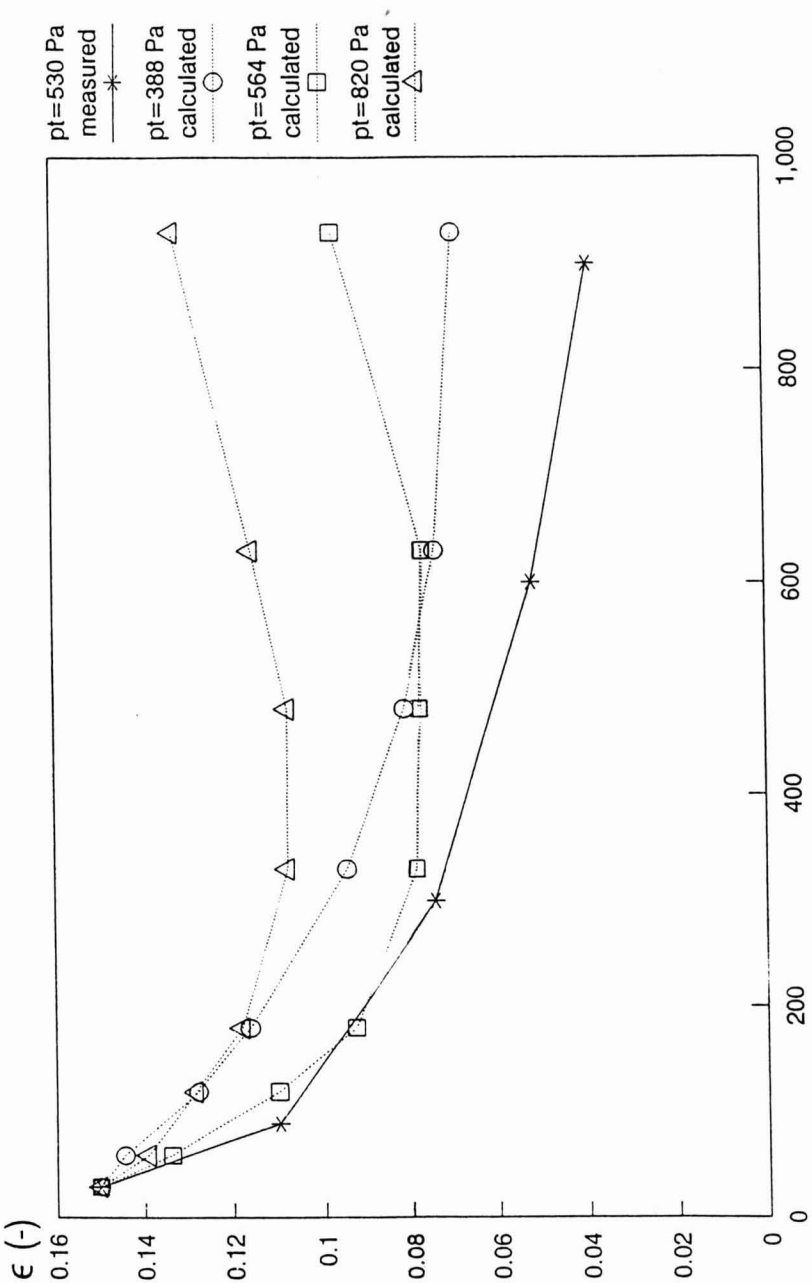

FIG. 5. THE COURSE OF THE CALCULATED POROSITY AND MEASURED POROSITY AS A FUNCTION OF TIME AT VARIOUS EXTERNAL PRESSURES, i(0) = 0.23, R = 0.06 m

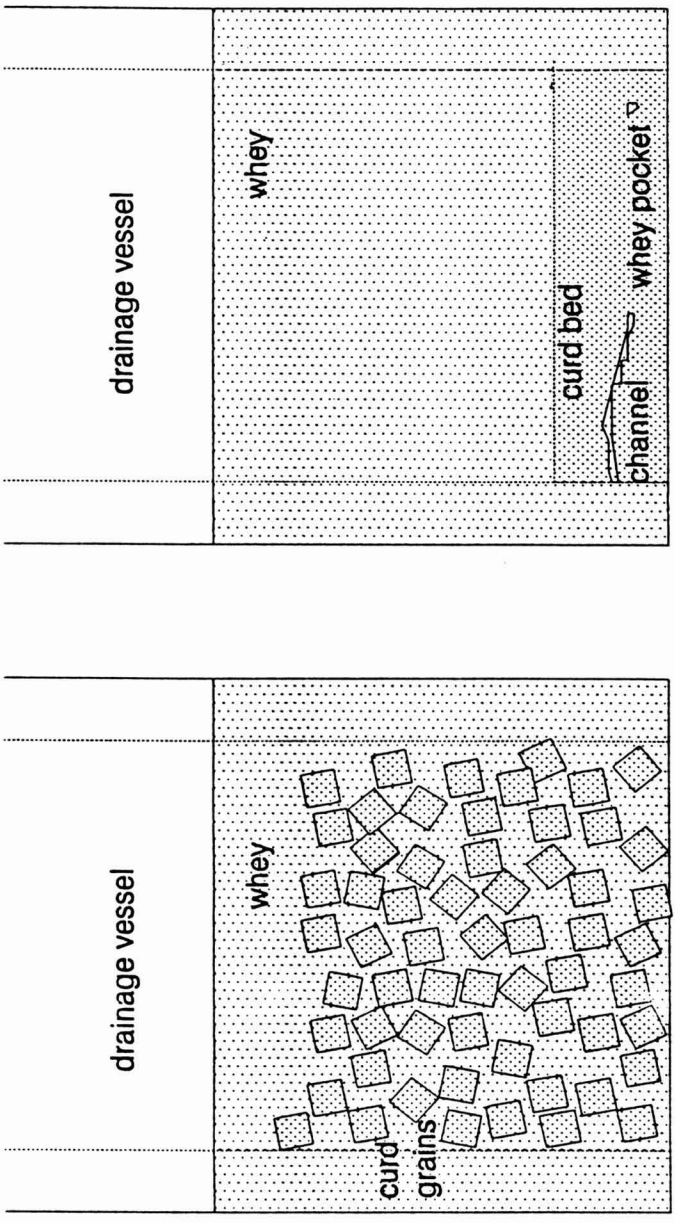

FIG. 6. SCHEMATIC CROSS-SECTION OF A CURD BED BEFORE AND AFTER PRESSING A CERTAIN PERIOD

DISCUSSION

The expression of one single curd grain can only be used as a model for the expression of a column of curd grains at low external stress. The limits of the external stress will probably be determined by the geometry of the column and the initial relative remaining volume i(0). At the conditions of our experiment ($0.29 < i(0) < 0.23$ and $R = 0.06$m, $t = 900$s), the limit is about 400 Pa; this may be higher in a case of more rigid curd grains. In practice, drainage equipment should allow a fast and complete removal of a certain amount of whey. Therefore, application of higher external stresses may be attractive. However, as shown above, the expression of a drainage column filled with curd grains can be greatly retarded compared to that of a single curd grain, while a liquid pressure gradient between the center and the outside of the curd column is still below the detection limits. This may be due to limited deformation possibilities for the curd grains inside the curd column and/or locally restricted flow of whey. Both causes may partly be set off by a slightly widening design of the drainage column. At high stress levels the single curd grain approach does not work, because liquid flow restrictions are not taken into account. However, high stress levels are rarely applied as they introduce an increased inhomogeneity of the curd blocks (Akkerman *et al.* 1994b).

In this paper we have tested the usefulness of the upscaled model by its ability to predict acceptable values for the porosity. One should realize that this is a very severe test. Indeed, the reconstruction of the porosity as parameter in an exponential curve is a notorious, ill-posed problem, and therefore it is very sensitive for the effects of errors either in the model or in the measurements. It may very well be that the upscaled single particle model is able to predict the volume of the curd mass, once an acceptable model (or a set of reliable measurements) for the porosity is available.

It should be realized that the drainage of a curd column is only one example of complicated expression behavior that cannot be described by current filtration models. The work of Trägårdh and Arvidsson (1984) shows that it is also very difficult to describe the expression of sugar-beet pulp with (modified) Terzaghi models. Study of such a system, with a comparable approach as given here, could be considered.

ACKNOWLEDGMENTS

The stimulating discussions with Prof. Dr. P. Walstra were highly appreciated by the authors. Further, we wish to thank the J. Mesdag foundation for financial support. Finally, we thank the referees for their helpful suggestions.

REFERENCES

AKKERMAN, J.C., BISPERINK, C.G.J. and RONTELTAP, A.D. 1992. A moving optical fibre technique for structure analysis of heterogeneous products: application to different foodstuffs. Food Struct. *11* 109–113.

AKKERMAN, J.C., BUIJSSE, C.A.P., SCHENK, J. and WALSTRA, P. 1994b. Drainage of curd: role of drainage equipment in relation to curd properties. Neth. Milk Dairy J. (In Press).

AKKERMAN, J.C., FOX, F.H.J. and WALSTRA, P. 1994a. Drainage of curd; expression of single curd grains. Neth. Milk Dairy J. *48*,1–17.

AKKERMAN, J.C., LEWIS, R.O. and WALSTRA, P. 1993. Fusion of curd grains. Neth. Milk Dairy J. *47*, 137–144.

KERKHOF, P.J.A.M. 1979. Private communication, Netherlands Dairy Research Institute, Ede, The Netherlands.

LECLERC, D. and REBOUILLAT, S. 1985. Dewatering by compression. In *Mathematical Models and Design Methods in Solid-Liquid Separation*, NATO ASI Series E no. 88, (A. Rushton, ed.) pp. 356–391, Martinus Nijhoff Publishers, Dordrecht, The Netherlands.

SCHWARTZBERG, H.G. 1983. Expression related properties. In *Engineering Properties of Food*, (M. Peleg and E. Bagley, eds.) pp. 423–471, Van Nostrand Reinhold/AVI, New York.

SHIRATO, M., MURASE, T. and IWATA, M. 1986. Deliquoring by expression: theory and practice. In *Progression in Filtration and Separation 4*, (R.J. Wakeman, ed.) pp. 181–287, Elsevier, Amsterdam, The Netherlands.

TRÄGÅRDH C. and ARVIDSSON, P.O. 1984. Consolidation theories applied to the expression of sugar-beet pulp. In *Engineering and Food*, Vol. II, (B.M. MacKenna, ed.) pp. 641–650, Elsevier, London.

WEIBEL, E.R. 1979. *Stereological Methods, Vol 1: Practical Methods for Biological Morphometry*, pp. 26–27, Academic Press, London.

FNP PUBLICATIONS IN FOOD SCIENCE AND NUTRITION

Journals

JOURNAL OF FOOD LIPIDS, F. Shahidi
JOURNAL OF RAPID METHODS AND AUTOMATION IN MICROBIOLOGY, D.Y.C. Fung and M.C. Goldschmidt
JOURNAL OF MUSCLE FOODS, N.G. Marriott, G.J. Flick, Jr. and J.R. Claus
JOURNAL OF SENSORY STUDIES, M.C. Gacula, Jr.
JOURNAL OF FOODSERVICE SYSTEMS, C.A. Sawyer
JOURNAL OF FOOD BIOCHEMISTRY, J.R. Whitaker, N.F. Haard and H. Swaisgood
JOURNAL OF FOOD PROCESS ENGINEERING, D.R. Heldman and R.P. Singh
JOURNAL OF FOOD PROCESSING AND PRESERVATION, D.B. Lund
JOURNAL OF FOOD QUALITY, J.J. Powers
JOURNAL OF FOOD SAFETY, T.J. Montville
JOURNAL OF TEXTURE STUDIES, M.C. Bourne and M.A. Rao

Books

OF MICROBES AND MOLECULES: FOOD TECHNOLOGY AT M.I.T., S.A. Goldblith
MEAT PRESERVATION: PREVENTING LOSSES AND ASSURING SAFETY, R.G. Cassens
S.C. PRESCOTT, M.I.T. DEAN AND PIONEER FOOD TECHNOLOGIST, S.A. Goldblith
FOOD CONCEPTS AND PRODUCTS: JUST-IN-TIME DEVELOPMENT, H.R. Moskowitz
MICROWAVE FOODS: NEW PRODUCT DEVELOPMENT, R.V. Decareau
DESIGN AND ANALYSIS OF SENSORY OPTIMIZATION, M.C. Gacula, Jr.
NUTRIENT ADDITIONS TO FOOD, J.C. Bauernfeind and P.A. Lachance
NITRITE-CURED MEAT, R.G. Cassens
POTENTIAL FOR NUTRITIONAL MODULATION OF AGING, D.K. Ingram *et al.*
CONTROLLED/MODIFIED ATMOSPHERE/VACUUM PACKAGING OF FOODS, A.L. Brody
NUTRITIONAL STATUS ASSESSMENT OF THE INDIVIDUAL, G.E. Livingston
QUALITY ASSURANCE OF FOODS, J.E. Stauffer
THE SCIENCE OF MEAT AND MEAT PRODUCTS, 3RD ED., J.F. Price and B.S. Schweigert
HANDBOOK OF FOOD COLORANT PATENTS, F.J. Francis
ROLE OF CHEMISTRY IN PROCESSED FOODS, O.R. Fennema, *et al.*
NEW DIRECTIONS FOR PRODUCT TESTING OF FOODS, H.R. Moskowitz
PRODUCT TESTING AND SENSORY EVALUATION OF FOODS, H.R. Moskowitz
ENVIRONMENTAL ASPECTS OF CANCER: ROLE OF FOODS, E.L. Wynder *et al.*
FOOD PRODUCT DEVELOPMENT AND DIETARY GUIDELINES, G.E. Livingston, R.J. Moshy, and C.M. Chang
SHELF-LIFE DATING OF FOODS, T.P. Labuza
ANTINUTRIENTS AND NATURAL TOXICANTS IN FOOD, R.L. Ory
UTILIZATION OF PROTEIN RESOURCES, D.W. Stanley *et al.*
VITAMIN B_6: METABOLISM AND ROLE IN GROWTH, G.P. Tryfiates
POSTHARVEST BIOLOGY AND BIOTECHNOLOGY, H.O. Hultin and M. Milner

Newsletters

MICROWAVES AND FOOD, R.V. Decareau
FOOD INDUSTRY REPORT, G.C. Melson
FOOD, NUTRITION AND HEALTH, P.A. Lachance and M.C. Fisher
FOOD PACKAGING AND LABELING, S. Sacharow

GUIDE FOR AUTHORS

Typewritten manuscripts in triplicate should be submitted to the editorial office. The typing should be double-spaced throughout with one-inch margins on all sides.

Page one should contain: the title, which should be concise and informative; the complete name(s) of the author(s); affiliation of the author(s); a running title of 40 characters or less; and the name and mail address to whom correspondence should be sent.

Page two should contain an abstract of not more than 150 words. This abstract should be intelligible by itself.

The main text should begin on page three and will ordinarily have the following arrangement:

Introduction: This should be brief and state the reason for the work in relation to the field. It should indicate what new contribution is made by the work described.

Materials and Methods: Enough information should be provided to allow other investigators to repeat the work. Avoid repeating the details of procedures that have already been published elsewhere.

Results: The results should be presented as concisely as possible. Do not use tables *and* figures for presentation of the same data.

Discussion: The discussion section should be used for the interpretation of results. The results should not be repeated.

In some cases it might be desirable to combine results and discussion sections.

References: References should be given in the text by the surname of the authors and the year. *Et al.* should be used in the text when there are more than two authors. All authors should be given in the Reference section. In the Reference section the references should be listed alphabetically. See below for style to be used.

RIZVI, S.S.H. 1986. Thermodynamic properties of foods in dehydration. In *Engineering Properties of Foods*, (M.A. Rao and S.S.H. Rizvi, eds.) pp. 133–214, Marcel Dekker, New York.

MICHAELS, S.L. 1989. Crossflow microfilters ins and outs. Chem. Eng. *96*, 84–91.

LABUZA, T.P. 1982. *Shelf-Life Dating of Foods,* pp. 66–120, Food & Nutrition Press, Trumbull, CT.

Journal abbreviations should follow those used in *Chemical Abstracts*. Responsibility for the accuracy of citations rests entirely with the author(s). References to papers in press should indicate the name of the journal and should only be used for papers that have been accepted for publication. Submitted papers should be referred to by such terms as "unpublished observations" or "private communication." However, these last should be used only when absolutely necessary.

Tables should be numbered consecutively with Arabic numerals. The title of the table should appear as below:

TABLE 1.
ACTIVITY OF POTATO ACYL-HYDROLASES ON NEUTRAL LIPIDS, GALACTOLIPIDS AND PHOSPHOLIPIDS

Description of experimental work or explanation of symbols should go below the table proper. Type tables neatly and correctly as tables are considered art and are not typeset. Single-space tables.

Figures should be listed in order in the text using Arabic numbers. Figure legends should be typed on a separate page. Figures and tables should be intelligible without reference to the text. Authors should indicate where the tables and figures should be placed in the text. Photographs must be supplied as glossy black and white prints. Line diagrams should be drawn with black waterproof ink on white paper or board. The lettering should be of such a size that it is easily legible after reduction. Each diagram and photograph should be clearly labeled on the reverse side with the name(s) of author(s), and title of paper. When not obvious, each photograph and diagram should be labeled on the back to show the top of the photograph or diagram.

Acknowledgments: Acknowledgments should be listed on a separate page.

Short notes will be published where the information is deemed sufficiently important to warrant rapid publication. The format for short papers may be similar to that for regular papers but more concisely written. Short notes may be of a less general nature and written principally for specialists in the particular area with which the manuscript is dealing. Manuscripts that do not meet the requirement of importance and necessity for rapid publication will, after notification of the author(s), be treated as regular papers. Regular papers my be very short.

Standard nomenclature as used in the engineering literature should be followed. Avoid laboratory jargon. If abbreviations or trade names are used, define the material or compound the first time that it is mentioned.

EDITORIAL OFFICE: DR. D.R. HELDMAN, COEDITOR, *Journal of Food Process Engineering*, Food Science/Engineering Unit, University of Missouri-Columbia, 235 Agricultural/Engineering Bldg., Columbia, MO 65211 USA; or DR. R.P. SINGH, COEDITOR, *Journal of Food Process Engineering*, University of California, Davis, Department of Agricultural Engineering, Davis, CA 95616 USA.

JOURNAL FOOD PROCESS ENGINEERING VOLUME 18, NUMBER 2

CONTENTS